

INFORMATION TO USERS

This manuscript has been reproduced from the microfilm master. UMI films the text directly from the original or copy submitted. Thus, some thesis and dissertation copies are in typewriter face, while others may be from any type of computer printer.

The quality of this reproduction is dependent upon the quality of the copy submitted. Broken or indistinct print, colored or poor quality illustrations and photographs, print bleedthrough, substandard margins, and improper alignment can adversely affect reproduction.

In the unlikely event that the author did not send UMI a complete manuscript and there are missing pages, these will be noted. Also, if unauthorized copyright material had to be removed, a note will indicate the deletion.

Oversize materials (e.g., maps, drawings, charts) are reproduced by sectioning the original, beginning at the upper left-hand corner and continuing from left to right in equal sections with small overlaps. Each original is also photographed in one exposure and is included in reduced form at the back of the book.

Photographs included in the original manuscript have been reproduced xerographically in this copy. Higher quality 6" x 9" black and white photographic prints are available for any photographs or illustrations appearing in this copy for an additional charge. Contact UMI directly to order.

UMI

A Bell & Howell Information Company
300 North Zeeb Road, Ann Arbor MI 48106-1346 USA
313/761-4700 800/521-0600

NOTE TO USERS

The original manuscript received by UMI contains pages with indistinct and/or slanted print. Pages were microfilmed as received.

This reproduction is the best copy available

UMI

Glaciological Investigations Beneath
An Active Polar Glacier

Kurt Marshall Cuffey

A dissertation submitted in partial fulfillment of
the requirements for the degree of

Doctor of Philosophy

University of Washington

1999

Program Authorized to Offer Degree: Geological Sciences

UMI Number: 9924081

Copyright 1999 by
Cuffey, Kurt Marshall

All rights reserved.

UMI Microform 9924081
Copyright 1999, by UMI Company. All rights reserved.

This microform edition is protected against unauthorized
copying under Title 17, United States Code.

UMI
300 North Zeeb Road
Ann Arbor, MI 48103

© Copyright 1999

Kurt Marshall Cuffey

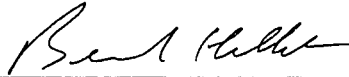
University of Washington
Graduate School

This is to certify that I have examined this copy of a doctoral dissertation by

Kurt Marshall Cuffey

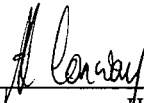
and have found that it is complete and satisfactory in all respects,
and that any and all revisions required by the final
examining committee have been made.

Chair of Supervisory Committee:

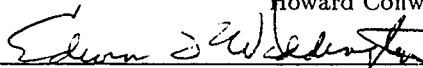


Bernard Hallet

Reading Committee:



Howard Conway



Edwin Waddington

Date: February 2, 1999

In presenting this dissertation in partial fulfillment of the requirements for the Doctoral degree at the University of Washington, I agree that the Library shall make its copies freely available for inspection. I further agree that extensive copying of this thesis is allowable only for scholarly purposes, consistent with "fair use" as prescribed in the U.S. Copyright Law. Requests for copying or reproduction of this dissertation may be referred to University Microfilms, 1490 Eisenhower Place, P.O. Box 975, Ann Arbor, MI 48106, to whom the author has granted "the right to reproduce and sell (a) copies of the manuscript in microform and/or (b) printed copies of the manuscript made from microform."

Signature Kent Cuffey

Date 2/2/99

University of Washington

Abstract

Glaciological Investigations Beneath
An Active Polar Glacier

by Kurt Marshall Cuffey

Chair of Supervisory Committee

Professor Bernard Hallet
Geological Sciences

Meserve Glacier, Antarctica, was used as a natural laboratory for research on the effective viscosity of subfreezing polycrystalline ice, and on the interaction of cold-based glaciers with their beds. A tunnel was excavated through basal layers of this glacier, which allowed sampling of ice for subsequent measurements of physical and chemical properties and allowed in-situ measurements of ice deformation and glacier sliding.

Analyses of deformation reveal a direct dependence of strain rate on crystal size, which reflects an important role for grain-size-sensitive deformation mechanisms such as grain boundary sliding. The sensitivity of strain rate to chemical impurity content and rock particle content is found to be very low. Variations of crystal size probably are an important control on shear enhancement in the ice sheets. The enhanced shear strain rate inferred from tilt of the Dye 3 borehole can be explained as a result of combined fabric and crystal size variations.

I infer that interactions between Meserve glacier and its bed are influenced by the presence of liquid water films at ice-rock interfaces despite the low temperature of -17°C . Such films allow slip at ice-rock interfaces and cause in-situ segregation of ice into clean lenses amidst dirty layers. Using slip rate and bed surface roughness measurements I infer a liquid

film thickness of at least tens of nanometers. Such films should generally be present in polar glaciers, and will have a thickness controlled by soluble impurities and temperature. Analyses of gas and isotopic composition of basal ices reveal that entrainment of bed material into this glacier actively occurs without bulk freeze-on and conventional regelation. Cold-based glaciers have the capacity to striate and erode their beds, and to create glacial landforms.

I reinterpret the clear and persistent relationship between $\delta^{18}\text{O}$ and δD of polar precipitation, which allows isotopic composition to be an important tool for studying glacier-bed interactions and deuterium excess measurements on ice cores to reveal subtropical paleoclimate. I argue that the isotopic composition of precipitation is determined by water-vapor equilibrium to temperatures as low as $-35\text{ }^{\circ}\text{C}$. This implies deuterium excess is not sensitive to cloud supersaturation.

TABLE OF CONTENTS

| | |
|---|-----------|
| List of Figures | iv |
| List of Tables | vi |
| Chapter 1: Introduction and Summary | 1 |
| 1.1 An In-Situ Rheology Experiment | 2 |
| 1.2 Basal Sliding at Subfreezing Temperatures | 3 |
| 1.3 Processes at Cold Glacier Beds | 4 |
| 1.4 Reconsidering the Meteoric Water Line | 5 |
| Chapter 2: The Rheology of Glacier Ice: Role of Crystal Size, Chemical Impurities and Rock Particles | 6 |
| 2.1 A Semi-Empirical Model | 11 |
| 2.1.1 The New Term | 12 |
| 2.2 Analysis of Meserve Glacier Data | 14 |
| 2.2.1 The Tunnel and Measurements of Ice Properties | 14 |
| 2.2.2 Ice Sampling. | 15 |
| 2.2.3 Using Fabric Data | 19 |
| 2.2.4 Analysis Method | 22 |
| 2.3 Results | 32 |
| 2.3.1 Optimal Models. | 32 |
| 2.3.2 A Mixed Grain Size and Ion Model is Necessary. | 33 |
| 2.3.3 Ions Act Through a Grain Size-Dependent Mechanism. | 36 |

| | | |
|---|--|-----------|
| 2.3.4 | Grain-Size Dependence | 36 |
| 2.3.5 | The Role of Ions. | 40 |
| 2.3.6 | The Role of Rock Particles. | 51 |
| 2.3.7 | Fabrics | 52 |
| 2.4 | Application to Other Sites | 52 |
| 2.5 | Conclusion | 59 |
| Chapter 3: Interfacial Water In Polar Glaciers and Measurements of Glacier Sliding at -17 °C | | 61 |
| 3.1 | Subfreezing Sliding: Theory | 62 |
| 3.2 | Sliding Observation | 63 |
| 3.3 | Interpretation of Sliding | 64 |
| 3.4 | Ice Segregation | 69 |
| 3.5 | Conclusion | 70 |
| Chapter 4: Entrainment Beneath Cold Glaciers | | 73 |
| 4.1 | Entrainment at Subfreezing Temperatures | 74 |
| 4.1.1 | Meserve Glacier Basal Layers | 75 |
| 4.1.2 | Gas Composition | 75 |
| 4.1.3 | Stable Isotope Composition | 77 |
| 4.1.4 | Entrainment Summary | 80 |
| 4.2 | Geomorphic Work of the Subfreezing Meserve Glacier | 81 |
| 4.3 | Mechanisms, Sliding, Interfacial Films | 82 |
| 4.4 | Striations and Abrasion | 85 |
| 4.5 | Conclusion | 85 |
| Chapter 5: Reconsidering the Polar Regions Meteoric Water Line | | 87 |
| 5.1 | Background | 87 |

| | |
|--------------------------|-----------|
| 5.2 A New View | 90 |
| Bibliography | 99 |

LIST OF FIGURES

| | | |
|------|---|----|
| 2.1 | Compilation of data used in strain rate analysis | 25 |
| 2.2 | C-axis data for U-grid | 27 |
| 2.3 | C-axis data for D-grid | 28 |
| 2.4 | Covariation of the variables | 30 |
| 2.5 | Monte Carlo simulation of strain rates | 31 |
| 2.6 | Model and measured strain rates compared | 34 |
| 2.7 | Additive models are inadequate | 37 |
| 2.8 | Inferred grain-size dependence | 38 |
| 2.9 | Constraints on ω | 39 |
| 2.10 | The roles of six ions considered | 41 |
| 2.11 | Constraints on non-linearity of ion softening | 44 |
| 2.12 | Generalized sensitivity to ions, and the fractional contribution of ions to grain-size-dependent deformation | 46 |
| 2.13 | Magnitude of the softening by ions | 47 |
| 2.14 | How η affects inferred sensitivity to ions | 48 |
| 2.15 | γ for various assumptions concerning the dominant impurity | 50 |
| 2.16 | How much of the Dye 3 residual enhancement does the new model explain . . | 55 |
| 2.17 | Depth profiles of the Dye 3 residual enhancement | 56 |
| 3.1 | Measurement of basal sliding | 65 |
| 3.2 | Measurement of rock roughness | 67 |
| 3.3 | Sketches of observed ice segregation features and cavities | 71 |

| | | |
|-----|---|----|
| 3.4 | Photograph of segregation ice | 72 |
| 4.1 | Marginal stratigraphy of Meserve Glacier | 76 |
| 4.2 | Gas composition measurements of Meserve ices | 78 |
| 4.3 | Co-isotopic data for Meserve ices | 79 |
| 4.4 | Erosional landform revealed by radio echo-sounding | 83 |
| 5.1 | Meteoric water line for glacial-age Dry Valleys precipitation | 89 |
| 5.2 | Modeled deuterium excess | 94 |
| 5.3 | Two independent tests of the model | 96 |

LIST OF TABLES

| | | |
|-----|---|----|
| 2.1 | Stratigraphic variability of ion content | 23 |
| 2.2 | Measured ice properties summary | 26 |
| 2.3 | Summary of optimal model parameters | 33 |
| 2.4 | Relative significance of various strain rate controls | 35 |
| 5.1 | Kinetic and equilibrium predictions compared | 98 |

ACKNOWLEDGMENTS

I wish to gratefully acknowledge the support and insight I have received over the years from my advisers at the University of Washington: Bernard Hallet, Howard Conway, Charlie Raymond, Ed Waddington and Tom Dunne. It was inevitable from the day I started applying to graduate schools that Bernard Hallet would become my primary adviser, due to his unique combination of intellectual power and breadth. To Howard Conway I am especially indebted for his decision to revisit the Meserve Glacier and for his perpetually positive attitude. In addition, I have greatly benefitted from the wisdom of Dave Montgomery, Steve Warren, Minze Stuiver, Greg Dash, John Wettlaufer, Sam Fain, Steve Burges, Steve Porter, Ron Sletten, Mark Kot, Marcia Baker, Dean Hegg, Art Rangno, and Al Rasmussen.

I am extremely grateful to Tony Gades, who has been a constant source of support and, in the course of the Meserve Glacier Project, a key colleague. In addition, Dave Morse, Eric Steig, Bonnie Light, Jon Stock, Rolf Aalto, Jim Roche, Kevin Schmidt, Tim Abbe, Steve Thompson and Kelin Whipple have all been particularly positive forces in my UW career. There have been many others.

I owe a huge debt of gratitude to colleagues outside the UW, without whom much of my research would not have been possible. In particular I thank Richard Alley, Gary Clow, Gerry Holdsworth, Sigfus Johnsen, and Shawn Marshall.

Success of the Meserve Glacier Project was made possible by contributions from numerous individuals. Most important are Howard Conway, Bernard Hallet, Charlie Raymond, Tony Gades, Ed Waddington, John Wettlaufer, Al Rasmussen, Ron Sletten, Nadine Nereson, Throstur Thorsteinsson, John Wright, Paul Mayewski, Sallie Whitlow, Mark Twickler, Glen Dunham, Scott Lea, Sam Fain, Kelli Barry, Bede Pittenger, Regi Lorrain, Jeff Sever-

inghaus, Joan Fitzpatrick, Eric Steig, Bruce Vaughn, Jim White, and Alex Wilson.

Much of the work presented here is a continuation of research begun by Gerry Holdsworth and Colin Bull over three decades ago, and many of my results were anticipated by them. Without the foundation they built, this work would probably not have happened.

I owe a special debt to Maynard M. Miller, founder and director of the Juneau Icefields Research Program, who made possible my introduction to real glaciers and began a series of opportunities that have lead to my present position.

More than all of the above combined, I thank those who have made my life in Seattle so wonderful: Pete, Jan, Zack, Nadia, Yun, and Karl. And I thank my family for all they have given me.

DEDICATION

To my dear Petey, my companion from the timberline larch grove above the lake with four points to the sunny summit of Sisyphus where the little devils play.

Chapter 1

INTRODUCTION AND SUMMARY

An important goal of modern global environmental research is to achieve a sound understanding of the earth's ice sheets and glaciers. There are several reasons for this. The ice sheets are a major control on global sea level and planetary albedo, and have the capacity to change the thermohaline circulation of the global ocean. Thus the ice sheets significantly impact the environment of even distant, heavily populated regions. Moreover, the ice sheets are capable of significantly changing their extent on time scales of centuries and millennia, extremely rapid changes for geomorphic features of their size. Ice sheets and glaciers are also important and unique repositories for information about past climates, as they are composed of atmospheric fallout (condensed water vapor, trace gases, and aerosols) and in places contain a continuous, high-resolution record of deposition spanning several hundred millennia. Glaciers and ice sheets interact with their beds, and so are also important geomorphic agents. Much of the mid to high-latitude and high-altitude landscapes of our planet have been shaped by glacial erosion and deposition.

The work presented here is fundamental research in glaciology, whose general purpose is to help investigators address the issues noted above. My work is one very small part of current efforts of this sort, and should be viewed as a small element in a very large and complex engine. The work is divided into four sections. Each involves, to varying degrees, field investigations at Meserve Glacier, an alpine glacier in Wright Valley, Antarctica (Holdsworth, 1974). There, following Holdsworth and Bull (1970) my colleagues and I excavated a tunnel into the glacier to expose basal ice layers for investigation, motivated by Holdsworth and Bull's discovery that the basal layers here are strongly stratified with

respect to impurities, and look much like the basal layers found beneath the center of the Greenland ice sheet (Gow et al., 1997). Attacking a small alpine glacier in this fashion provides relatively easy access to a large section of basal ice; by contrast the only information we have about basal ice of the ice sheets is from the few ice cores that have penetrated to sufficient depth, and these are single cylinders never more than 25 cm in diameter. The temperature and stress regime beneath Meserve Glacier are similar to those in significant portions of the ice sheets.

For the remainder of this chapter I introduce, in abstract form, the four investigations I have conducted under the auspices of the Meserve Glacier Project. The conceptual connection between these is noted.

1.1 An In-Situ Rheology Experiment

Central to our understanding of the earth's great ice sheets is our knowledge of the rheology of polycrystalline ice, the material relationship between stress and deformation rate. For example, if one wishes to predict the fate of the Greenland ice sheet in a warmer-than-present climate using a numerical model (e.g. Huybrechts et al., 1991) it is necessary to incorporate an accurate rheologic relation for ice into the calculations. At present, the effect of impurities on rheology is poorly known (but natural ice is seldom pure), and a role for crystal size is generally discounted (a recent exception being the work of Goldsby and Kohlstedt (1997)).

To improve understanding of the deformation properties of polycrystalline glacier ice, and in particular the role of crystal size, chemical impurities, and rock particle impurities, I analyze in-situ strain rates in the basal layers of the Meserve Glacier, Antarctica, following Holdsworth and Bull. Strain rates were measured on the walls of a subglacial tunnel, and ice properties (texture, fabric, and impurity content) were measured. I propose a simple empirical model describing strain rate variations due to variations in crystal size and impurity content, and I use all relevant data to constrain model parameters. I conclude that there is a direct dependence of strain rate on crystal size, which reflects an important role

for a grain-size-sensitive deformation mechanism such as grain boundary sliding. Chemical impurities are found to act through a grain-size-sensitive mechanism, but they do not dominate this component of the deformation. The sensitivity of strain rate to chemical impurity content is very low, such that in the ice-age ices of the Greenland ice sheet, there is probably an immeasurable contribution of chemical impurities to strain rate enhancement (the increase of shear strain rate relative to that expected for Glen's Law), though I cannot exclude enhancements as high as 1.5. According to my analyses rock particles have no direct rheologic effect in the Meserve ices. I resurrect the idea (Barnes et al., 1971) that variations of crystal size probably are an important control on shear enhancement in the ice sheets, though this effect is generally dominated by variations of crystal fabric, as has been concluded by most recent investigators. The enhanced shear strain rate of ice-age ice in southern Greenland, as inferred from tilt of the Dye 3 borehole, can be explained as a result of combined fabric variations and crystal size variations, with these two ice properties accounting for roughly 70% and 30% of the average enhancement, respectively.

1.2 Basal Sliding at Subfreezing Temperatures

To conduct the rheology experiment, it was necessary to infer the disposition of chemical impurities in the ice. I concluded that a significant fraction (5% to 20%) of the chemical impurities in the study site ices reside in liquid layers (interfacial films) at the surfaces of rock particles embedded in the ice. This may seem surprising due to the very low temperature of the ice (-17 °C). The presence of liquid layers of this sort in cold ice may have important consequences for interpretation of ice core paleoclimate records. Here I present independent evidence for the existence of such layers.

I have observed sliding at the cold ice-rock interface beneath the Meserve Glacier, and the segregation of ice into clean lenses amidst the dirty basal layers of this glacier. I interpret these as manifestations of thin water films at ice-rock interfaces. I use Shreve's (1984) theory for sub-freezing sliding, and measurements of rock surface roughness, to infer the nominal film thickness to be at least tens of nanometers, based on the measured rate of slip. Such

water films should exist around rocks in most polar ices. These films probably have high solute concentrations due to the efficient rejection of solutes from growing ice, and due to the ability of solutes to exchange (by diffusion) between films and the veins and grain boundaries in polycrystalline ice, where impurities reside (the concentration of impurities in grain boundaries is probably several orders of magnitude higher than in the bulk). The role of interfacial films should be considered in analyses of ice core data. For example, such films may allow migration of particles, facilitate homogenization of isotopes and chemicals, and provide media (liquid and substrates) for chemical reactions.

1.3 Processes at Cold Glacier Beds

The presence of interfacial films, and associated slow slip at ice-rock interfaces, imply that cold-based glaciers can interact with their beds in ways that facilitate entrainment of rock material from the bed into the ice. This has important consequences for the efficacy of cold-based glaciers as geomorphic agents, and for the generation of the rheologically-distinct dirty basal layers of the ice sheets. Is there evidence that entrainment occurs at glacier beds despite subfreezing temperatures?

Here I present measurements of the gas content and isotopic composition of debris-rich basal layers of Meserve Glacier, which has basal temperature well below the bulk freezing point. These show that debris entrainment has occurred without alteration of the glacial ice, and provide the most direct evidence to date that active entrainment occurs at the beds of cold glaciers, without bulk freeze-on or conventional regelation (for which there is no thermodynamic constraint on the amount of water present at equilibrium). The debris export resulting from such entrainment may be sufficient to explain the development of the U-shaped trough in which the Meserve glacier rests. In addition to making some cold-based glaciers important geomorphic agents, entrainment at subfreezing temperatures provides a general mechanism for formation of dirty basal layers of polar glaciers and ice sheets. I note the accumulating evidence pointing to the need to abandon the assumption that cold-based glaciers do not slide and erode their beds.

1.4 Reconsidering the Meteoric Water Line

The use of the isotopic composition of ice to infer melt and refreeze processes, an approach that was not available when Holdsworth and Bull conducted their work, is predicated on the observation that the deuterium and oxygen isotope ratios in precipitation define a very clear line on a plot of $\delta^{18}O$ versus δD . This trend (called the Meteoric Water Line) is one of the most spectacular and universal features of earth's environmental geochemistry, being both exceedingly clear and persistent, across space and through time. Through it, nature is trying to tell us something important. Yet, despite over three decades of study, a satisfactory explanation for this line has not been presented. Here I show that adopting an unconventional view of how isotopic composition of precipitation is determined over the ice sheets suggests an answer to this puzzle.

Is the isotopic composition of precipitation largely determined by liquid water even at temperatures as low as $-35^{\circ}C$? Although contrary to current thinking, an affirmative answer to this question directly solves the decades-old puzzle of why there is a clear and persistent linear relation between deuterium and oxygen isotope ratios in polar regions precipitation. This view firmly supports the use of ice core deuterium excess measurements ¹ to learn past climates; according to the traditional view, deuterium excess should be very sensitive to cloud properties (degree of supersaturation in particular), variations of which would obscure the source-region climate signal.

¹Deuterium excess refers to the quantity $\delta D - 8 \delta^{18}O$. The average deuterium excess is the intercept of the Meteoric Water Line.

Chapter 2

**THE RHEOLOGY OF GLACIER ICE: ROLE OF CRYSTAL SIZE,
CHEMICAL IMPURITIES AND ROCK PARTICLES**

An appropriate rheologic relation for polycrystalline ice is a keystone in our understanding of earth's ice sheets and glaciers. The empirical rheologic relation most used by glaciologists is the generalized Glen's Law (Nye, 1957; Paterson, 1994) which describes strain rate as a non-linear function of stress and temperature. Glen's Law (hereafter GL) is usually interpreted to be a manifestation of dislocation motion, a combination of easy glide on basal planes and dislocation climb normal to basal planes (Duval et al., 1983; Alley, 1992), the latter being rate-limiting. A rheology dominantly reflecting these mechanisms is independent of crystal size. Incompatible deformations in polycrystals may be accommodated by diffusional creep, which is crystal size-dependent, but this mechanism has not been suggested to dominate ice deformation.

Several decades ago, Barnes et al. (1971) recognized that the increase of apparent activation energy in GL at temperatures approaching the melting point (greater than about -10°C) most likely reflects an increasing role for a deformation mechanism such as grain boundary sliding, and accommodation by transport along grain boundaries, possibly in liquid films. Recently, Goldsby and Kohlstedt (1997; Peltier, 1998) have argued that, at stresses typical of terrestrial ice, GL reflects important contributions from grain boundary sliding at all earth temperatures. An important consequence of grain boundary sliding is that polycrystalline ice rheology will depend importantly on grain size (Barnes et al. (1971); Goldsby and Kohlstedt (1997)) (a grain is a single crystal for most applications in glaciology). No grain-size dependence is permitted in the usual implementation of Glen's Law.

GL is without question a useful tool, but it does fail to describe significant strain rate variations that have been measured in the ice sheets. A “fudge-factor” coefficient called enhancement (E) is introduced as a multiplier of the stress term to describe these variations. E is quantitatively very important, in some instances varying by one order of magnitude. Three situations for which E is important are:

1. calculating flow of the Greenland ice sheet and Canadian Arctic ice caps, at the scale of whole ice sheet models and at the scale of the ice-divide regions which are particularly relevant to ice core studies. The lower portions of these ice bodies (consisting of ice deposited during the last ice-age) are rheologically soft, with an average E relative to overlying Holocene ice of 2.5 (Fisher and Koerner, 1986; Dahl-Jensen and Gundestrup, 1987; Paterson, 1991).
2. understanding the flow of dirty basal layers (DBL) which have a high rock content. For example, E in such layers beneath Dye 3 and GISP2 are 4 and 7, respectively (Dahl-Jensen and Gundestrup, 1987; Clow and Gundestrup, unpublished). A most surprising yet uncontroversial measurement by Echelemeyer and Zhongxiang (1987) shows $E=120$ for a rock-rich ice beneath an alpine glacier (the Urumqi) in the Tien Shan. Even if they are thin, such extremely soft layers can contribute significantly to the overall flow of an ice mass (Echelmeyer and Zhongxiang, 1987).
3. analyzing the distribution of velocities across ice-stream shear margins, for the purpose of learning basal characteristics and force balance partitioning for these ice streams. Estimates of E for the shear margins are as high as 12 (Echelemeyer et al., 1994).

Laboratory experiments have conclusively shown (Budd and Jacka, 1989; Jun et al., 1996) that a significant source of E is variations in ice-crystal c -axis fabric strength (fabric meaning the statistics of orientations). The dependence of viscosity on fabric strength is a consequence of the strong deformation anisotropy of single ice crystals (Lliboutry and Duval, 1985). Deviations of fabric from isotropic can plausibly account for nearly a factor of 10

variation in E (Shoji and Langway, 1988; Jun et al., 1996), and it is reasonable to suggest that this is the *only* important control on E in natural settings. Paterson (1991) reviewed all relevant data on the subject and concluded that crystal fabric variations cause most of the softening of the ice-age ices, noted above. Analyses of tilt of the Dye 3 borehole have shown, however, that fabric cannot be the sole control (Dahl-Jensen and Gundestrup, 1987; Paterson, 1991); a recent, detailed study strongly suggests that fabric effects account for no more than 70 % of the E variations at Dye 3 (Thorsteinsson et al., in press). Nonetheless, Paterson's conclusion that crystal fabric variations are dominant is sound.

Many researchers have noted that E variations in the ice sheets correlate strongly with rock particle content, chemical impurities, and crystal size (Dahl-Jensen and Gundestrup, 1987; Fisher and Koerner, 1986) and have suggested that these are a major control on E . In recent years, crystal-size variations have been discounted, for several reasons. First, Jacka (1984) has shown that crystal size evolves to an "equilibrium" value for a given strain rate, and therefore is clearly a consequence of strain-rate. This does not, however, mean this equilibrium value is independent of possible crystal size-dependent deformation mechanisms. Further, Dahl-Jensen et al. (1997) have shown that the equilibrium crystal-size is not purely a function of strain rate but also of impurity content. Second, the apparent dominance of dislocation creep over grain-boundary sliding and diffusional creep as the mechanism responsible for GL argued against a direct grain-size dependence. Third, Paterson (1991) cites laboratory experiments on ices from Vostok (Pimienta et al., 1988) and Dye 3 (Shoji and Langway, 1988). Paterson's argument is weak, primarily because both data sets contain a large range of crystal fabrics, whose effects could obscure a modest, but important, grain size dependence. Also, most of these tests were conducted at stress levels much higher than those in ice sheets, which favors dislocation creep mechanisms, according to Goldsby and Kohlstedt (1997). Further, the Shoji and Langway analysis used inferred grain size rather than measured grain size (their Table III), except for their Figure 1 which shows a better correlation of E with grain size than with sonic velocity (a proxy for fabric strength). Direct evidence from the ice sheets arguing against a grain size-dependent rheology is lacking.

In any case, having discarded grain size from the list of strain-rate controls, investigators have attributed E variations unaccounted for by fabric variations to chemical impurities and/or rock particles (Paterson, 1991; Thorsteinsson et al., in press). Laboratory experiments have shown that single ice crystals become substantially softer upon doping by acids (HF and HCl) that can substitute in the crystal lattice. One set of experiments examined the rheologic effects of an important natural salt, $NaCl$, and found that this impurity stiffens ice single crystals (Riley et al., 1978). The relevance of these studies to the ice sheets is unclear, as most impurities will be interstitial, if in the crystal, and the dominant acids in the ice sheets are sulphuric and nitric, and these are neutralized in the dust-rich ice-age ices of Greenland. Further, impurities most likely segregate to grain boundaries (Paren and Walker, 1971). Accumulation of impurities at grain boundaries would likely facilitate grain boundary-dependent deformation mechanisms like sliding and diffusion (Holdsworth and Bull, 1970; Barnes et al., 1971; Fisher, 1987).

Studies of rheologic effects of dispersed rock particles have shown widely conflicting results (see review in Budd and Jacka, 1989), with substantial stiffenings and softenings both reported at 10% volume. Some of this variation may be meaningful. If rock particles embedded in ice are surrounded by liquid films, they may act as soft inclusions because ice can negotiate them by regelation and boundary slip (Echelmeyer and Zhongxiang, 1987). If no liquid is present, rocks will act as hard inclusions and stiffen the ice in a local region around each particle due to viscous effects (e.g. Durham et al., 1992) and due to interaction with dislocations (Ashby, 1969). If grain boundary sliding is important, particles can stiffen the polycrystal by pinning grain boundaries (Ashby, 1980). At concentrations high enough for particle-particle interactions to become important, stiffening most likely occurs (Hooke et al., 1972), though the one observation of Echelmeyer and Zhongxiang (1987) in a frozen till with 60 to 70% rock content contradicts this in a spectacular fashion. Recent reviews of ice rheology have concluded that rock particles are unlikely to be significant at the low concentrations found in the ice sheets, with the possible exception of the dirty basal layers, for which a direct role of rock particles is a leading contender.

To discern the contributions to E of all these factors (fabrics, impurities, and crystal size) several, complementary, approaches are valuable. Laboratory experiments ("ice-squeezing") have produced important results but have two difficulties. First, they are generally conducted at stresses higher than those of interest in the ice sheets. This is a particular problem in view of Goldsby and Kohlstedt's (1997) claim that while dislocation creep dominates at high stresses, grain-boundary sliding becomes important at lower stresses typical for glaciers and ice sheets. Second, laboratory experiments on polycrystals do not control the crystal fabric and the grain size. The difficulty this causes for interpretation is illustrated by the study of Dahl-Jensen et al. (1997). In the course of her experiments, crystal size and fabric continually evolved, rendering the final ice textures rather different from the original. It would be desirable to determine an instantaneous strain rate at the beginning of such experiments, but this would raise other questions concerning possible annealing of ice samples and other ice properties that will be different under steady state creep.

Thus, in-situ deformation studies, such as analyses of tilt of the deep boreholes in the ice sheets are extremely valuable, despite the fact that stress is inferred, not measured. The results of these studies have not, however, been generally diagnostic because variations in enhancement, fabric, most impurities, and crystal size are strongly correlated (high-enhancement ices generally having strong fabrics, high rock and ion contents, and small crystals).

The study presented here is an in-situ ice deformation study. Following Holdsworth and Bull (1970), my colleagues and I excavated a tunnel through the basal layers of the Meserve Glacier, an alpine glacier in Wright Valley, Antarctica. The basal layers of this glacier have a high but variable impurity content (Holdsworth, 1974). Many of these impurities appear to be derived from entrainment of bed material. The strength of correlations between candidate rheologic controls here is therefore much weaker than in the ice-age ices of the ice sheets, providing a fresh perspective on this old problem (and a resurrection of Holdsworth and Bull's efforts). The fabric strength is also much more uniform here than in the ice sheets, with most ices of the basal Meserve having a very well-developed single maximum

normal to the planes of shear (Anderton, 1974). Total ion contents in the Meserve basal ices average 200 micromoles/L, a factor of 20 greater than the dirtiest ice-age ices from Greenland, but vary over a huge range, from 35 to 880 micromoles/L.

The goal of this study is to propose a simple empirical model for E variations due to variations in crystal size and ionic and solid impurities, and to use measurements of strain rate and ice properties for Meserve glacier ices to constrain model parameters. I explore the applicability of the resulting calibrated model to the ice sheets. The results obtained here are essentially for one temperature ($-17\text{ }^{\circ}\text{C}$) and one stress (approximately 0.5 bar). Fortunately, these conditions are important ones for many glaciologic problems.

I fully acknowledge that the results of this analysis depend entirely on this one glacier and therefore may be peculiar to it. This paper is one small part of the community-wide effort to understand ice rheology better.

2.1 A Semi-Empirical Model

I assume that the enhancing effects of grain-size and impurities can be represented by a scalar coefficient (E_{∞}) that multiplies a 2nd-rank tensorial function ($\underline{\underline{\dot{\epsilon}^F}}$) of crystal fabric and stress (an “anisotropic flow law” for clean polycrystalline ice which is equivalent to the GL for an isotropic fabric)

$$\underline{\underline{\dot{\epsilon}}} = A(T) E_{\infty} \underline{\underline{\dot{\epsilon}^F}}(\underline{\underline{\tau}}, \underline{\underline{S}}) \quad (2.1)$$

in which $\underline{\underline{\dot{\epsilon}}}$ is strain rate, A is a strongly increasing function of temperature as inferred from numerous studies and compiled by Paterson (1994), $\underline{\underline{\tau}}$ is the deviatoric stress tensor, and $\underline{\underline{S}}$ a tensorial description of crystal fabrics such as the average Schmid tensor (Azuma and Higashi, 1985; Alley, 1988). Obviously, a “true” E_{∞} is likely a function of temperature, but I have no capacity to resolve temperature dependence here; A in this study will be a constant coefficient for the temperature at which strain rates were measured ($\approx -17\text{ }^{\circ}\text{C}$).

I also are not proposing here any additions or alterations to $\underline{\underline{\dot{\epsilon}^F}}$ relative to the several proposals for it in the literature. I follow Thorsteinsson et al. (in press) in considering

two end-member views of the function $\underline{\underline{\dot{\epsilon}^F}}$, the Azuma model (Azuma, 1994; Azuma and Goto-Azuma, 1996) which assumes uniform strain rate throughout the polycrystal and the Sachs model which assumes uniform deviatoric stress (van der Veen and Whillans, 1994; Thorsteinsson et al., in press). For a single deformation component, these end-members differ primarily by a constant multiple, such that $\underline{\underline{\dot{\epsilon}^F}}$ will vary with crystal fabric twice as much in the Azuma formulation as in the constant stress models. Thus, because the prefactor A is not known *a priori* to better than a factor of approximately five (Paterson, 1994), and because A multiplies $\underline{\underline{\dot{\epsilon}^F}}$, in-situ studies such as this one cannot resolve which of these models is more appropriate (Thorsteinsson et al., in press) for most fabrics. Though unfortunate, this does assist my analyses by reducing the effective number of free parameters in the model.

2.1.1 *The New Term*

In proposing a form for E_{∞} I am guided by the following considerations

1. algebraic and conceptual simplicity
2. following Goldsby and Kohlsted (1997), we suppose that bulk strain rate is the sum of a grain-size-dependent mechanism(s) and grain-size-independent mechanisms
3. I allow that the dependence of E_{∞} on ion content may be non-linear, due to lattice saturation effects (e.g. the laboratory experiments of Nakamura and Jones (1970) showing sub-linear dependence) or due to non-linear dependence on the grain boundary ion content (e.g. the strain rate mechanism depends on the grain-boundary thickness in a non-linear fashion, and this thickness is proportional to bulk ion concentration)
4. Rock particle content may correlate with strain-rate either because particles affect rheology directly, or because (indirectly) a certain fraction of the measured bulk ion content is actually derived from rock-surface interfacial films (Dash et al., 1995; Cuffey et al., in press; Chapter 3) or the rock surface itself. This fraction of the ions is not

residing in grain boundaries or within the crystal lattice and therefore does not directly affect the rheology of ice with widely scattered mineral particles.

The class of models I explore describes variations of E_{∞} relative to its mean as

$$\frac{E_{\infty}}{\langle E_{\infty} \rangle} = 1 + \omega D^{-m} \left[1 + \sum_i \gamma_{\lambda}^i C_i^{\lambda} (1 + \eta A_r)^{-\lambda} \right] + \beta V_r \quad (2.2)$$

Here D is the average grain size (diameter in mm), m is a constant (found, but not forced, to be positive), and ω is a positive number reflecting the relative importance of the size-dependent component to the size-independent component. In the limit $\omega \rightarrow \infty$ the grain-size-dependent component completely dominates the rheology, while in the limit $\omega \rightarrow 0$ it is negligible. Normalizing to the constant $\langle E_{\infty} \rangle$ indicates that I do not know the extent to which the term multiplying ω is present in the standard compilations for flow-law prefactors A (Budd and Jacka, 1989; Paterson, 1994).

The D -dependent component is enhanced by ions $i = SO_4, Cl, \dots$ of bulk measured concentration C_i , according to a simple power relation with exponent λ and prefactor γ_{λ}^i . The inferred prefactors not only depend on the ion considered, but also necessarily on the non-linearity. The notation γ_{λ} is therefore a necessity. I have measurements of 9 ions. Using all 9 ions in the sum would not produce meaningful results, as many of the ions are strongly correlated. Typically I use only three ions, which are representatives of strongly correlated ion groups. Most commonly I use SO_4 , Cl , and inferred acidity (denoted +), so for example the coefficient multiplying ωD^{-m} is

$$1 + \left(\gamma_1^{SO_4} C_{SO_4} + \gamma_1^{Cl} C_{Cl} + \gamma_1^{+} C_{+} \right) (1 + \eta A_r)^{-1} \quad (2.3)$$

in the case of a linear dependence on concentration.

The fractional reduction of measured ion content to account for storage on/in rocks depends on a constant η (units of length) and the measured area of rock per volume of ice (A_r). I choose to represent this fractional reduction using a divisor $(1 + \eta A_r)$ rather than a coefficient $(1 - \eta A_r)$ because the divisor ensures there will be no change of sign at large A_r . In the analyses I have tried both and found that it makes little difference.

Equation (2.2) implies that ions act only via a grain-size dependent mechanism, for example by facilitating grain-boundary sliding. I prefer such a mechanism because most ions will be interstitial, if in the crystal interior, and because the concentration of ions in grain-boundaries is likely very much higher than the concentration of ions in the crystal interiors. Most importantly, I will justify this *post-facto* below; I have found that models for which grain-size and ions are separate, additive terms in E_{ps} are unacceptable. Writing a more general form for equation (2.2) which allows this possibility has a high cost in simplicity, so I address such additive models separately below.

Finally, the term βV_r permits a direct rheologic effect of fractional rock volume V_r (volume of rock per volume of ice), according to a single constant β . A_r and V_r are very strongly correlated, and both are generally correlated with ionic content. Thus the direct rheologic effect may be difficult to separate from the “ion storage” effect. The dependence on V_r was kept strictly linear for simplicity, which appears reasonable as the highest V_r values are only ≈ 0.02 .

2.2 Analysis of Meserve Glacier Data

I use measurements of ice properties and in-situ strain rates to find best-fit values for free parameters in equation (2.2) using standard geophysical inverse procedures.

2.2.1 The Tunnel and Measurements of Ice Properties

In the austral summer of 1995-96 my colleagues and I excavated a 20-meter-long tunnel into the basal layers of the Meserve Glacier, at the northeast margin beside the Holdsworth and Bull (1970) camp. The tunnel was approximately two meters high and one meter wide. It was excavated with chain saws, pick-axes and shovels. The tunnel entered the glacier normal to the marginal cliff, and curved up-slope to parallel the flow-line (see Figure 2 of Holdsworth, 1974). The total extent of my excavations was paltry compared to the earlier efforts of Holdsworth and colleagues (Holdsworth, 1974, Figure 7).

Strain Rates

I excavated two alcoves (0.7 meters in depth, \sim 1.2 meters wide, \sim 2.0 meters high) for the strain-rate measurements, one at 8 meters from the tunnel entrance, and the other at 16 meters. The rear walls of these were smoothed, and regular arrays of metal bolts were frozen into place in drill holes. The plane of the grid at 8 meters (hereafter referred to as the D-grid [downflow]) was angled approximately 10 degrees from the flow-line, and was positioned to take advantage of prominent layering of the stratigraphy, seen as three bands of “amber”-colored rock-particle-rich ice amidst white, bubbly, clean ice. The plane of the grid at 16m (hereafter referred to as the U-grid [upflow]) was parallel to the flow line, and had a simpler stratigraphy, with one prominent amber layer.

The D-grid had 18 horizontal rows of bolts, spaced 0.1 m apart vertically, and three columns, separated by 0.1 m. The U-grid had 17 horizontal rows of bolts and three columns, with similar separations. Distances between neighboring bolts were measured with micrometers, once in late December 1995, once in late January 1996, and once in December of 1996. I calculated strain rates from changes in relative bolt positions, using standard techniques (Rasmussen and Waddington, 1993), yielding 17 measurements of strain rates at the D-grid and 16 at the U-grid, each with a redundancy of four. Inferred strain rates using the January 1996 and December 1996 data are nearly identical, indicating the measurement error is very small relative to the signal (for shear strain rates) and that no measurable temporal change of the strain rates occurred.

2.2.2 Ice Sampling.

I extracted, by chainsaw, six vertical columns of ice from the tunnel walls, from 7.0 m, 7.5 m, 9.5 m, 10.5 m, 11 m, and 16.5 m from the tunnel entrance. Ice from these was used for chemistry, particle, and density measurements, and to make thin sections.

Chemistry

Complete vertical profiles of major ion content were obtained for the 16.5 m and 9.5 m columns, and for a vertical profile through the amber-layer banding and adjacent white ice at 7.5 m. Columns were subsampled at approximately 4 cm resolution in the stratified portions, and at 10 cm resolution in the upper white ices. Major ion concentrations (*Na*, *K*, *Mg*, *Ca*, *NH₄*, *Cl*, *NO₃*, *SO₄*) for these samples were obtained by ion chromatography at the University of New Hampshire glaciochemistry lab using standard, stringent cleaning and filtering procedures (Buck et al., 1992; Mayewski et al., 1997). Average charge imbalance was 5% (missing negative charges, likely bicarbonate). Samples with missing positive charge were few, except for those from the upper portion of the 9.5 m profile. where approximately 5% positive charges were missing. I assume these to be H^+ .

Repeat measurements on the same samples revealed a very high reproducibility of chemistry measurements (to within a few percent). A few samples were run without immediately filtering rock particles, and these had up to 10 % higher ion contents. Rock particles were immediately filtered for all the measurements used here.

Particles

Twins of all samples for chemistry analysis were saved and weighed, and rock mass fraction determined by melting, filtering, drying and weighing (filter pore size was 2.5 micron). Subsequently, particles were re-suspended and agitated, and grain-size distributions measured using a laser-light scattering and extinction instrument (the Model 770 AccuSizer of Particle Sizing Systems, Santa Barbara, California, operated by the Batelle Pacific Northwest Laboratory, Richland, Washington). Particle size distributions were found to be quite consistent throughout the “amber” ices, with a mean size of approximately 0.2 to 0.7 mm, as found by Holdsworth (1974). An estimate of rock surface area per volume of rock was made for each sample by approximating the particles as spheres.

Some of the size-distribution measurements for the clean ices were questionable due to the low total rock content. This possible error has little consequence for subsequent

analyses, due to the near-zero values for rock volume in these ices.

Void Fraction

Prior to melting to extract rock particles, I measured the “twin” samples’ density, using an isostatic weighing procedure. Void fraction was then estimated from these bulk density measurements, the rock mass measurements, and an assumed density for ice crystals ($920 \text{ kg} \cdot \text{m}^{-3}$) and for rocks ($2650 \text{ kg} \cdot \text{m}^{-3}$).

Thin Sections

I prepared thin sections from the ice columns using standard procedures (separating ice slices with a band saw, smoothing one surface, affixing it to transparent plates using freeze-on and/or glue and reducing the ice to sub-millimeter thickness). The rock-rich amber ices presented a special challenge. The smoothing and thinning of amber ice slices was done with sand paper with various grit sizes (finer grit being used toward the end of the task); abrasion and chipping rapidly destroyed metal blades, necessitating the more laborious task of “sanding”. Before freeze-on, visibly protruding rock particles were plucked from the surface to ensure a smooth contact. A total of 45 thin sections were prepared.

Crystal Size

Thin-sections were photographed under crossed polarizers, and crystal size measured from the photographs using the linear intercept method. The average length per grain was multiplied by 1.5 to approximate the crystal diameter (Underwood, 1970).

C-axis Fabrics

For 35 of the thin sections I measured c-axis orientations for at least 100 grains, using crossed polarizers and a Rigsby Stage (Langway, 1958). Proper corrections for refraction effects were made, following Kamb (1962). Selection of grains for orientation measurement was randomized by dropping a pointer onto the thin section. Thus my c-axis fabrics are

“area-weighted”, which is proper for rheologic calculations. Thin sections were taken parallel to the plane of shear, with a $\pm 10^\circ$ uncertainty in the orientation of the normal to the thin section, and a $\pm 10^\circ$ uncertainty in the azimuth relative to the flow direction. In many cases, the uncertainty on the orientation relative to the shear plane was smaller, because visible, bed-parallel strata guided the cutting of the thin section. The azimuth is known so well because the elongate bubbles provide a built-in directional indicator (Holdsworth, 1969, Figure 8; Holdsworth, 1974).

The amber ices again presented a special difficulty, due to their very small grain sizes (0.6 mm apparent diameter seen in section). In his study of Meserve ice petrography, Anderton (1974) did not obtain any fabric data for the amber ices, but noted that they appeared to have a strong fabric. I was able to obtain fabric data by using optical binocular magnifying glasses (manufactured by Donegan Optical Company, Lenexa, Kansas) which provided an effective magnification of $\sim 2\times$. The main difficulty proved not to be the uncertainty in identifying the angular position of maximum extinction (as one might suppose) but rather the task of tracking a single grain through rotations of the stage. A successful measurement was obtained in only approximately 30% of the attempts. This, plus the small absolute sizes, almost certainly introduced a “large-grain” bias to the resulting fabric data in addition to the intentional one for proper area-weighting; I probably did not measure any orientations for grains with the average apparent diameter of 0.6 mm or less.

Excepting this problem, I am confident that the fabric data I obtained for amber ices are accurate. The amber-ice fabrics are quite similar to the fabrics obtained from white ices, with the strong shear-normal single maximum that is characteristic of simple shear flows. For one of the amber ice thin sections, I prepared a companion section from amber ice a few centimeters higher in the column, but with a tilt of 35° relative to the original. The inferred fabric had 7° broader dispersion of c-axes, most likely reflecting a greater error in identifying extinction position for grains that are significantly tilted relative to the thin-section plane or its normal.

2.2.3 Using Fabric Data

I calculate $\underline{\dot{\epsilon}}^F$ directly from c-axis fabric data and assumed stress tensors according to Azuma (1994) and van der Veen and Whillans (1994), the latter being an application of the model due to Sachs. After the fact, I found that the fabric relations and various stress assumptions I use make little difference to the final results, and my analysis has little resolving power for distinguishing amongst them. Some readers may wish to skip this section. I denote calculations of $\underline{\dot{\epsilon}}^F$ using the Azuma and Sachs models as $\underline{\dot{\epsilon}}^{F,A}$ and $\underline{\dot{\epsilon}}^{F,S}$, respectively.

Considering a single crystal, assumed to deform by basal glide in two orthogonal directions k with Burger's vectors B_i^k in the global coordinate system x_i (i.e. a convenient coordinate system for the glacier as a whole), the resolved shear stress on the basal planes of a crystal with c-axis orientation vector c_j is $\tau^k = B_i^k c_j \tau_{ij}$. The tensor $B_i^k c_j$ is called the Schmid tensor and denoted S_{ij}^k .

In the Sachs formulation, the stress acting on each crystal is assumed to be simply the bulk stress τ_{ij} and the bulk deformation is the average over all crystals (N in number) of the deformations caused by the shear stress resolved on the basal planes

$$\dot{\epsilon}_{ij}^{F,S} = \frac{A_S}{N} \sum_{g=1}^N \sum_{k=1,2} S_{ij}^{k,g} \left(S_{pq}^{k,g} \tau_{pq} \right)^n \quad (2.4)$$

where the sums over spatial directions $p, q = 1, 2, 3$ are indicated by repeated indices and the superscript F, S indicates the Sachs model is being used. A superscript F, A will indicate the Azuma model.

The Azuma formulation (Azuma, 1994) assumes the slip direction is the direction of maximum resolved stress on the basal planes (see Appendix 1 of Azuma, 1994), with a corresponding Schmid tensor S_{ij}^* . The average value of S_{ij}^* for all grains is computed (effectively replacing the polycrystal with a single crystal having average properties), and the uniform bulk deformation rate is

$$\dot{\epsilon}_{ij}^{F,A} = A_A \langle S_{ij}^* \rangle \left(\langle S_{pq}^* \rangle \tau_{pq} \right)^n \quad (2.5)$$

where the brackets $\langle \rangle$ indicate the average over all N grains and again there are sums over $p, q = 1, 2, 3$. The prefactors differ by $A_A = 2A_S$ (Thorsteinsson et al., in press).

To use these formulae for calculating $\dot{\epsilon}_{ij}^F$ I need to specify how the stress varies relative to its mean, and the relative magnitudes of the various deviatoric stress components (the mean value is unimportant because I treat the prefactor A as a free parameter). I adopt two end-member views of the stress, one in which the stress perturbation caused by the tunnel is ignored, and one in which I maximize its effect. This stress perturbation causes tunnel closure, and I have measured tunnel closure rates at one cross-section in the tunnel, 15 m from the tunnel entrance. The closure rate was determined by measuring relative distance changes between markers (metal bolts inserted and frozen into drill holes in the tunnel wall) arranged in a line spanning both walls and ceiling of the tunnel (following Holdsworth, 1974). Thus I have directly measured the closure velocity into the tunnel, and the shear strain rate caused by this motion relative to the no-slip bed (the small slip rate reported in Chapter 3 did have a component into the tunnel, but this few $\text{mm} \cdot \text{yr}^{-1}$ slip is unimportant in this context).

Define a coordinate system with (x_1, x_2, x_3) being flow-parallel, flow-normal bed-parallel, and bed-normal directions, respectively (also being sub-parallel to the long axis of the tunnel, into the tunnel normal to the tunnel side walls, and bed-normal). The stresses associated with the closure motions are a longitudinal closure stress τ_{22} acting normal to the tunnel wall, and a closure shear stress τ_{23} acting on horizontal planes but perpendicular to the dominant down-flow shear stress τ_{13} .

I assume the dominant shear stress acting on the ice τ_{13} depends on height above the bed (x_3) and is enhanced by increases in void ratio V_b and has the form

$$\tau_{13} = \frac{(1 - \frac{x_3}{H})^\nu}{(1 - V_b)} \quad (2.6)$$

in which, x_3 is zero at the bed, H is the ice thickness, V_b is the volume fraction of bubbles, and ν the power characterizing the effective spatial variation of stress with depth. This ν does not necessarily equal unity as it would if the weight of overburden controls the stress

because it also reflects the variation in shear stress due to gradients in longitudinal stress τ_{11} which I do not know, but which will generally oppose the upward decrease of τ_{13} caused by the decrease of overburden. Most importantly, the magnitude of τ_{13} variation is almost certainly small due to the small size of my strain grids relative to the glacier thickness. I have used values for ν of 0.0, 0.3, 0.7 and 1.0, inclusive, and found that none of the results presented below depend on this number in any significant fashion. My strain-rate measurements provide a direct measurement of longitudinal strain-rate along-flow, which is approximately zero. This may primarily reflect the near-vertical *c*-axis fabric and therefore does not mean the longitudinal stress τ_{11} has a negligible effect on the (unknown) τ_{13} gradient.

With regard to the tunnel effects, the two end-member stresses I consider are CASE 1 (the tunnel has no effect on the stress):

$$\tau_{22} = 0 \quad (2.7)$$

$$\tau_{23} = 0 \quad (2.8)$$

and CASE 2 (there is a longitudinal stress into the tunnel, with a magnitude proportional to closure velocity, and there is a shear stress associated with tunnel closure over a no-slip bed):

$$\tau_{22} = \tau_{22}^{max} \left[\frac{u_c}{u_c^{max}} \right]^{1/n} \quad (2.9)$$

$$\tau_{23} = \tau_{13} \left[\frac{\dot{\epsilon}_{23}}{\dot{\epsilon}_{13}} \right]^{1/n} \quad (2.10)$$

For the maximum value τ_{22}^{max} of the closure stress I use one-quarter of the overburden pressure, or $1/4$ (2 bar) = 0.5 bar, which I estimate to be approximately equal to τ_{13} . One may be inclined to use one-half the overburden pressure for the maximum deviatoric stress τ_{22}^{max} , but for a non-linear fluid such as ice the large stress-coupling lengths cause a broad low-pressure zone around a subglacial tunnel (Weertman, 1972). In any case,

these calculations are illustrative. u_c in equation 2.9 is measured closure rate, which has a maximum value of $u_c^{max} = 0.04 \text{ m} \cdot \text{yr}^{-1}$, and the ratio of the two bed-parallel shears is estimated from the direct measurements. These two stress scenarios are used explicitly in equations (2.4) and (2.5) to calculate possible variations of the strain rate $\dot{\epsilon}_{13}$, which is the subject of all the analyses presented below. The absolute value of the stress τ_{13} does not matter in this context, only the relative values.

According to these rheologic relations the shear $\dot{\epsilon}_{13}$ will depend only weakly on the other stress components due to the strong crystal fabrics (a result very different from the classic isotropic Glen's Law if these stresses are used; however, if one assumed Glen's Law to be true, the stresses estimated directly from closure measurements would be very small relative to the dominant shear, so the net result would be the same). I do not consider explicitly any stresses τ_{12} , as these will act as an intermediate case between these two extremes.

Thus I have four end-member stress-fabric models: Azuma with no tunnel stresses, Azuma with full tunnel stresses, Sachs with no tunnel stresses and Sachs with full tunnel stresses. Denote the $\dot{\epsilon}_{12}$ components of these $\dot{\epsilon}^{F,A}$, $\dot{\epsilon}_T^{F,A}$, $\dot{\epsilon}^{F,S}$, and $\dot{\epsilon}_T^{F,S}$, respectively. I describe the "true" $\dot{\epsilon}_{12}^F$ as a linear mixture of these. Introduce two free model parameters e_{AS} and e_T which are each restricted to the range $[0,1]$. Then

$$\dot{\epsilon}_{13}^F = e_{AS} \left[(1 - e_T) \dot{\epsilon}^{F,A} + e_T \dot{\epsilon}_T^{F,A} \right] + (1 - e_{AS}) \left[(1 - e_T) \dot{\epsilon}^{F,S} + e_T \dot{\epsilon}_T^{F,S} \right] \quad (2.11)$$

2.2.4 Analysis Method

Common Reference Frame

To interpret strain rate variations in terms of measured and derived ice properties, it is first necessary to compile all data in one common spatial reference frame. For this I use the 33 0.1m vertical intervals corresponding to the strain rate measurements. I determined average chemical and physical properties for each of these 0.1m intervals using linear combinations (which are weighted averages) of the measured values from samples in the stratigraphic layers composing the intervals. More precisely, the value for the j^{th} property in the i^{th} grid

Table 2.1: Comparison of major ion concentrations (for two stratigraphic horizons) at two locations separated by 3 meters along flow. Units are micromoles per liter.

| | Up-flow Samples | | | | Down-flow Samples | | | |
|--------------------|-----------------|------------------|-----------------|-------------------------------|-------------------|------------------|-----------------|-------------------------------|
| | Na ⁺ | Ca ²⁺ | Cl ⁻ | SO ₄ ²⁻ | Na ⁺ | Ca ²⁺ | Cl ⁻ | SO ₄ ²⁻ |
| Amber Ice : | 161 | 50 | 190 | 41 | 190 | 52 | 198 | 35 |
| White Ice : | 14 | 6 | 23 | 5 | 12 | 7 | 22 | 9 |

interval, P_{ji} , is calculated in terms of the k measured values for this property M_{jk} as

$$P_{ji} = \sum_k a_{ik} M_{jk} \quad (2.12)$$

where the coefficients a_{ik} are restricted to the range $[0,1]$ and subject to the requirement $\sum_k a_{ik} = 1$ (typically there are one to four non-zero terms in the sum). The a_{ik} values were selected *a priori* from stratigraphic maps of the tunnel walls that show explicitly: (1) that specific stratigraphic layers contained in the strain-rate grid intervals correlate precisely with certain stratigraphic layers in the measured profiles of ice properties, and (2) that the 0.1 m (vertical) by 0.5 m (horizontal) areas of ice surface centered on each of the 33 strain grid rows consist of quantifiable proportions of the various stratigraphic layers.

The extrapolation/interpolation procedure (1) is justified because the between-layer variability of ice properties is much greater than the along-flow variability, a direct consequence of large shear strain. For example, the top-most amber ice layer in the D-grid was sampled both 2 m up-flow and 1 m down-flow from the grid (Table 2.1), and the micromolar ionic concentration differs by 10% between these two sites. For the white ice 0.2 m above the top of this amber, the up-flow and down-flow difference is 17%. By contrast, the amber and white ices differ in average ion content by a factor of 920% at the upstream site, and 990% at the downstream.

The partitioning procedure (2) is more difficult to justify conceptually, as it contains

two approximations: that the rheologic properties of a mixed layer equal a linear mixture of the rheologic properties of sub-layers, and that the relative proportions of various layers seen on the strain grid wall equal the volumetric proportions, to whatever depth into the wall is relevant to determining the strain rate. However, circumstance provides better justification than concept. The complete range of variability between stratigraphic layers is unambiguously represented, because many of the grid levels require no partitioning at all, being all one layer. In such cases, having more than one non-zero term a_{ik} simply reflects averaging of repeat measurements of the same stratigraphic layer. Moreover, the stratigraphic layers are generally characterized by a horizontal span much greater than the size of the strain grids, and much greater than their vertical extent.

All the final data used in the analyses are shown in Figure 2.1, after translation to the common reference frame. Table 2.2 lists minima, means and maxima for all these parameters. The c-axis fabric data derived from many of the thin sections are shown in Figures 2.2 and 2.3.

Inversion Procedure

My task is to find values for the free parameters in equations (2.2) and (2.11) that best describe the measured strain rates in terms of the data in all the other panels of Figure 2.1. This is only a meaningful exercise if the model variables vary independently to some extent. Figure 2.4 shows correlations of the most important ice properties. This diagram is encouraging; in contrast to the ice-age ices of the ice sheets, here there is significant independent variation of crystal size, ionic content, fabric enhancement, and rock content. Sulphate and Chloride vary independently to a significant degree. On the other hand, rock surface area and volume are very strongly correlated, suggesting it will be difficult to separate direct rheologic effects of rock particles from "ion storage" effects. The ions fall into several distinct groups, within which the correlation is very strong. These groups are the sulphate group (SO_4 and Ca), the chloride group (Cl and Na), the nitrate group (NO_3 , K , Mg), unbalanced positive charges (presumed acidity and denoted +), and ammonia (NH_4).

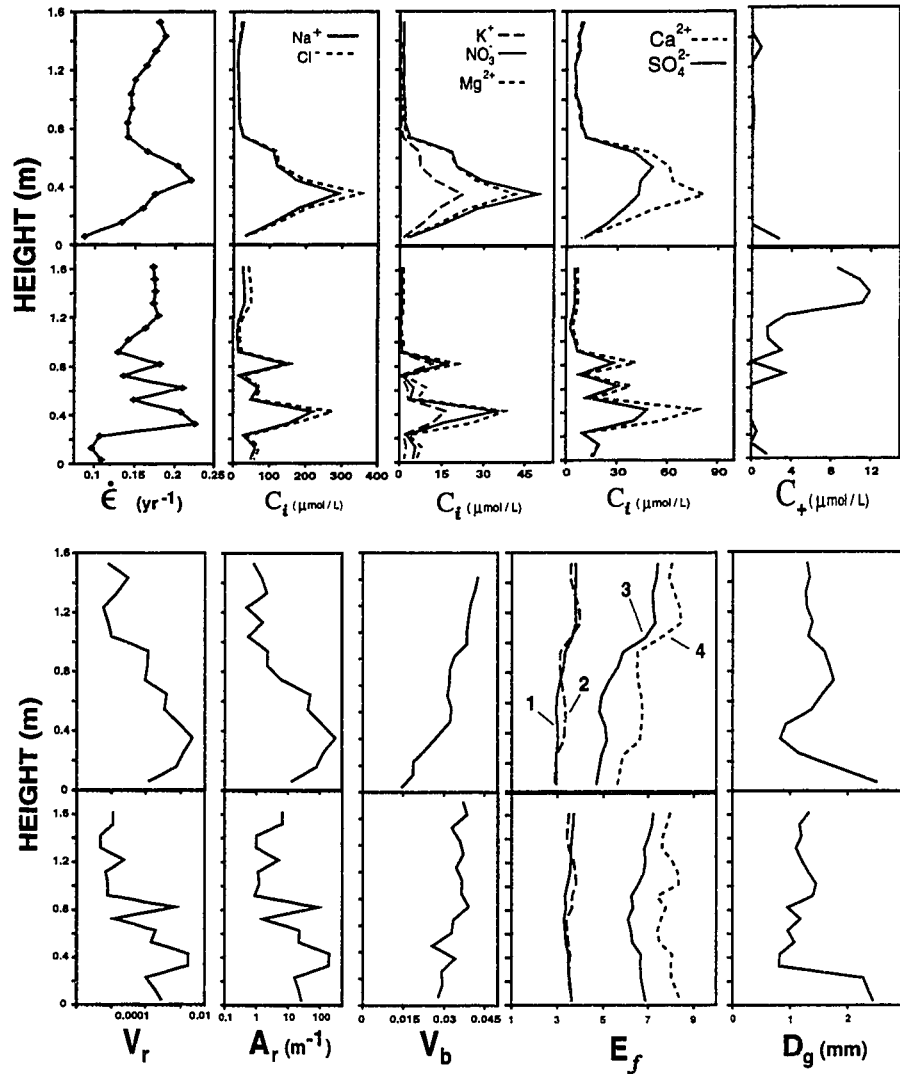


Figure 2.1: Measured strain rates and all other ice properties used in the rheology analysis. Top(bottom) panels are U-grid(D-grid) data. All variables are as in the text, except E_f which is the enhancement of down-flow shear rate due to fabric relative to isotropic ice, calculated using distinct models: 1. uniform stress model without tunnel stresses, 2. uniform stress model with tunnel stresses, 3. uniform strain rate model without tunnel stresses, 4. uniform strain rate model with tunnel stresses.

Table 2.2: Summary of measured ice properties in Meserve basal ices. C_T is the total ionic content. E_A , E_S , $E_{A,T}$ and $E_{S,T}$ are shear enhancements relative to isotropic ice calculated according to Azuma and Sachs (A and S) with and without tunnel closure stresses (T indicates such stresses are included). All other variables as defined in text. Uncertainties on single measurements, as determined by repeat measurement of identical samples, are approximately ± 1.5 micromoles per liter for ions (increasing to ± 3 micromoles per liter in the most impure samples), ± 0.003 for V_b , and ± 0.06 mm for D . Uncertainty on the E values results primarily from uncertainty of the thin section orientations, and is approximately $\pm 10\%$. Uncertainty on single measurements of the rock content were estimated not from repeat measurements on the same sample, but from measurements on adjacent samples in the same stratigraphic layers, and are approximately $\pm 15\%$ in the amber ices.

Summary of Meserve Ice Properties (grid values)

| | <u>Minimum</u> | <u>Mean</u> | <u>Maximum</u> | <u>Units</u> |
|------------------|----------------|-------------|----------------|------------------------|
| Na | 11.8 | 65.1 | 291. | $\mu\text{mol L}^{-1}$ |
| NH ₄ | 0.07 | 0.44 | 1.28 | $\mu\text{mol L}^{-1}$ |
| K | 0.27 | 3.98 | 22.3 | $\mu\text{mol L}^{-1}$ |
| Mg | 0.73 | 8.80 | 41.1 | $\mu\text{mol L}^{-1}$ |
| Ca | 3.90 | 22.5 | 81.4 | $\mu\text{mol L}^{-1}$ |
| Cl | 12.1 | 76.14 | 353. | $\mu\text{mol L}^{-1}$ |
| NO ₃ | 0.41 | 8.40 | 49.3 | $\mu\text{mol L}^{-1}$ |
| SO ₄ | 2.49 | 16.99 | 51.0 | $\mu\text{mol L}^{-1}$ |
| C _T | 37.3 | 202.3 | 881. | $\mu\text{mol L}^{-1}$ |
| C ₊ | 0. | 1.3 | 11.9 | $\mu\text{mol L}^{-1}$ |
| V _b | 0.014 | 0.033 | 0.043 | |
| V _r | 5e-05 | .0033 | 0.021 | |
| A _r | 0.5 | 41.4 | 308. | m ⁻¹ |
| E _A | 4.70 | 6.30 | 7.42 | |
| E _S | 2.93 | 3.43 | 3.82 | |
| E _{A,T} | 5.64 | 7.45 | 8.46 | |
| E _{S,T} | 2.87 | 3.48 | 4.00 | |
| D | 0.81 | 1.40 | 2.51 | mm |

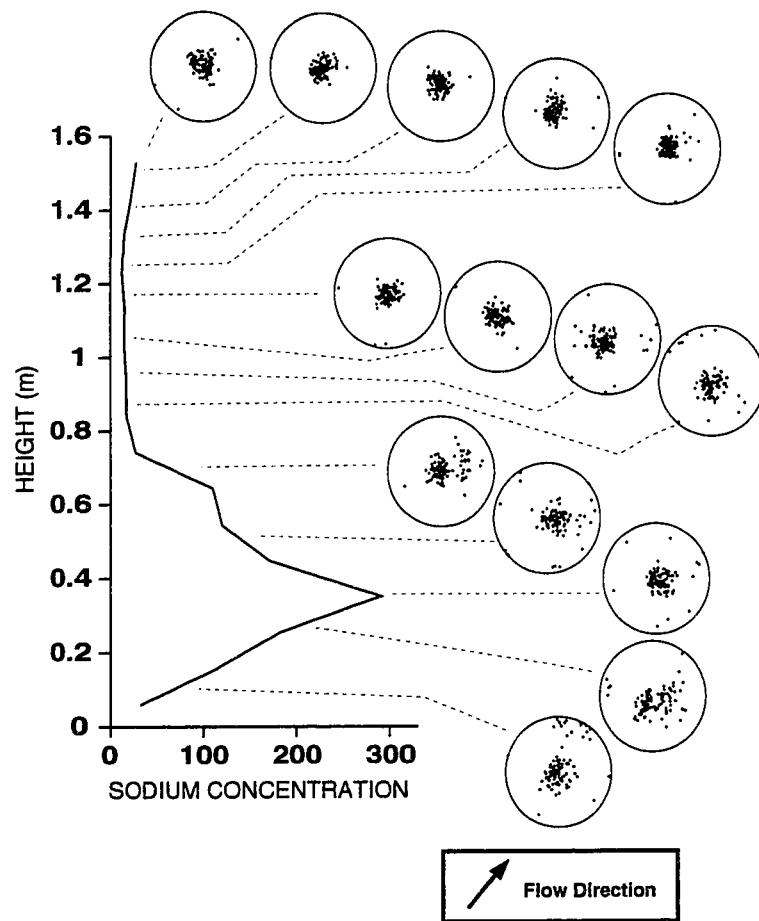


Figure 2.2: C-axis orientations for thin sections near the U-grid, and corresponding stratigraphic positions (stratigraphy here represented by the micromolar sodium concentration). Each thin section has at least 100 measured orientations. Note the generally stronger clustering of c-axes high in the profile.

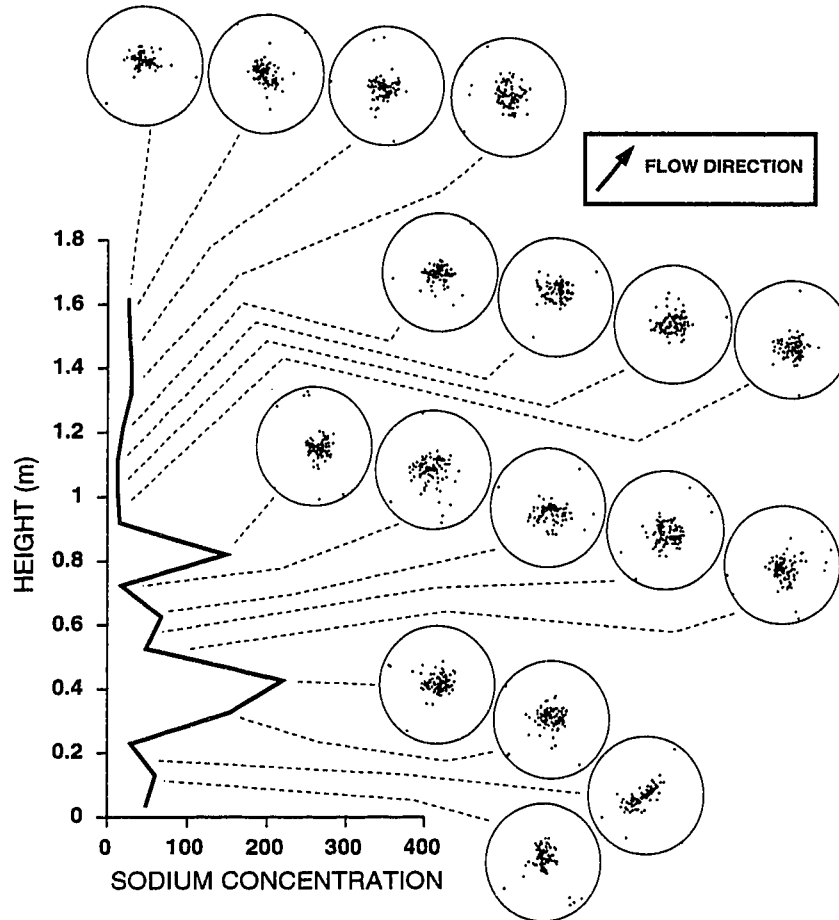


Figure 2.3: C-axis orientations for thin sections near the D-grid, and corresponding stratigraphic positions (stratigraphy here represented by the micromolar sodium concentration). Each thin section has at least 100 measured orientations. Not shown here are five additional sections which show the same lack of variability as a function of height above the bed.

Further, the nitrate and chloride groups correlate strongly in the amber ices and therefore are difficult to treat separately. Ammonia occurs at very low concentrations and is not correlated with strain-rates, so I will not consider it further.

Free parameters in the strain rate model that I wish to optimize are: A , ω , m , γ^{SO_4} , γ^{Cl} , γ^+ , λ , η , β , e_{AS} and e_T . In optimizations for which all these parameters are free, 22 degrees of freedom remain. For many optimizations I fix $\gamma^{Cl}=0$ and $\beta=0$, the e parameters, and the power pertaining only to C_+ , for reasons discussed below. I define a chi-square performance index in terms of observed and modelled strain rates ($\dot{\epsilon}^o$ and $\dot{\epsilon}^M$)

$$\chi^2 = \sum_{i=1}^{33} \frac{(\dot{\epsilon}_i^M - \dot{\epsilon}_i^o)^2}{(\sigma_\epsilon^2 + \sigma_P^2)_i} \quad (2.13)$$

in which σ_ϵ is the variance of measured strain rates, and σ_P is the variance in predicted strain rate due to uncertainties of all input parameters.

Optimal model parameters are those for which χ^2 is minimized. I perform the minimization using iterative application of singular value decomposition. This was supplemented with “shaking” (forced arbitrary changes of parameters, as in simulated annealing procedures (e.g. Press et al., 1992, p. 436) to allow escape from local minima which were found to exist in some regions of the parameter space.

I used a preliminary solution (which proved to be very close to the final solution) to calculate σ_P . I estimated, based on reproducibility of measurements, and especially on ambiguity in the interpolating and partitioning procedures, that a reasonable, somewhat conservative, error for values of most input parameters is $\pm 20\%$. I then used a Monte Carlo procedure to generate 80 separate strain rate predictions, forcing each input parameter to be perturbed by uniform random variables between $\pm 20\%$, generated using the Matlab random number generator. σ_P is the variance of the resulting strain rate predictions (Figure 2.5) at each grid point (which, of course, are approximately normally distributed).

Average values for σ_ϵ and σ_P are 2% and 7% of the measured strain rates, respectively.

Confidence intervals for model parameters were defined based on $\Delta\chi^2 = \chi^2 - \chi_{min}^2$, the decrease of performance relative to that for the optimal model. As described in, for

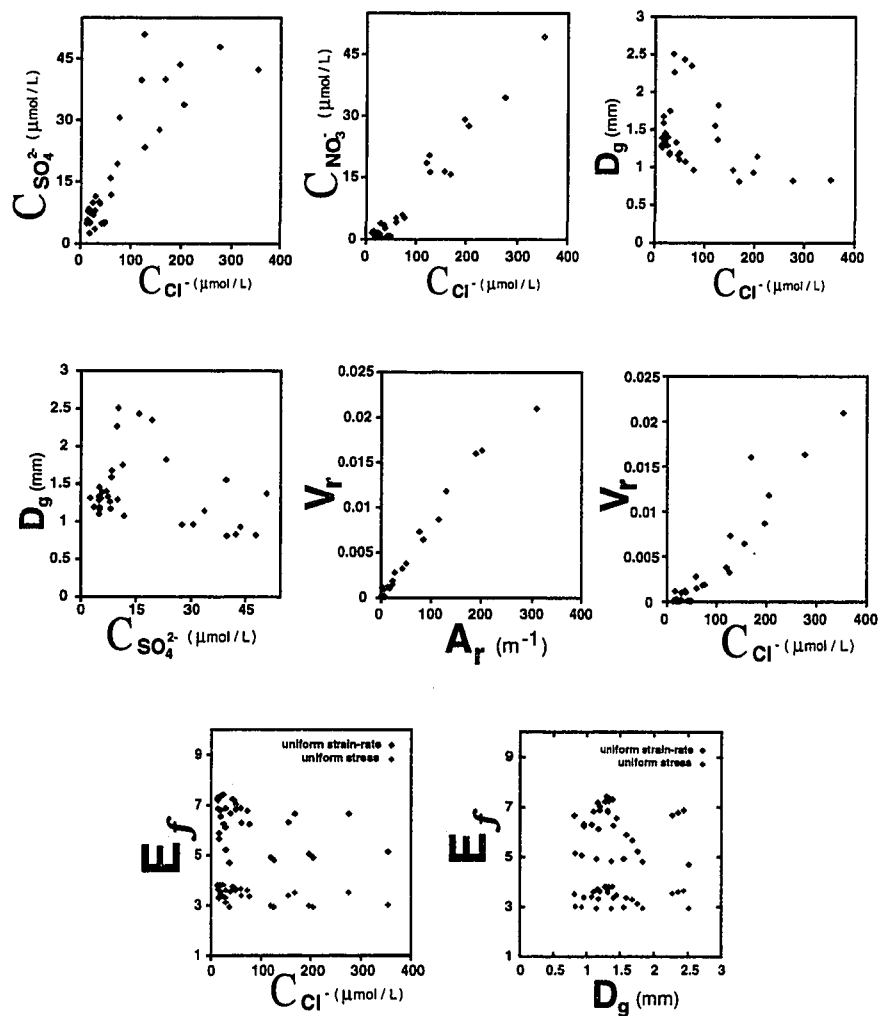


Figure 2.4: Covariation of many of the variables shown in Figure 2.1.

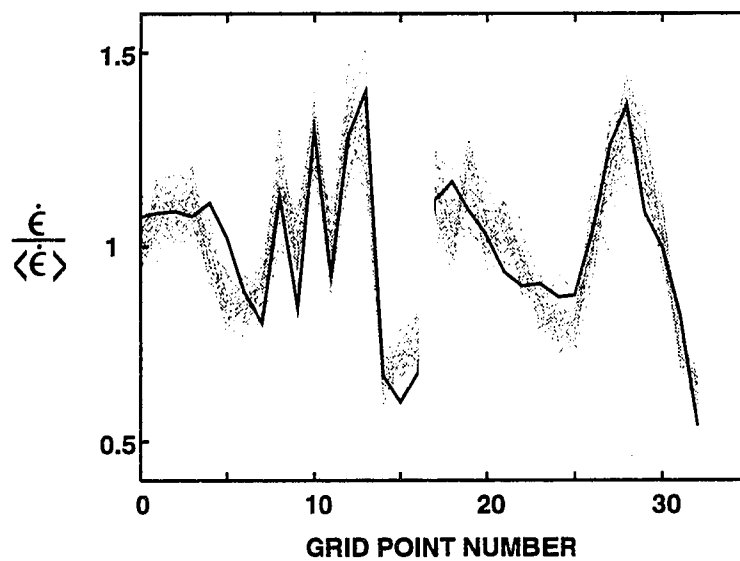


Figure 2.5: Measured strain rates (solid line) for all 33 grid points (corresponding to the measured strain rates) used in the rheology analysis, plus 30 of the re-calculated strain rates based on randomly perturbed input parameters. Strain rate is shown normalized to mean.

example, Press et al. (1992, p.688-693), a combination of arbitrarily fixed model parameters μ in number (where μ is less than or equal to the total number of model parameters) is statistically acceptable at a given confidence level if the $\Delta\chi^2$ for this model (after optimizing the non-fixed parameters) does not exceed the value of the χ^2 distribution with μ degrees of freedom that corresponds to this confidence level. In this fashion, I evaluate the statistical acceptability of variants of the general model that are defined by specified values for parameters.

A really unacceptable model is one that can be rejected with 99.5 % confidence. To discuss such horrible models, I therefore define an index of horribility \mathcal{H} in terms of a model's $\Delta\chi^2$ and the .995 probability $\Delta\chi_{.995}^2$ as

$$\mathcal{H} = \frac{\Delta\chi^2}{\Delta\chi_{.995}^2} - 1 \quad (2.14)$$

Models with $\mathcal{H} > 0$ can be firmly rejected. I define a similar index relative to 95% confidence as

$$\mathcal{A} = \frac{\Delta\chi^2}{\Delta\chi_{.95}^2} - 1 \quad (2.15)$$

Models with this acceptability index $\mathcal{A} < 0$ are acceptable at this confidence.

2.3 Results

Results clearly indicate that crystal size is an important control on strain rate, and that ions (not rock particles) are a significant softening agent at the high concentrations present in the Meserve Glacier ices.

2.3.1 Optimal Models.

The optimal model incorporating 11 free parameters (Table 2.3) has $\chi^2=23.0$, which is comparable to the degrees of freedom (22), indicating the model is generally adequate (Figure 2.6), though not spectacular. Experimentation has shown that a sparser model (Table 2.3) with five free parameters (ω , m , γ^{SO_4} , γ^+ , η) is nearly as acceptable ($\chi^2=32.7$

Table 2.3: Summary of optimal model parameters, and those for the reduced model.

| Optimal Model Parameters | | | Reduced Model Optimal Parameters | |
|---------------------------------|-----------------------|---------------------------------|---|----------|
| | <u>best value</u> | <u>95 % confidence interval</u> | | |
| e_T | 0.0 | [0, 0.6] | ω | ∞ |
| e_{AS} | 0.2 | [0, 0.92] | m | 0.60 |
| ω | ∞ | [0.15, ∞] | $\gamma_1^{SO_4}$ | .019 |
| m | 0.64 | [0.46, 2.2] | γ_1^+ | .088 |
| λ | 1.53 | [0.48, 3.7] | η | .0073 |
| $\tilde{\gamma}_{1.53}^{SO_4}$ | .0020 | $[1.30, 3.17] \times 10^{-3}$ | | |
| $\tilde{\gamma}_{1.53}^{Cl}$ | -9.7×10^{-5} | $[-17, +2] \times 10^{-5}$ | | |
| $\tilde{\gamma}_{1.53}^+$ | .0053 | $[1.11, 10.2] \times 10^{-3}$ | | |
| η | .0019 | $[-0.2, +8.5] \times 10^{-3}$ | | |
| β | 1.87 | [-22, +8.3] | | |

for 28 degrees of freedom), indicating that the grain-size and ionic parameters are dominant in determining the optimal model. Variations of crystal size and, to a lesser extent, chemical content, dominate strain rate variations at the study site (Table 2.4).

2.3.2 A Mixed Grain Size and Ion Model is Necessary.

The only acceptable models are those for which both grain size and ions are important. I have experimented with all plausible models for which, in addition to stress and fabric, only rocks are important ($m=0, \gamma^i=0$), only ions are important ($m=\beta=\eta=0$), only rocks and ions are important ($m=0$), only grain size is important ($\gamma^i=\beta=\eta=0$), or only grain size and

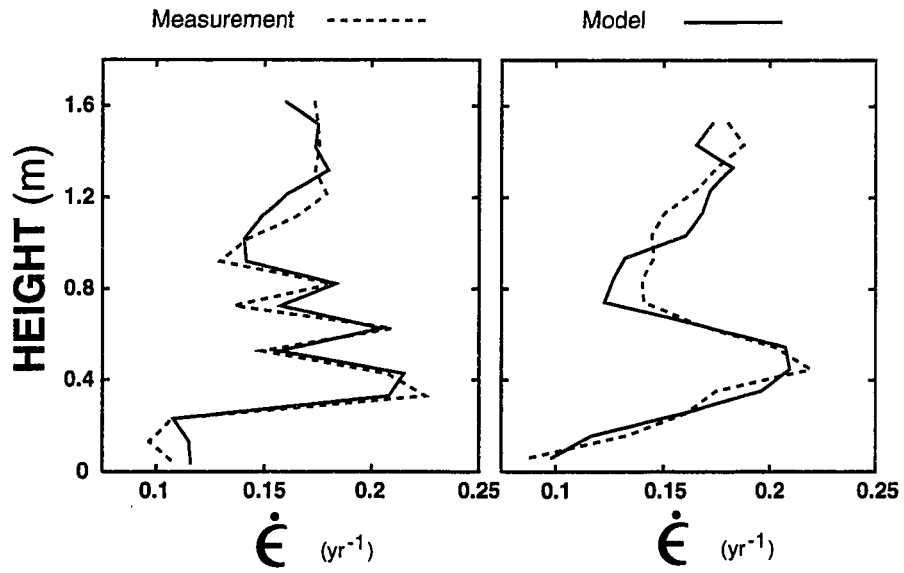


Figure 2.6: Model and measured strain rates for the D-grid (left) and the U-grid (right). The model shown here is optimal.

Table 2.4: Relative significance of ice properties in controlling strain rate variations in the Meserve Glacier basal layers. These rankings were calculated by removing each variable from the optimal model and recording the increase of model-measurement mismatch. The relative magnitudes of these mismatch increases are proportional to the relative contributions reported here.

**Significance Ranking of Strain-Rate Controls
(in Meserve Basal Layers)**

| <u>RANK</u> | <u>VARIABLE</u> | <u>RELATIVE CONTRIBUTION</u> |
|-------------|---------------------------|------------------------------|
| 1 | Crystal Size | 1.00 |
| 2 | Principal Ion(s) | 0.54 |
| 3 | Crystal Fabrics | 0.24 |
| 4 | Particles (Ion Storage) | 0.23 |
| 5 | Acidity (?) | 0.15 |
| 6 | Particles (Direct Effect) | 0.00 |

rocks are important ($\gamma^i=0$). All such models are soundly rejected. Pure grain-size models have \mathcal{H} in the range 1.9 to 2.2, pure ion models have \mathcal{H} in the range 5 to 9, pure rock models have \mathcal{H} in the range 7 to 8, and mixed ion-rock models have \mathcal{H} in the range 4.5 to 9. The corresponding $\Delta\chi^2$ are approximately 50 for the pure grain size models, and 85 to 165 for the others. With reference to Figure 2.5, a model with $\Delta\chi^2 = 50$ has each point, on average, worse than the optimal model by twice the width of the gray zones.

2.3.3 Ions Act Through a Grain Size-Dependent Mechanism.

An alternative to equation (2.2) is the class of additive models

$$\frac{E_{\infty}}{\langle E_{\infty} \rangle} = 1 + \omega_a D^{-m} + \sum_i \gamma_{\lambda}^i C_i^{\lambda} (1 + \eta A_r)^{-\lambda} + \beta V_r \quad (2.16)$$

These are found to be unacceptable (Figure 2.7) for all values of the grain-size-importance parameter ω_a . This justifies *post facto* the multiplicative relation between ions and grain size in equation (2.2). Physically, this means that ions are most likely affecting rheology through a grain size-dependent deformation mechanism. As discussed above, concentrated impurities at grain boundaries will enhance liquid layers there, and such layers likely facilitate grain boundary sliding, and mass transfer along grain boundaries. The latter will help polycrystalline ice accommodate the incompatible deformations that are a necessary consequence of the strong single-crystal mechanical anisotropy. Thus the ions are acting to increase the effective temperature of the polycrystal, with respect to the relative importance of different deformation mechanisms and accommodation processes as explained by Barnes et al. (1971).

2.3.4 Grain-Size Dependence

I find that strain-rate depends on the inverse of crystal diameter to a power m in the range 0.5 to 0.75 as a bulk average (meaning in the limit of large ω ; Figure 2.8). This average dependence may be interpreted (Figure 2.8) as reflecting either (1) a grain size-dependent deformation mechanism with a low value for $m \approx 0.6$ but which is substantially more

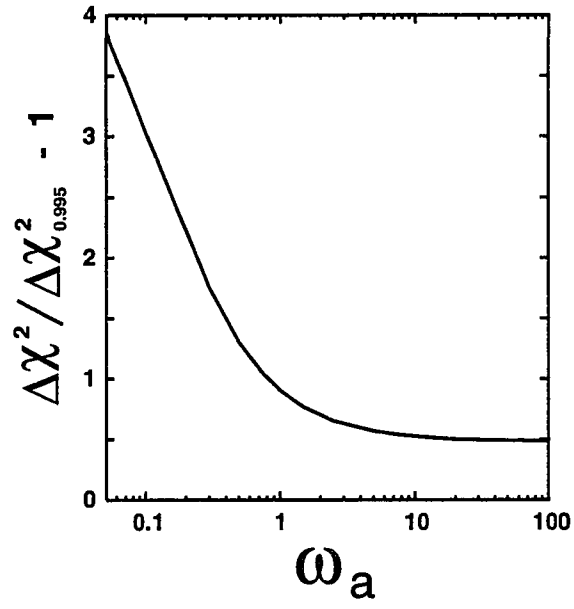


Figure 2.7: Horribility index \mathcal{H} for purely additive models.

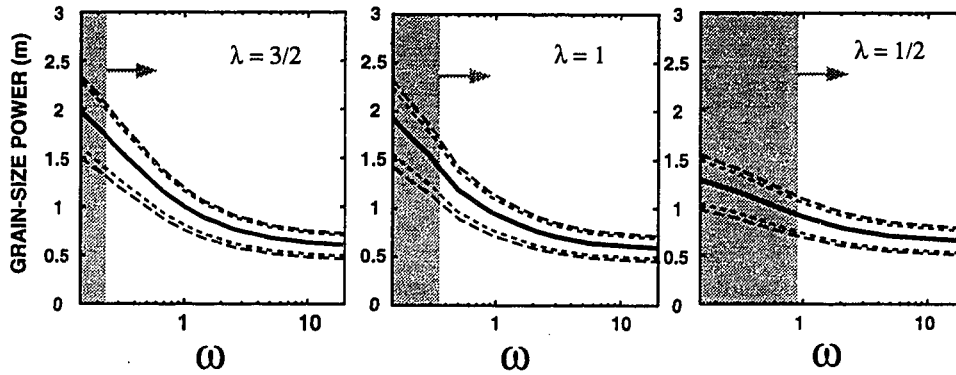


Figure 2.8: Inferred grain-size power dependence m in D^{-m} as a function of grain-importance parameter ω . Results are shown for three specific values of solute exponent λ . 90 and 95 % confidence intervals for m at given ω are shown. In addition, the 95 % confidence region for ω lies to the right of the shaded areas.

important to bulk rheology than grain size-independent mechanisms such as dislocation creep, or (2) a grain size-dependent deformation mechanism depending strongly on grain size (m in the range 1.3 to 2.2) but which is substantially less important to bulk rheology (at $D = 1$ mm) than the size-independent mechanisms. Intermediate cases are entirely admissible.

Unfortunately, with the present data set I cannot constrain the relative magnitudes of these components (i.e. the parameter ω) other than to say the D -dependent component must be at least 10% as large as the other in the limit as ion content tends to zero (Figure 2.9) and if I demand high confidence. At low confidence, results suggest that the D -dependent component must be at least 50% as large as the other, in the low-ion limit.

In any case, the grain-size dependence almost certainly results from an explicitly grain-size dependent deformation mechanism such as grain boundary sliding or diffusional creep. Goldsby and Kohlstedt (1997) and Duval et al. (1983) suggest that for these mechanisms,

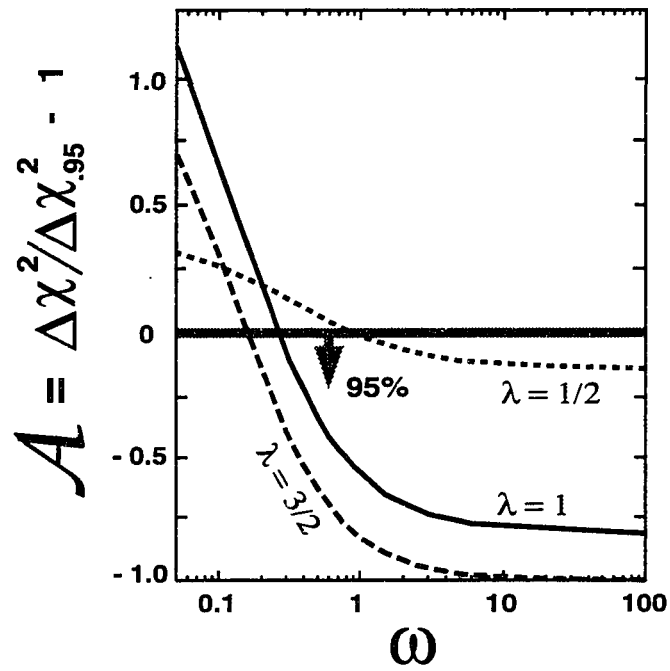


Figure 2.9: Decrease of model performance relative to optimal model, as a function of ω and λ . Clearly models with $\omega > 1$ are all equally good. Also, the $\lambda = 1/2$ models, though acceptable at 95 % confidence, as indicated by the threshold, are not very good.

strain rate is inversely proportional to grain size raised to a power m of 1.4, or 2 to 3, respectively, either of which is consistent with our results.

The alternative interpretation, that grain-size is determined by strain rate, which here is determined by an unidentified and unmeasured quantity, seems highly unlikely. This would imply that substantial variations of strain rate are caused by a physical quantity that is neither grain size nor a major impurity nor a consequence of mechanical anisotropy, and which is not correlated with either impurities or fabrics.

2.3.5 The Role of Ions.

Many results concerning ions are rather ambiguous. The most important result is that the sensitivity of strain rate to ion content appears to be rather low at $T = -17^\circ\text{C}$, such that a 2 micromolar concentration of sulphate plus chloride (a quantity typical of the impure ice-age ices in Greenland) will enhance strain rate by no more than 30%, and plausibly will have an immeasurably small effect. This conclusion has already been reached by Lipenkov et al. (1989) based on analyses of Vostok ice, and by Paterson (1991) based on analyses of borehole tilt at Law Dome (Etheridge, 1989). Irrespective of this magnitude, I find that the net effect of ionic impurities is to soften the ice, as has been generally believed (Holdsworth and Bull, 1970; Budd and Jacka, 1989).

Which Ions are the Softening Agents?

Meserve Glacier data suggest that SO_4 and/or Ca are the most effective softening agents on a per-molar basis (Figure 2.10). The conclusion that $\text{SO}_4(\text{Ca})$ is the principal softening agent results primarily from two features of the strain-rate data (Figure 2.1): the magnitude of the middle of the three strain rate spikes in the lower part of the D-grid, and the position of the strain rate maximum in the U-grid. Thus this conclusion, though statistically strong, is largely a consequence of a small number of data points and therefore should be viewed with more caution than other results presented here.

To determine which ions are the most likely softening agents, I determine how well the

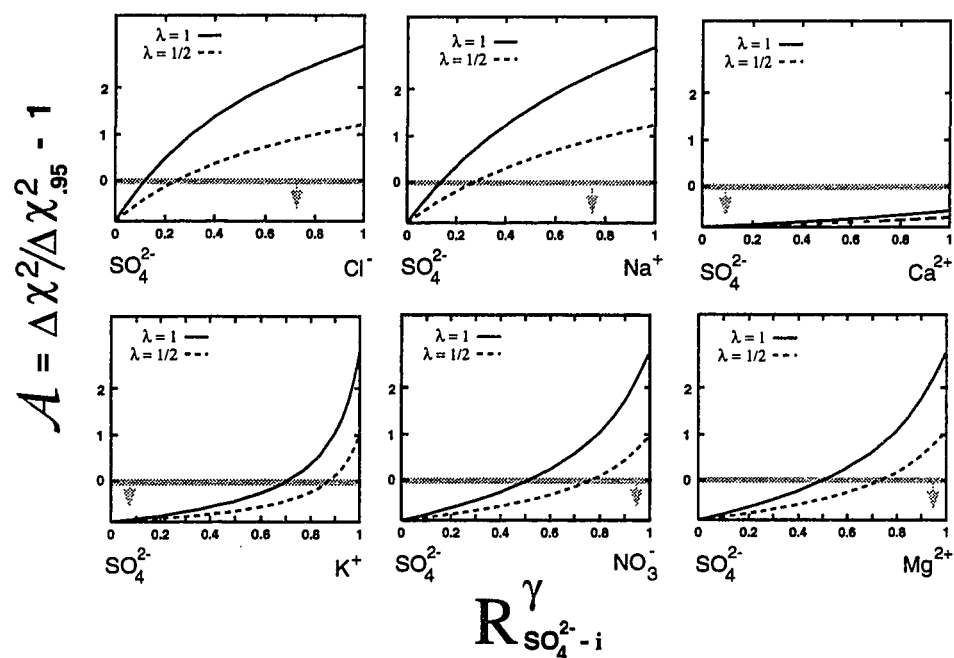


Figure 2.10: Decrease of model performance as a function of relative softening efficacy of six ions, relative to SO_4 . 90 % confidence region is below the bars, as indicated by the arrows. When the x-axis value is 0.5 in these graphs, the two ions considered have an equal per-molar softening effect. At the 0 and 1 positions on the x-axis, the indicated ion is much more effective than the other.

strain rate variations can be explained given various assumptions about which ions cause the softening and what their relative γ values are. Suppose I require that softening results from C_+ and two of the principal ions (SO_4 and one other, denoted i). Then the ionic sum in equation (2.2) is $\gamma_{\lambda}^{SO_4} C_{SO_4}^{\lambda} + \gamma_{\lambda}^i C_i^{\lambda} + \gamma_{\lambda}^+ C_+^{\lambda}$. Further I require γ^i to be positive (γ^{SO_4} is positive too, but this is a result of the optimization). Then if I fix the relative sensitivity of the two ions at some ratio γ^i/γ^{SO_4} , how good a model can I find? Because the ratio γ^i/γ^{SO_4} varies from 0 to ∞ , it is easiest to define a new variable, R^γ that ranges from 0 to 1

$$R_{a-b}^\gamma = \frac{\gamma^a/\gamma^b}{1 + \gamma^a/\gamma^b} \quad (2.17)$$

and that has a value 0.5 when the two γ are equal.

Results for such experiments show (Figure 2.10) that sulphate and calcium are the most likely softening agents, and that *Na* and *Cl* are unlikely to cause a per-molar softening larger than 1/5 of that due to SO_4/Ca . A per-molar softening by *K*, NO_3 , or *Mg* that is equivalent to that for SO_4 is possible, the small quantities of these ions in the Meserve ices preventing a more definitive statement.

Stiffening Agents?

Optimal model results indicate that *Cl* (and hence *Na*) may actually cause a weak stiffening, the 95% confidence intervals on $\gamma_{1.5}^{Cl}$ and γ_1^{Cl} being $(-1.7 \times 10^{-4}, +2 \times 10^{-5})$ and $(-4.5 \times 10^{-3}, +5 \times 10^{-4})$, respectively. A stiffening due to *NaCl* is consistent with the experiments of Riley et al. (1978) for single crystals, but opposes my view of ions acting in polycrystalline ice through disordering effects on grain boundaries. It is possible that the rather strong correlation of *Cl* with rock content causes the ion storage effect to obscure the true role of *Cl*, which is instead lumped with the sulphate/calcium sensitivity (see “ SO_4 as a Proxy...” section below).

Linearity?

The large variation of ion concentrations in the stratified ices of my study site makes it possible to constrain the non-linearity λ to some extent. However, the generally small size of the ionic terms and the partial correlation with crystal size make the confidence limits on λ broad. At 90 % confidence, λ is in the range 0.52 to 3.5 (Figure 2.11). This precludes a very low sensitivity ($\lambda < 0.5$) and therefore argues against an important role for a saturation value of concentration beyond which further addition of impurity has no effect (Nakamura and Jones, 1970). This is consistent with ions acting through grain boundary effects rather than through changes of lattice properties. The best-fit λ , approximately 1.5, shows very little variation as a function of the parameter ω (Figure 2.11).

How Soft is Soft?

What is the absolute magnitude of the softening effect of ions? At the Meserve study site the inferred ionic softening corresponds to an average enhancement of approximately $1 + \gamma_1^{SO_4} C_{SO_4} = 1 + (0.02) * (20) = 1.4$ and a maximum in the most impure layers of approximately 2.

For generalized use, γ must be interpreted properly in terms of ω and λ . First, consider the role of ω . Expanding equation (2.2) and writing the ion term simply as γC for convenience

$$E_{\text{ice}}/\bar{E}_{\text{ice}} = 1 + \omega D^{-m} + \omega \gamma C D^{-m} \quad (2.18)$$

or, to within a constant multiple (for given values of ω and D)

$$E_{\text{ice}} \propto 1 + \frac{\gamma}{1 + D^m \omega^{-1}} C \quad (2.19)$$

Thus I define a generalized ionic sensitivity $\tilde{\gamma}$ as

$$\tilde{\gamma} = \frac{\gamma}{1 + D^m \omega^{-1}} \quad (2.20)$$

It is this sensitivity that I can infer from the data analysis, rather than γ , because I am unable to significantly constrain ω . In the limit $\omega \rightarrow \infty$, $\tilde{\gamma} = \gamma$. For a given value of λ ,

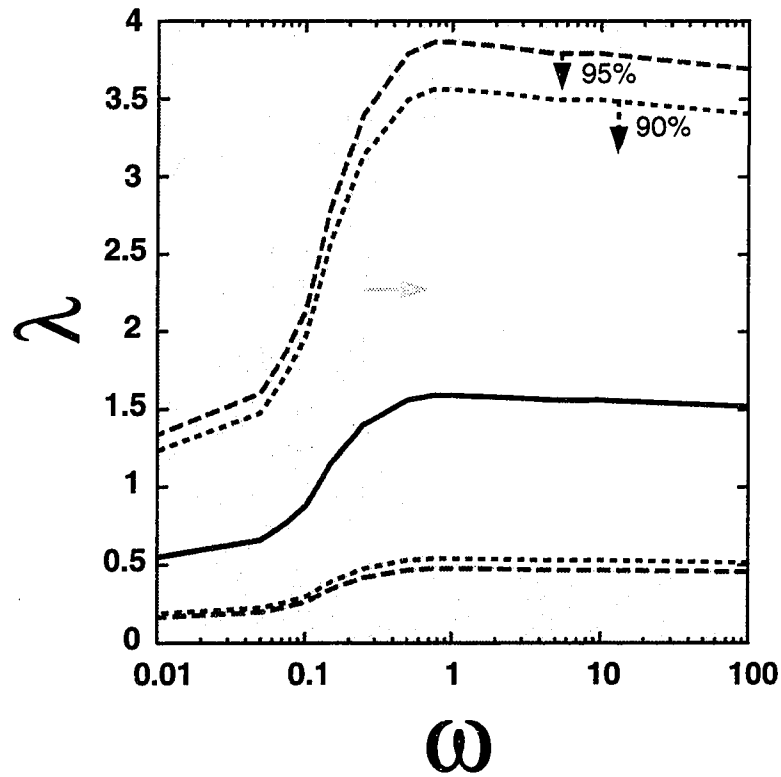


Figure 2.11: Acceptable models (at 95 % confidence) are within the white region in ω - λ space. The solid line is the optimal λ value for given ω , and the dashed lines are the 90 and 95 % confidence intervals obtained if one assumes a specific value for ω is the “true” value.

inferred $\tilde{\gamma}$ is nearly constant over the entire range of statistically admissible ω (Figure 2.12). It is undefined at the limit $\omega \rightarrow 0$, but I have already rejected such models firmly.

The magnitude of $\tilde{\gamma}_\lambda$ is a very important parameter at lower ion contents, as the enhancement due to a 1 micromolar ion concentration is simply $1 + \tilde{\gamma}_\lambda$. Inferred $\tilde{\gamma}_\lambda$ inevitably varies strongly with λ (Figure 2.13). The factor of seven range in λ (Figure 2.11) causes a four orders of magnitude uncertainty in the value of $\tilde{\gamma}$. However, all $\tilde{\gamma}$ are small enough for $\lambda > 1$ that the corresponding enhancement is no more than a few percent at 1 micromolar concentrations (Figure 2.13). For the low end of the admissible λ range, $[0.5, 1]$, the 1 micromolar enhancement could be as high as 30%.

This result is independent of ω , which makes $\tilde{\gamma}$ a very convenient parameter. This is apparent from the following. In general, if the strain rate without any ions present is a multiple of $1 + \omega D^{-m}$, and the ions change the strain rate to a new value $(1 + KC)(1 + \omega D^{-m})$, the unit ion enhancement is $1 + K$. The new strain rate value is also $1 + \omega D^{-m}(1 + \gamma C)$, requiring that $K = \gamma(1 + D^m \omega^{-1})^{-1} = \tilde{\gamma}$.

This is an over-estimate for the effect of ions if I am mis-interpreting the role of rocks. Suppose that there is neither a measurable “ion storage” effect, nor a direct rheologic effect (due to their less than 2 % volume), so that $\eta = \beta = 0$ in equation (2.2). Then inferred $\tilde{\gamma}$'s are reduced by approximately a factor of 0.4 (Figure 2.14).

Considering only the grain size-dependent deformation, what fraction of this deformation results explicitly from the presence of ions according to my results? This fraction is simply $\gamma C / (1 + \gamma C)$ or

$$f_i = \frac{C}{C + [\tilde{\gamma}(1 + D^m \omega^{-1})]^{-1}} \quad (2.21)$$

At a 1 micromolar concentration, and a grain size of 1 mm or greater, this fraction is less than 30 % for admissible values of λ and ω (Figure 2.12). In the Meserve Glacier ices, with average $C_{SO_4} \approx 20$, this fraction could be as high as 70 % (at the lowest value for ω), but is more likely 30 to 50 %. Thus I suggest that the grain size-dependent deformation rate has been approximately doubled by the presence of ions, on average.

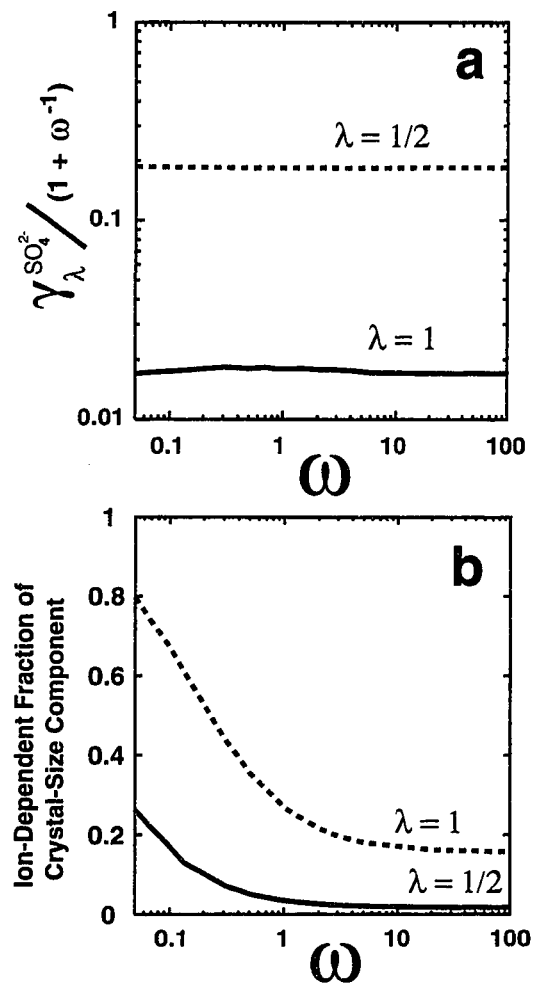


Figure 2.12: a. The inferred generalized sensitivity to the dominant impurity (here assumed to be sulphate) as a function of ω , for two values of λ and at a grain size of $D = 1$ mm. b. The inferred fraction of the grain-size dependent deformation which is due to the presence of ions, shown for the specific case of a 1 micromolar sulphate concentration.

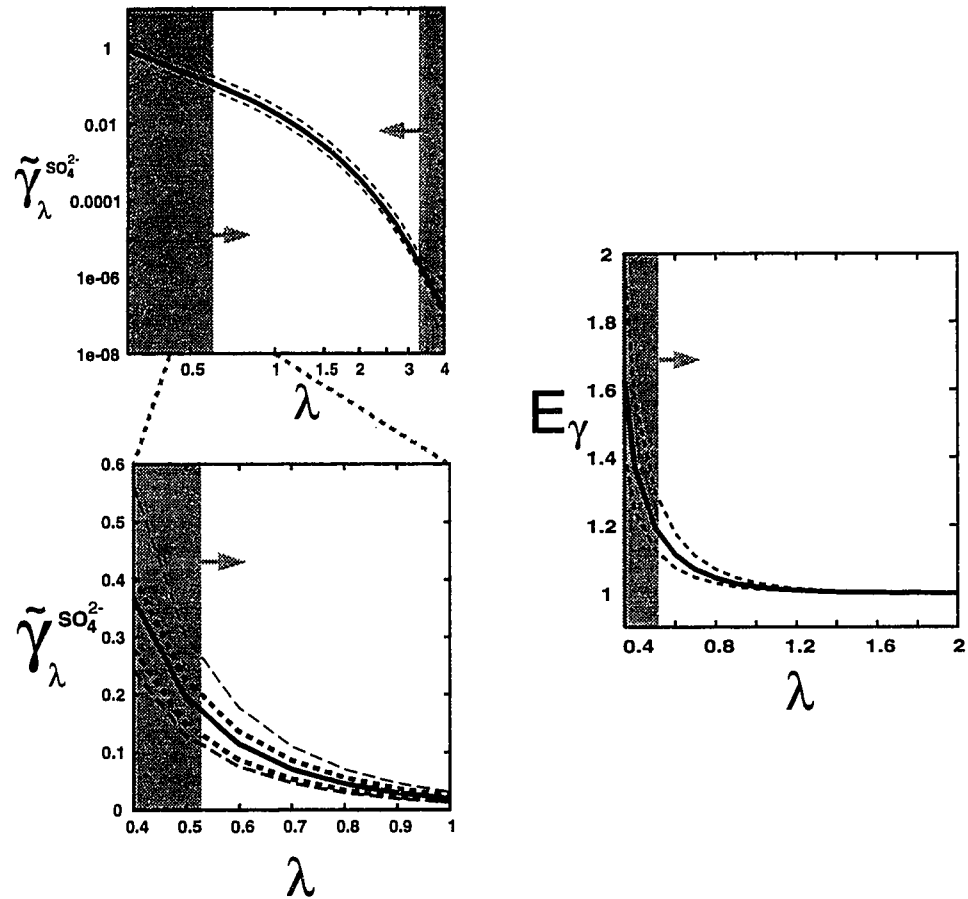


Figure 2.13: Inferred generalized sensitivity of strain rate to the dominant impurity (here assumed to be sulphate), and the corresponding strain rate enhancement for the interval $\lambda = [0.4, 2]$. The shaded regions are unacceptable at 90% confidence. Note the log-log scale of the upper left panel, and the linear-linear scale of the others.

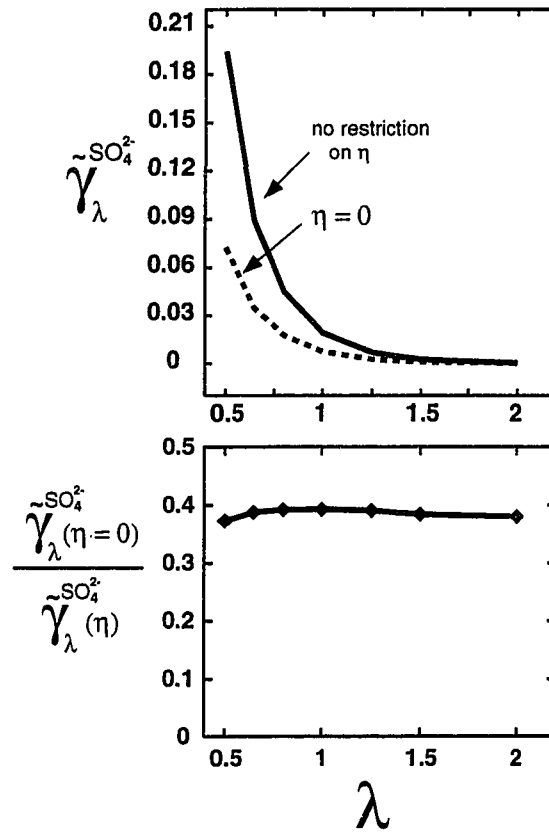


Figure 2.14: Forcing $\eta=0$, which implies there is no ion storage along ice/rock interfaces, reduces the inferred sensitivity to dominant impurity by approximately 60 %. Top panel shows the inferred sensitivities with and without this restriction on η . Bottom panel shows their ratio.

Sulphate as Proxy for Other Ions

Figure 2.13 presents ionic sensitivity results in terms of $\tilde{\gamma}^{SO_4}$. Suppose that SO_4 is not the actual softening agent, but rather is merely acting as a proxy for another ion or combination of ions (denoted i) with which it is correlated. In this case, an alternate sensitivity can be used to calculate ionic enhancement. This alternate is, to a good approximation,

$$\gamma_\lambda^i = \gamma_\lambda^{SO_4} \frac{\bar{C}_{SO_4}^\lambda}{(\bar{C}_i)^\lambda} \quad (2.22)$$

where the \bar{C} are average ion concentrations in the Meserve ices (Table 2.4). For example, suppose that SO_4 and Ca are equally effective softening agents. Then the enhancement one should estimate from a data set of C_{Ca} and C_{SO_4} is $1 + \gamma(C_{Ca} + C_{SO_4})$ with $\gamma = \gamma^{SO_4} C_{SO_4} / (C_{SO_4} + C_{Ca}) = 0.43\gamma^{SO_4}$, for the case of $\lambda = 1$.

A particular interesting case concerns combinations of SO_4 and Cl , because these are the two dominant anions in ice-age ices of the ice sheets. Suppose that SO_4 and Cl both are softening agents, with equal molar-specific sensitivities. Then the molar-specific sensitivity most consistent with my data is (Figure 2.15) approximately half that for SO_4 alone, or $0.08(0.008)$ for $\lambda = 0.5(1)$.

The Role of Acidity?

The optimal models all ascribe an important softening effect to C_+ , which I presume to be acidity. This results primarily from the correlation of C_+ with the strain rate increase in the upper part of the D-grid (Figure 2.1), which is only partially explained by variations of grain size and principal ions.

I have explored a class of models in which the power-law dependence for C_+ is different from that for the principal ions (such as sulphate). For example, I have treated the ion softening term as $\gamma_\lambda^{SO_4} C_{SO_4}^\lambda + \gamma_\lambda^+ C_+^{\lambda^*}$ where λ^* is an arbitrary positive constant. The resulting λ^* is very poorly constrained, and at 95% confidence is in the range (0.02,3.5), with an optimal value of $\lambda^* = 0.4$. Example sensitivities are $\gamma_1^+ = 0.0231$ and $\gamma_{0.1}^+ = 0.501$ for $\lambda=1$ and $\lambda=0.1$, respectively.

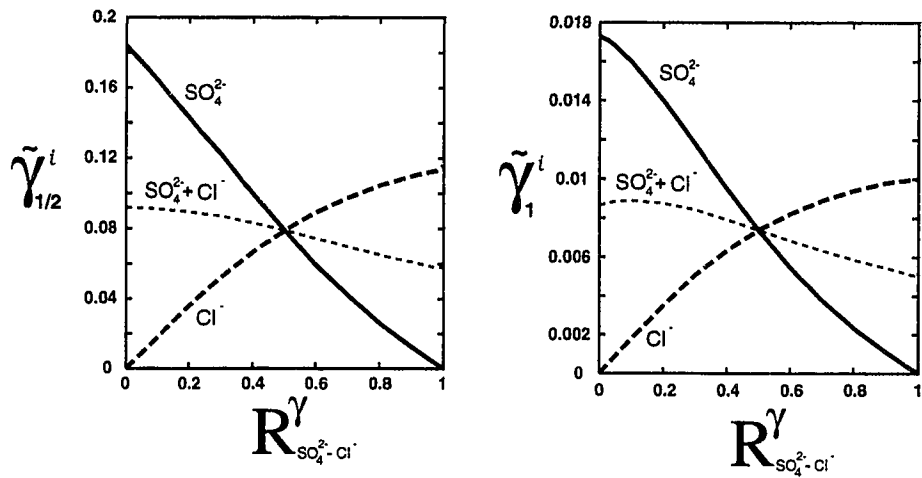


Figure 2.15: Inferred generalized sensitivity of strain rate to dominant impurity, for various definitions of “dominant impurity”. The impurity enhancement due to some impurity (or combination of impurities) C is in all cases $1 + \gamma C$. These graphs show the appropriate $\tilde{\gamma}$ to use for various C and R . The solid line is the one to use if C is assumed to be only sulphate. The thick dashed line is the one to use if C is assumed to be only chloride. The thin dashed line is the one to use for the sum $C = SO_4 + Cl$.

If I set $\gamma^+ = 0$, which is statistically unacceptable but motivated by the importance of this term relative to the paucity of data supporting it, the optimal grain size power m decreases by 1.4 %, and $\gamma_{1.5}^{SO_4}$ increases by 15%. Thus, the results presented in this paper do not significantly depend on my use of a C_+ term.

2.3.6 The Role of Rock Particles.

I find no evidence for a direct influence of rock particles on rheology, as even an extremely restrictive confidence interval (60 %) for β includes $\beta = 0$. That the optimal value, $\beta = 1.87$, is positive therefore should not be interpreted as evidence for a direct softening effect of rock particles, but most likely results as a correction to the relatively large inferred ion-storage effect, as a result of the near-perfect correlation between A_r and V_r , and the fairly strong correlation of these with major ions.

Optimized models all have positive η , most probably indicating that a significant fraction of ions are stored on the surfaces of rock particles, probably in liquid films (Dash et al., 1995; Chapter 3). The optimal value for η is 0.0019 m, but if I set $\beta=0$ so that the βV_r term cannot reflect ion storage, then the optimal $\eta=0.0021$ m, with a 95% confidence interval from -0.0004 to 0.0085. The inferred fraction of ions stored at particle surfaces is

$$1 - \frac{1}{1 + \eta A_r} = \frac{\eta A_r}{1 + \eta A_r} \quad (2.23)$$

which has a mean value in the Meserve ices of 0.065 (and may be as high as 0.17 or negligible, if 95% confidence stipulated). Suppose all this ion storage occurs in ice-rock interfacial liquid films of average thickness h , then the fraction of stored ions is also $h A_r C_h C^{-1}$ where C_h and C are concentrations in the film and the bulk, respectively. If C_h is determined by the *NaCl* liquidus, and so is an approximately 3 mol/L brine (at -17 °C), then using the measured average value of $C/A_r = 2.6 \times 10^{-5} \text{ m} \cdot \text{moles} \cdot \text{L}^{-1}$, h is approximately 55 nm on average (or in the range 0 to 150 nm according to the 95% confidence interval on η).

This h has splendid but perhaps fortuitous agreement with the film thickness (20 to 40 nm) inferred in Chapter 3 based on analysis of measured slip at ice-rock interfaces. The

ices adjacent to these interfaces have a lower total ion content than the average (100 vs. 200 micromoles/L), implying the inferred h would be lower than 55 nm here.

A possible complication is that models for which I require chloride to be a softening agent ($\gamma^{Cl} > 0$) have substantially higher η values, with a mean of .0076 m. This corresponds to a higher h , approximately 150 nm. Such a large film thickness was not rigorously excluded by the slip analysis (Chapter 3), as I could only constrain the lower limit firmly in that study.

2.3.7 *Fabrics*

The Meserve strain rate analysis has revealed nothing about the relative merits of the uniform-stress vs. uniform-strain rate assumptions. The optimal model uses the uniform-stress model ($e_{AS} = 0.2$). However, the 90% confidence interval on e_{AS} is (0,0.92), indicating no distinction can be made. This failure is not surprising, because the predictions of these models primarily differ by only a constant multiple.

2.4 *Application to Other Sites*

Results from the Meserve Glacier strain rate analysis can shed light on strain rate variations at other locations. In particular, it may be profitable to explore the usefulness of grain-size dependent rheologies (cf. Peltier, 1998). Confidence in the applicability of my results should decrease rapidly as stress and temperature conditions diverge from those at my study site (roughly 0.5 bar and -17 °C), while increasing modestly with the glaciologist's sense of desperation. I note that my results are quite limited as a predictive quantitative tool, due to the limited constraint placed on λ and, especially, ω . Their utility is largely conceptual.

What to Use

I have generated the hypothesis that strain rate enhancement in ice sheets and glaciers should vary about its mean, in addition to variations caused by non-uniformity of fabric,

stress, and temperature, according to

$$\frac{E_{\text{psa}}}{\langle E_{\text{psa}} \rangle} = \frac{1 + \omega D^{-m} + \tilde{\gamma}_\lambda C^\lambda (1 + \omega D^{-m})}{1 + \omega \langle D^{-m} \rangle + \tilde{\gamma}_\lambda \langle C^\lambda (1 + \omega D^{-m}) \rangle} \quad (2.24)$$

where the parameters ω and λ must be chosen from their broad range of acceptable values. In particular I would recommend the three cases $\omega > .15$ if $\lambda=1.5$, $\omega > .25$ if $\lambda=1.0$, and $\omega > .9$ if $\lambda=0.5$, which will cover the range of model behaviors. For each pair of values (ω , λ), the following parameterizations give appropriate values for m and γ :

$$m(\omega) = 0.58 \left(1 + \frac{4.3}{1 + 5\omega} \right) \quad \lambda = 1.5 \quad (2.25)$$

$$m(\omega) = 0.58 \left(1 + \frac{3.8}{1 + 5\omega} \right) \quad \lambda = 1.0 \quad (2.26)$$

$$m(\omega) = 0.64 \left(1 + \frac{1.56}{1 + 3\omega} \right) \quad \lambda = 0.5 \quad (2.27)$$

$$\tilde{\gamma}_\lambda^{SO_4} = \exp(-4\lambda) + \exp(-6\lambda) \quad (2.28)$$

where the latter is to be used if C_{SO_4} is used as the measure of ionic content. For the alternative measures of ionic content C_{Ca} , $C_{SO_4} + C_{Ca}$, $C_{SO_4} + C_{Cl}$, and C_{Cl} , $\tilde{\gamma}$ given by equation (2.28) should be multiplied by factors of 0.77, 0.89, 0.44, and 0.64.

For ices with negligible ion present, two convenient end-members (representing large and small ω cases) for estimating the change in shear strain rate due purely to a change in crystal size from D_1 to D_2 (D in mm) are

$$\frac{E_1}{E_2} = \left[\frac{D_2}{D_1} \right]^{0.6} \quad (2.29)$$

$$\frac{E_1}{E_2} = \frac{1 + 0.2D_1^{-1.8}}{1 + 0.2D_2^{-1.8}} \quad (2.30)$$

The largest grain-size variations in the ice sheets are typically one order of magnitude, e.g. 5 to 0.5 mm at Dye 3, and 25 to 2.5 mm at Summit (Herron et al., 1985; Langway et al.,

1988; Alley and Woods, 1996; Thorsteinsson et al., 1997; Tison et al., 1994). The possible enhancement due to grain-size variation alone is thus 4.0 to 1.7 at Dye 3 and 4.0 to 1.04 at Summit. A factor of 4 enhancement is very large, being larger than the average ice-age ice enhancement at Dye 3, and half of the total enhancement variation at GISP2 (Clow and Gundestrup, in prep.). However, even the upper limit for these estimates is substantially smaller than the potential factor of 10 variation due to fabric (Budd and Jacka, 1989).

The Dye 3 Borehole

The tilt of the Dye 3 deep borehole reveals an average enhancement for ice-age ice of approximately 2.5 there, with a maximum of 4 (Dahl-Jensen and Gundestrup, 1987). Temperature varies from -17 to -12 °C at these depths. Recently, Thorsteinsson et al. (in press) have done a thorough analysis of the contribution of fabric variation to this enhancement, and found that fabric can account for no more than 70 % of the average enhancement. Their residual correlates roughly with particle content and ions/crystal size. Dahl-Jensen and Gundestrup (1987) recognized the strong correlation between Dye 3 enhancement and dust content, crystal size, and concentrations of several ions, and proposed that any of these may be dominantly controlling strain rate there. Here I show that the effect of variations in crystal-size, as proposed here, can explain up to 90% of the residual enhancement identified by Thorsteinsson et al. (in press) after accounting for crystal fabric effects.

Using crystal size, sulphate, and chloride data from Herron et al. (1985), Langway et al. (1988) and Herron and Langway (1985) we calculate E_{res} for the bottom section of the Dye 3 borehole, for various values of ω and λ . The strain rate and properties in the Holocene ice immediately above the climate transition are used to constrain the reference value for E_{res} . Thus I am calculating variations in enhancement, not its absolute value. Models with ω in the range 0.9 to 3 are very strongly correlated with the residual enhancement (Figure 2.16 and 2.17). For the $\lambda = 0.5$ model, the contribution of ions to the residual enhancement is on average $\approx 7\%$. For the higher λ ones, it is only a fraction of a percent. Thus I suggest that crystal-size variations are responsible for more than 90% of the residual enhancement

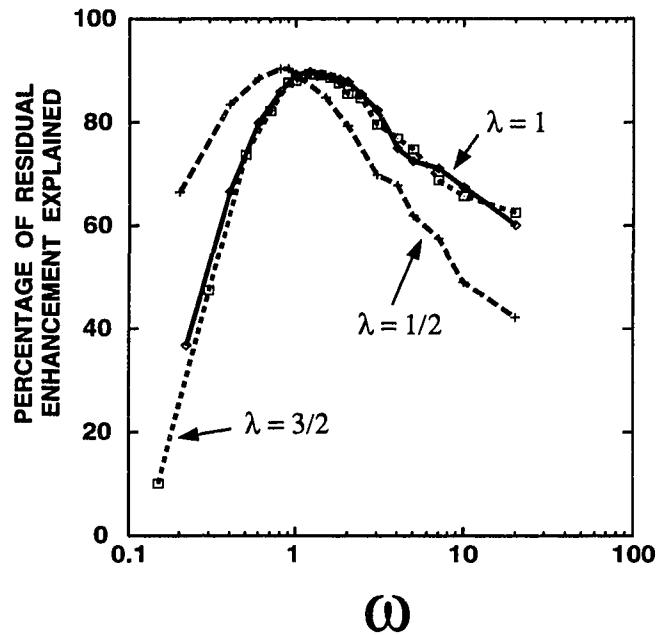


Figure 2.16: Percentage of variance of the non-fabric residual enhancement inferred from tilt of the Dye 3 borehole (Thorsteinsson et al., in press) that can be accounted for with various models which were deemed acceptable in the Meserve strain rate analysis.

at Dye 3. For the ice-age ice as a whole, the 2.5 average enhancement can be explained as 70% crystal fabric, 25 to 30% crystal size, and less than 5 % chemistry. This is actually an over-estimate for the role of chemicals, because I have not considered the potential softening effect of acids in the Holocene ice.

I note that, in the Langway et al. (1988) data on crystal size, average diameters are 2 mm in the 30m immediately above the basal silty ice. Paterson (1994, p. 287) cites a manuscript by Thorsteinsson stating crystal diameters here should be 3 mm instead. Adopting this value

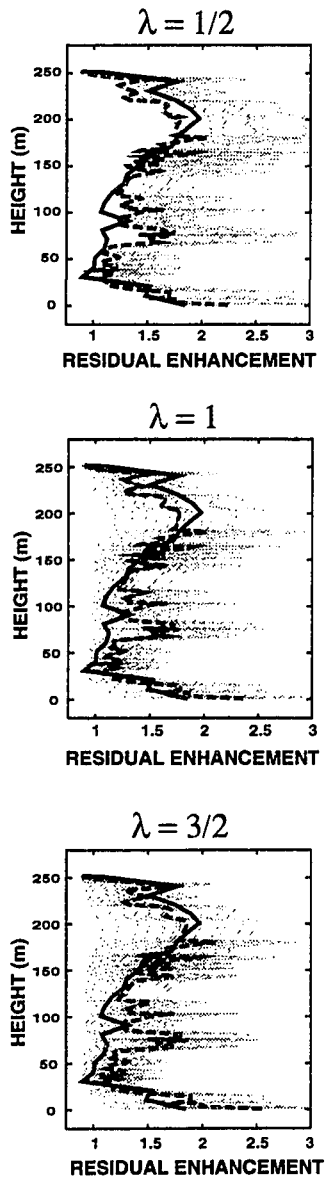


Figure 2.17: Dye 3 non-fabric residual enhancement inferred by Thorsteinsson et al. (in press) as a function of height above the bed (solid line). Dashed lines show my model results for various values of ω . The best model is shown as a dark dashed line.

for my calculations would improve my results further, eliminating much of the remaining discrepancy.

The GISP2 Borehole

Tilt of the GISP2 borehole (Clow and Gundestrup, in prep.) reveals a decrease of E from $E=8$ at 600 m above the bed to $E=1$ at 50 m above the bed, and then a step increase to $E=7$ in the thin silt-rich basal layer (described by Gow et al., 1997). Both of these changes are correlated with changes in fabric strength (Gow et al., 1997) and crystal size. Throstur Thorsteinsson (unpublished calculations, University of Washington, 1999) has converted the observed p-wave velocity anisotropy (Gow et al., 1997, Fig. 9) to a fabric enhancement, which shows that the fabric change likely accounts for a factor of $E=3$, or somewhat less than half the total enhancement variation.

Crystal diameter varies from 2.5 mm 600 m above the bed to 10 mm or more 50 m above the bed (Alley and Woods, 1996; Gow et al., 1997, Fig. 6), and back approximately to 2 mm in the basal silty ices (Gow et al., 1997, Fig. 11) According to my rheologic hypotheses, these grain size variations could account for a factor of $E = (10/2.5)^{0.6} = 2.3$ which is just sufficient to account for the missing enhancement (using coarser grains than 10 mm would increase this number). The uncertainty concerning an appropriate ω makes this little more than a suggestion, however. The basal temperature at GISP2 is -9°C , permitting a larger role for crystal size variations to be more likely here than at Dye 3 and Meserve.

Agassiz Ice Cap

Analyses of Fisher and Koerner (1986) revealed that enhanced flow of Ice-Age ice at Agassiz Ice Cap correlated best with dust content, calcium concentration, and crystal size. They observed enhanced closure rate of their borehole where it intersected ice-age ices, a result that at first sight precludes a significant role for crystal fabric, which is oriented unfavorably for this deformation. Paterson (1991) pointed out that this enhancement decreased through time (from a factor of 2.6 in the first year, to a factor of 1.3 three years later), probably as

a consequence of recrystallization, and that therefore impurities are not a credible source for the enhancement. Such a “fabric-only” hypothesis cannot, however, explain the initial factor of 2.6 enhancement without a suspiciously rapid recrystallization in the ice-age ice.

Here I point out that allowing a significant dependence of enhancement on inverse crystal size provides an explanation consistent with both the initial enhancement of the closure, and its decrease through time. The initial crystal size difference could explain the initial softness of the ice-age ice. Subsequently, the Holocene ice would become finer grained as it recrystallizes, reducing the contrast with the ice-age ice.

A Note on the Role of Chemical Impurities

If I am correct that crystal size variations are an important (though not dominant) control on shear enhancement in the ice-age ices, the root cause of such enhancement variations is then the chemical impurity content of these ices, despite the lack of a direct mechanistic connection. This is because the chemicals slow grain growth by pinning grain boundaries (Alley et al., 1986), causing impure ices to be fine grained. Paterson (1991) has argued that chemical impurities are also the root cause of important fabric variations, because the impurities cause finer grains, which more readily develop a strong fabric.

Urumqi

There is at present no sound explanation for the surprising and very important discovery by Echelmeyer and Zhongxiang (1987) that frozen ice-laden till can be two orders of magnitude softer than adjacent glacial ice. These authors suggest that the softening results from low friction of particle-particle and ice-particle interactions due to the presence of liquid films. Such an effect seems necessary because ice comprises only 38 % by weight of this frozen layer. Here I point out that the very fine crystal sizes (approximately 0.5 mm) observed in intergranular ice may have an important (though probably not dominant) role in the overall softening of the till. The temperature (-4 °C) at this field site is much closer to the pressure-melting temperature than the other sites noted above.

2.5 Conclusion

The deformation properties of polycrystalline glacier ice probably depend directly on crystal size, at stresses, temperatures and impurity contents typical of polar ice sheets and glaciers. This suggests an important role for grain-boundary processes as suggested by Barnes et al. (1971) and supports Goldsby and Kohlstedt's (1997) view that Glen's Law reflects contributions from both grain size-dependent and independent deformation mechanisms. Grain size variations probably contribute importantly to enhanced shear of ice-age ices in the northern hemisphere ice caps, and to enhanced shear of silt-rich basal layers. In the former, variations of crystal fabric are at least as important, and probably dominant, in agreement with Paterson's (1991) review. In contrast to Paterson, I attribute residual enhancement variations within ice-age ices to variations of crystal size, not to those of ionic content.

Some ions (possibly SO_4 or Ca) are important softening agents at high concentrations, but probably not at concentrations typical of the ice sheets (as recognized by Budd and Jacka (1989)). When ions do affect rheology, it is most likely through a grain-size dependent mechanism such as grain boundary sliding. This is consistent with the view that chemical impurities increase the effective temperature of ice polycrystals with respect to deformation mechanisms, as envisioned by Barnes et al. (1971) and subsequent investigators like Fisher (1987). Rock particles are probably irrelevant at concentrations found in ice sheets. Thus I argue that the rheology of glacier ice is almost entirely controlled by its physical properties, texture and fabric.

All my results should be viewed as hypotheses. Further studies of in-situ deformation, preferably supported by direct measurements of stress, will shed light on these rheologic issues, and will continue to complement laboratory experiments.

Future work may also shed light on the two main unresolved issues concerning interpretation of the Meserve Glacier data. These are

1. the paucity of information concerning the relative importance of grain size-dependent

vs. grain size-independent mechanisms at a given grain size (as given by my parameter ω)

2. the ambiguous role of some major ions (*Cl* or *Na* in particular). I have inferred that these act as weak stiffening agents, but this may contradict my interpretation that ions affect rheology through an influence on grain boundaries. Alternatively, all these ions have a softening effect, which I was not able to discern for *Cl/Na* due to correlations with rock content and interfacial film volume.

Chapter 3

**INTERFACIAL WATER IN POLAR GLACIERS AND
MEASUREMENTS OF GLACIER SLIDING AT -17 °C**

The presence of interfacial water films at the surfaces of rock particles embedded in polar glaciers and ice sheets may have important consequences for research on these ice bodies ¹. Interfacial films can complicate the interpretation of ice core paleoclimate records by, for example, facilitating diffusion of isotopes and chemicals through the polycrystalline ice, providing a medium for chemical reactions and ion storage, and causing size-dependent migration of particles due to temperature gradients (Gilpin, 1979). Interfacial films may also affect bulk mechanical properties and help explain why the impure basal layers of ice sheets deform so easily (Dahl-Jensen and Gundestrup, 1987; Echelmeyer and Zhongxiang, 1987). The role of interfacial films in these problems remains unexplored ².

Interfacial films exist due to a reduction of the chemical potential of water very close to the surface of a foreign solid (Gilpin 1979; Dash et al 1995), which depresses the melting point as an inverse function of the film thickness. Soluble impurities can depress the melting point and induce film growth, as can molecular-scale roughening of the surface (Beaglehole and Wilson, 1994). There is firm and abundant laboratory experimental evidence for the presence of interfacial films between ice and foreign solids (Dash et al., 1995).

Here I report and interpret observations of two macroscopic manifestations of interfacial water in the basal layers of an active polar glacier, at a temperature of approximately -17 °C. My first observation is of glacier sliding over basal boulders, apparently facilitated by a high

¹A closely related problem concerns the presence of liquid films at grain boundaries in polycrystalline ice. Attention was focussed on grain boundary liquid films by Barnes et al. (1971) and Paren and Walker (1971). The behavior and importance of such films remains largely unexplored.

²Echelmeyer and Zhongxiang did note the possible importance of these films

solute concentration in the interfacial water and/or by roughness-induced surface disorder. In addition to allowing us to estimate the interfacial film thickness, this measurement is interesting because until recently glacier sliding was thought not to occur under cold-based glaciers. There are only two reported measurements of such sliding, at considerably higher temperatures of $-4\text{ }^{\circ}\text{C}$ and $-1\text{ }^{\circ}\text{C}$ (Echelmeyer and Zhongxiang, 1987 and Hallet et al, 1986, respectively). The second observation is of ice segregated into clean lenses amidst rock-rich layers, which I infer to result from natural filtration of rock particles by mass transfer through a very thin film at the surfaces of englacial boulders. I hope that these observations will encourage glaciologists and paleoclimatologists to consider the role of interfacial films in current analyses of ice cores and glacier deformation.

3.1 *Subfreezing Sliding: Theory*

Water films at an ice-rock interface enable sliding by allowing the ice to negotiate very small roughness elements on the bed by regelation. Shreve (1984) has shown that the rate-controlling process in subfreezing sliding is the viscous flow of water in this film; the sliding rate is therefore sensitive to film thickness, h , the flux of water scaling with h^3 .

Gilpin's (1979) interfacial film theory, which he calibrated using measurements of motion of wires and particles through ice, implies a melting point depression of $bh^{-\alpha}$, where b and α are empirical constants. Shreve (1984) blended Gilpin's results with the theory of glacier sliding over a bed whose topography has an arbitrary roughness (Nye, 1969). Shreve also suggested that to incorporate the effects of dissolved solutes one can assume the contributions of interfacial forces and dissolved solutes to the chemical potential are additive. Thus, the melting point depression, $\bar{\theta}$, relative to the bulk pressure-melting point for clean ice is

$$\bar{\theta} \approx bh^{-\alpha} + M(C) \quad (3.1)$$

in which the function M defines the liquidus in terms of solute concentration C . Note that C may be written in terms of solute per area of interface C^* as C^*h^{-1} . Though physical

models of interfacial films show that effective values for b and α will change with solute concentration, the additive form of (3.1) is a good approximation at high solute contents (Wettlaufer, 1998) and is supported by direct measurements of film thickness at a salty interface (Beaglehole and Wilson, 1994) and of unfrozen water content of salty frozen soils (Tice et al., 1984). Shreve's expression for the sliding rate u_b as a function of shear stress τ_b , ice viscosity η_i , and the spectral power density of bed topography S_b is

$$u_b = \pi \tau_b \left[\eta_i \int_0^\infty \Omega(k) S_b(k) dk \right]^{-1} \quad (3.2)$$

where the function Ω , which is integrated over all wave numbers k , is most strongly controlled by the thickness of the interfacial water layer (Shreve's equation 12a). The derivation of (3.2) is entirely independent of values for Gilpin's parameters b and α , and the inferred u_b is negligibly sensitive to them if one calculates the integral in terms of a specified h . Replacing Gilpin's inferred spatially varying pressure in the film with a correct physical statement for the pressure difference between ice and film (Wettlaufer and Worster, 1995) has no mathematical consequence for Shreve's calculation. Thus I consider equation (3.2) useful for quantitative estimates insofar as its assumptions are met. Two assumptions which are violated at my study site (small bedrock roughness and linear rheology) strengthen the conclusions below because they cause equation (3.2) to over-predict sliding rate for a given h (cf. Gudmundsson, 1997).

3.2 *Sliding Observation*

In the austral summer of 1995-96 my colleagues and I excavated a tunnel along the bed of the Meserve Glacier to expose impure basal layers for study, following Holdsworth (1974). Here I observed cavities in the lee of boulders on the bed, as reported by Holdsworth. The cavity roofs are striated, with a wavelength correlated to the grain roughness of the crystalline plutonic rocks at the up-flow margins of the cavities. This suggested sliding occurs at the ice-rock interface up-flow of the cavities and motivated us to install (by freeze-on) displacement markers on the ice at the interface whose positions could be measured relative

to fixed bolts on the rock, using a micrometer, and to insert a displacement transducer 1 mm above the bed, and another at 30 mm. These were all just upstream of a prominent cavity, at a distance of approximately 16 meters from the ice margin, which is a 20-meter high cliff. I also inserted a displacement transducer 1 mm above the bed at a location on the opposite side of the tunnel, not upstream of a cavity. All these markers moved downglacier over the periods of measurement (up to ten months) at a rate more than an order of magnitude faster than that due to shear strain (which has a maximum observed value of 0.2a^{-1} here), and therefore were measuring sliding³ (Figure 3.1). Enhanced shear at the interface due to a more favourable orientation of ice crystals there (a possibility raised by Barnes et al., 1971) cannot explain my data because the fabric throughout the ice where strain rate measurements were made is already a tight, vertical single maximum and therefore already as soft as possible.

The markers showed a sliding rate of about $8\text{ mm}\cdot\text{a}^{-1}$ near the lip of the prominent cavity, decreasing to $2\text{ mm}\cdot\text{a}^{-1}$ some 20 cm up-flow. The decrease away from the cavity is probably due to a concentration of down-flow shear stress at the cavity lip. Finite element model calculations of this stress concentration indicate the shear stress declines to the far-field value within approximately 15 cm for a cavity of this size. Thus the $2\text{ mm}\cdot\text{a}^{-1}$ value is an appropriate value for sliding rate driven by the average basal shear stress unperturbed by nearby cavities. This is quite similar to the $3\text{ mm}\cdot\text{a}^{-1}$ measured on the opposite side of the tunnel. All sliding rates here refer to the component of slip parallel to the tunnel.

3.3 Interpretation of Sliding

The measured sliding rate is considerably higher than one would estimate from Gilpin's results ($0.2\text{ mm}\cdot\text{a}^{-1}$ according to Shreve (1984)) and deserves explanation. The principal unknown quantity is the mean thickness of the interfacial film, and I now use equation (3.2) to estimate it. To accomplish this, I first measured the detailed topography of the rock surface adjacent to the sliding cavity, and from this calculated the spectral power density

³Shear strain can account for $0.2 \times 1 = 0.2\text{mm} \cdot \text{yr}^{-1}$.

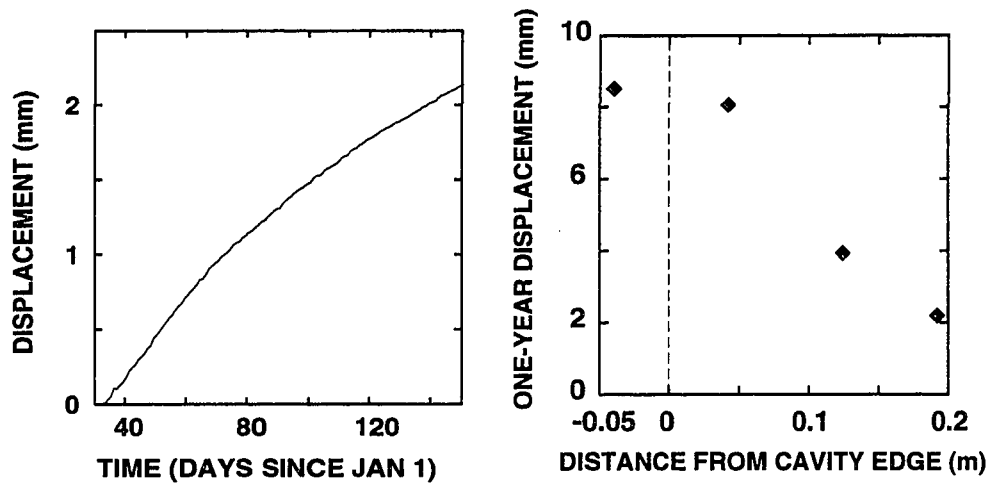


Figure 3.1: Left Panel. Example of continuous time displacement measurement spanning four months of 1996, using an armature LVDT, anchored in the basal boulder and inserted 1 mm above ice/rock interface. The curvature is probably due to displacement of the ice into the tunnel and toward the transducer. LVDT measurements showed noise of magnitude 0.015 mm about the mean. Right Panel. The net slip during 1996 at four locations on the ice rock interface, as a function of distance upglacier from the cavity edge.

S_b . The resulting S_b (Figure 3.2) approximates a power-law over seven orders of magnitude, and is on average $S_b(k) = 0.05k^{-3}$. This is rougher than the example bed used by Shreve, and so the observed rapid sliding is not a consequence of an unusually smooth interface.

The actual measurement of rock topography was done (mostly on two separate samples of the surface) using four methods at different spatial scales: tape and compass survey ($k < 10^2 \text{ m}^{-1}$), contour tool profiling (for $10^2 < k < 10^3$), optical interferometry (Zygometrics NewView 200; $10^3 < k < 3 \times 10^5$), and contact-mode Atomic Force Microscopy ($10^6 < k < 5 \times 10^7$). Wavenumbers $10^2 < k < 10^5$ proved to be the only significant ones in the integral (3.2).

For the η_i it is not appropriate to use standard tabulated values as the basal ices of the Meserve Glacier are unusually soft (Holdsworth, 1974), and because the tunnel affects the stress state. Instead I use $\eta_i = \tau_b/n\dot{\epsilon}_b$, in which $\dot{\epsilon}_b$ is my in-situ measurement of shear strain rate for ice of this impurity content (0.1a^{-1}), and $n=3$ is the non-linearity of ice creep. The down-flow (tunnel-parallel) shear stress is a multiple E of the weight-slope product. E is an enhancement term accounting for the presence of the ice cliff, and is 1.4 to 2 according to two-dimensional finite element calculations we have made for non-linear creep of a sloping ice body with a terminal cliff. I use the low estimate $E = 1.4$ because this gives a lower limit for η_i and hence h . I find $\eta_i \approx 4 \times 10^{12} \text{ Pa s}^4$. This substitution for η_i eliminates τ_b from the numerator in (3.2), but η_i remains an important parameter in Ω .

For these values, and the measured spectral power density, (3.2) indicates that a liquid film of thickness approximately 20 to 40 nm is necessary for sliding to occur at the measured

⁴Here the local surface slope and thickness are approximately 0.15 and 25 m, respectively, so I estimate the basal shear stress is at least $1.4 \times 0.15 \times 25 \times 9.8 \times 917 = 4.7 \times 10^4 \text{ Pa}$, in which 9.8 and 917 are gravitational acceleration and ice density, in m-k-s units. The finite element calculations are an adaptation of the Raymond (1983) finite element code, in which a stress-free lateral boundary has been introduced to one end of a flow-line. The grid was focussed toward the base and toward the marginal cliff. The results $E=1.4$ (at a distance of one cliff height in from the margin) was found for a model of a parallel-sided slab of a power-law fluid ($n=3$) with a soft basal layer (viscosity reduced to 0.25 its normal value, in a layer that is one-tenth of the total ice thickness). Other models, such as those for linear-viscous bodies and those lacking a soft basal layer produced higher values for E . Thus my stress estimate is likely a minimum value. This implies I may be underestimating the ice viscosity and hence, ultimately, underpredicting the liquid film thickness, as stated in the text

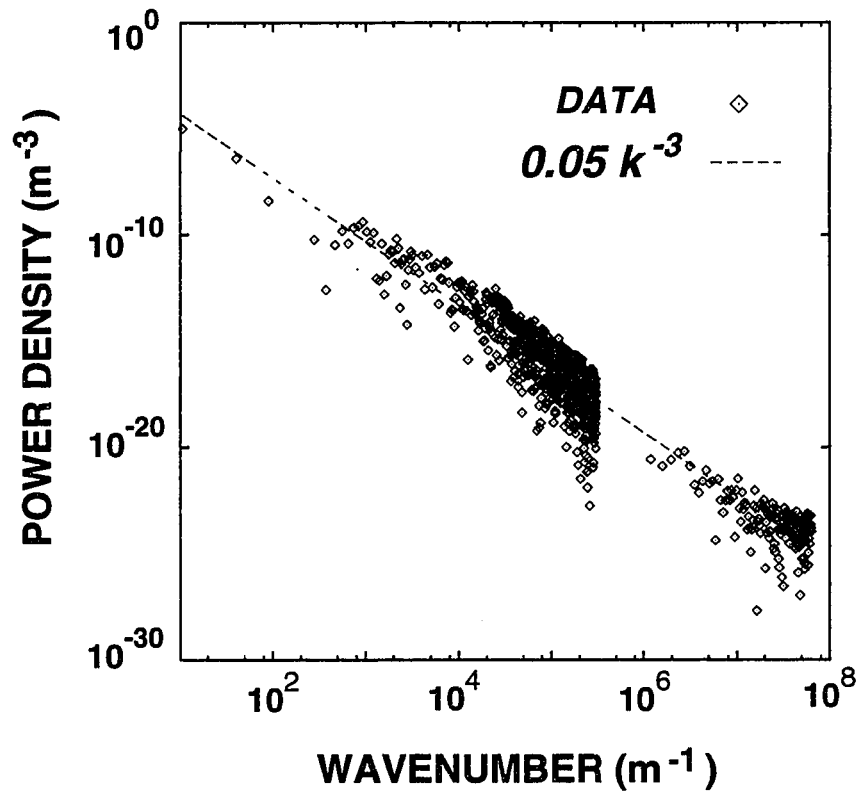


Figure 3.2: Measured spectral power density of rock surface. For consistency with Nye (1969), wavenumbers k are defined unconventionally as the inverse of wavelength, without a coefficient of 2π .

rate. Uncertainties on the measured physical quantities and the physics of the problem conspire to make this result tightly constrained in the lower limit, but not the upper ⁵. All plausible thicknesses are sufficiently large to make the interfacial term in (3.1) very small (20 nm is one order of magnitude larger than the film thickness predicted from Gilpin, 1979). Consequently the interfacial film likely has a very high solute content (a situation analogous to that produced in experiments of Beaglehole and Wilson, 1994). If this is the primary reason for the thick film, its solute concentration must be $C \approx \tilde{\theta}/M$, which is approximately 3 moles/L based on the NaCl liquidus (Wettlaufer et al., 1997; 70% of soluble impurities here are NaCl). The relatively rapid sliding of this polar glacier in this view is made possible by a brine layer at the ice-rock interface.

Though high, a 3 molar solute concentration is plausible; the total salt per area of bed in the layer, approximately 9×10^{-5} moles m^{-2} , is equivalent to the salt per unit area in a $10^{-3}m$ thickness of ice, which is approximately 1/3 the diameter of ice crystals here (the bulk solute concentration of ice just above the sliding interface is 10^{-4} molar, as measured by the U. New Hampshire glaciochemistry lab (Buck et al., 1992)).

The impurity concentration in grain boundaries and veins in polycrystalline ice is several orders of magnitude higher than that of the crystal lattice (Alley et al, 1986). Further, as ice freezes from water, as during regelation cycles, it rejects solutes at a very high efficiency (Gross et al., 1975). Interfacial films will generally intersect grain boundaries, allowing solutes to exchange. Because of this, and the refreezing accompanying regelation, the solute concentration of interfacial films will generally be orders of magnitude higher than the bulk concentration of adjacent ice, and this makes for generally thicker films, especially in ices with a temperature not far from the bulk phase boundary.

Thus solutes are also a likely explanation for the high sliding rate measured by Echelmeyer and Zhongxiang (1987). Without solutes they could only account for 10% of their measured $0.18 m \cdot a^{-1}$ slip rate, despite the relatively low roughness of this interface ($0.004 k^{-3}$). At

⁵In addition to the uncertainty on the stress estimate (see footnote [4]), the upper limit is not well constrained because the derivative of slip velocity with respect to film thickness rapidly decreases in magnitude as film thickness increases, according to the Shreve (1984) formulation.

-4 °C, solutes will dominate film thickness at concentrations of ~ 0.5 mol/L (for NaCl), which is 10^4 times greater than typical solute concentrations of glaciers in the Tien Shan (Wake et al, 1989). A 10^4 concentration difference between grain boundaries and bulk ice is expected (Gross et al., 1975; Alley et al., 1986). The Hallet et al (1986) measurements also show unexpectedly rapid slip, but I do not interpret these because the slip rate was not steady, and the temperature was close to the bulk melting temperature.

3.4 Ice Segregation

Water films also can explain structures observed within the glacial ice. The dirtiest basal layers of the Meserve Glacier contain $\sim 1\%$ by volume of finely dispersed silt-sized rock particles, which give these layers a pronounced yellow-brown color (Holdsworth, 1974). Within these layers are sparsely distributed larger rock clasts. The shear of ice around these clasts induces two pressure shadows on opposite sides of the rock surface, and it is common to observe small cavities separating the clast and ice in these positions (Holdsworth, 1974).

If an interfacial film is present, the pressure gradient along the rock surface will drive a net flow toward the cavities. A small rate of net melt must occur adjacent to the interface to maintain film thickness. At the cavity, the water will accumulate as ice, either by direct refreezing or by evaporation into the cavity and subsequent deposition. The small thickness of the water film will prevent transport of all but the finest particles so the accumulating ice will be free of them; the rock surface and its interfacial film act as a natural filtering system.

I have observed (Figures 3.3 and 3.4) pronounced clear ice zones, which stand in contrast to the adjacent amber-colored ice, adjacent to the low-pressure regions of clasts, and tailing off as thin zones far up- and down-flow (similar to S-shaped strain figures seen in metamorphic rocks). It is likely that these clear ice zones are accumulations of the sort envisioned here ⁶; segregation of clean ice is difficult to envision in situ by any other mechanism. This

⁶Gow et al. (1997) report similar features from the silt-rich basal ice near the base of the Greenland ice

process may have an important role in the formation of foliation in creeping dirty glacier ice and other heterogeneous media.

3.5 Conclusion

Observations of glacier sliding and ice segregation beneath the Meserve Glacier are best explained as manifestations of unfrozen water in films at ice-rock interfaces, despite the low temperature of -17°C . Estimated film thickness is at least 20-40 nm. Here these water-dependent phenomena are strengthened and made easily discernible by the unusually high solute content of this ice, but interfacial films and resultant phenomena should be present in most polar ice masses. The role of interfacial films in possibly modifying ice core records and ice deformation properties should be carefully considered by researchers of these subjects. Films in most natural glacier ices are likely thicker than implied by Gilpin (1979) due to concentrated impurities. ⁷

sheet, as sampled in the Greenland Ice Sheet Project-2 ice core.

⁷Much of this chapter was published as Cuffey et al. (1999).

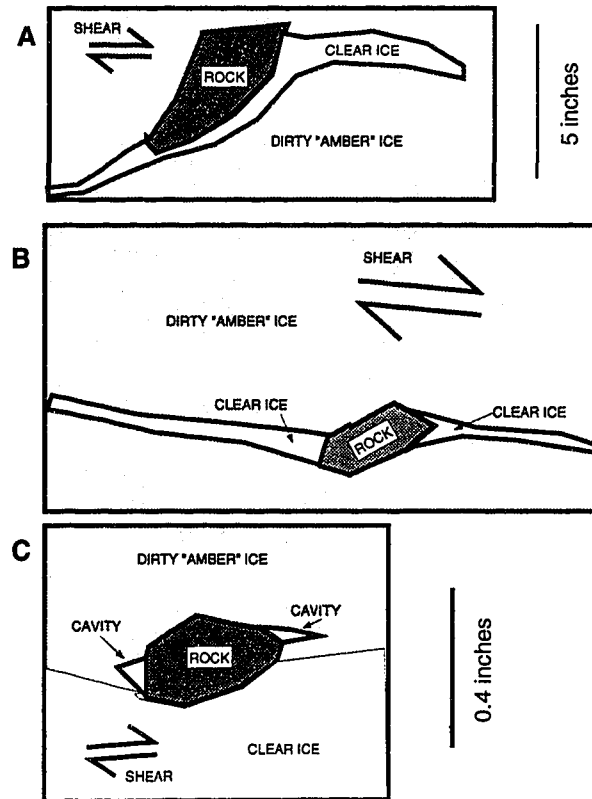


Figure 3.3: Sketches of three rocks and adjacent ice, observed in basal layers of the Meserve Glacier. A and B. Rocks with clear ice zones in pressure-shadow positions. C. A rock with cavities in pressure shadows but no clear ice, as observed by Holdsworth (1974, his Figure 17, page 34).

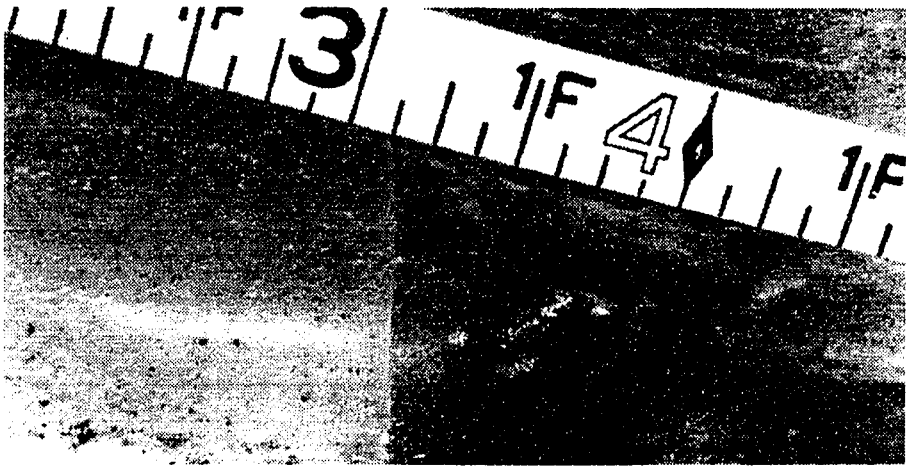


Figure 3.4: Photograph of the rock and ices in panel B of Figure 3.3. The scale is a tape measure with English units, the numbers 3 and 4 indicating inches.

Chapter 4

ENTRAINMENT BENEATH COLD GLACIERS

Dirty basal ice layers are present at many locations beneath polar glaciers and ice sheets whose basal temperatures are lower than that for bulk pressure-melting (Koerner, 1989; Gow et al., 1997). These layers are important because they usually deform more rapidly than clean ice and can contribute importantly to the flow of the ice mass (Echelmeyer and Zhongxiang, 1987; Dahl-Jensen and Gundestrup, 1987) and, in addition, because they may limit the time-span of useful paleoclimate information inferred from ice core analyses. In some cases, these layers clearly are relicts of past climatic conditions and ice sheet configurations that are drastically different from the modern ones, as under central Greenland (Souchez, 1997; Souchez et al, 1995). In general, however, dirty basal layers will be present irrespective of such historical circumstance only if entrainment of debris into basal ice occurs actively at subfreezing temperatures. Here I present a case study that provides the best example to date (as far as I know) of entrainment occurring at subfreezing temperatures. This result was anticipated over two decades ago by Holdsworth (1974).

Motivated by my recent high resolution continuous measurements of slow sliding at the Meserve Glacier base (Chapter 3), I also renew the challenge against two common assumptions that geomorphologists make concerning cold-based ice masses. The first is that cold-based glaciers do not slide or abrade their beds (e.g. Summerfield, 1991, p. 271), and hence that striated rock surfaces are evidence for past warm-bed conditions (Summerfield, 1991). The second is that cold-based glaciers do not accomplish significant geomorphic work, and hence that landforms of glacial erosion beneath subtemperate ice masses are relicts of past warm-bed conditions (e.g. Richardson and Holmlund, 1996). Note that I do not challenge the basic contention that cold-based ice masses are weak erosive agents

relative to temperate ones.

Central to a proper physical picture of processes in subfreezing ice is the recognition that thin layers of water, called interfacial films, exist at the interfaces between ice and immersed foreign solids, such as rocks, at temperatures well below (tens of degrees Centigrade) the bulk pressure-melting point. These films allow slip, and therefore abrasion, to occur at the ice-rock interface despite bulk subfreezing temperatures. As discussed below, they will also facilitate entrainment of rock debris from the glacier bed by cold ice, by permitting mechanisms additional to those cited by Sugden and John (1976, p. 163).

4.1 *Entrainment at Subfreezing Temperatures*

Mechanisms for entrainment of coarse rocks at subfreezing glacier soles have been envisioned for quite some time (Sugden and John, 1976), but direct evidence of subfreezing entrainment is lacking. Observations of rock debris entrained in the terminal ice of polar glaciers (e.g. Mercer, 1971) do not provide the necessary evidence because the mechanism for entrainment in these cases is ambiguous. Entrainment could occur by melt and re-freeze at the margins of these glaciers prior to advance, by active shearing of over-ridden stony permafrost, from supraglacial sources, or by normal melt-freeze entrainment processes in temperate ice (Alley et al., 1997) either far up-flow or at some time in the past when the ice was thicker or the climate warmer.

Analyses of the composition of dirty basal layers beneath polar glaciers have mostly concluded that entrainment occurred under warm-bed conditions via bulk melting and re-freezing, whether current (Sugden et al., 1987; Zdanowicz et al., 1996; Souchez et al., 1988), or past (Souchez, 1997; Koerner, 1989). An exception is the work of Tison et al (1993), who suggest that debris travels from the bed upward along shear bands at subfreezing temperatures. Though this interpretation may be correct, the gas composition of the dirty ices studied by Tison et al. and the scatter of their isotopic data indicate significant alteration by water, and therefore one cannot exclude bulk melt and re-freeze as the entrainment mechanism (this could have happened at the glacier margin when it was retracted relative

to its present position).

4.1.1 Meserve Glacier Basal Layers

In the austral summer of 1995-96, my colleagues and I excavated a 20m-long tunnel through basal ice of the Meserve Glacier, an alpine glacier in Wright Valley, Antarctica. Earlier studies here (Holdsworth and Bull, 1970) revealed dirty basal layers despite the low temperature of -17 °C, and I wished to study these using gas and isotopic composition techniques not available to Holdsworth and colleagues. The dirty basal layers contain dispersed fine rock particles (up to 2.5 % silt and fine sand) and larger boulders, and have a yellow-brown “amber” hue (Munson designation: 2.5Y 4/4 to 7/4).

The margin of the Meserve glacier’s ablation zone is a 20m high vertical cliff (see Holdsworth, 1974), from which ice blocks fall to accumulate in an apron of marginal debris at the cliff foot. This apron also contains wind-blown snow and re-frozen meltwater. On the warmest days of summer, the glacier surface and this marginal apron melt. Recent advance of the glacier and over-riding of this marginal debris has generated a three-layer stratigraphy of basal ice layers (Holdsworth and Bull, 1970) within 20m of the margin. Clean bubbly glacier ice overlies stratified amber layers, which over-lie cleaner ice (but still containing rocky layers) which is former marginal apron (Figure 4.1). The boundaries between these units are blurred by physical mixing, manifested as interfingering and recumbent folding of distinctive layers.

4.1.2 Gas Composition

As snow densifies to form glacier ice on polar glaciers, air is trapped in bubbles that are approximately 8% of the total volume. The molar fraction gas content is thereafter fixed in a glacier such as the Meserve, with ratios between various gas species very similar to those of the atmosphere. If melt occurs subsequently, and the water equilibrates with either the open atmosphere (if the melt occurs in the marginal apron, for instances) or bubbles having atmospheric composition, the differing solubilities of the gas species results in a gas

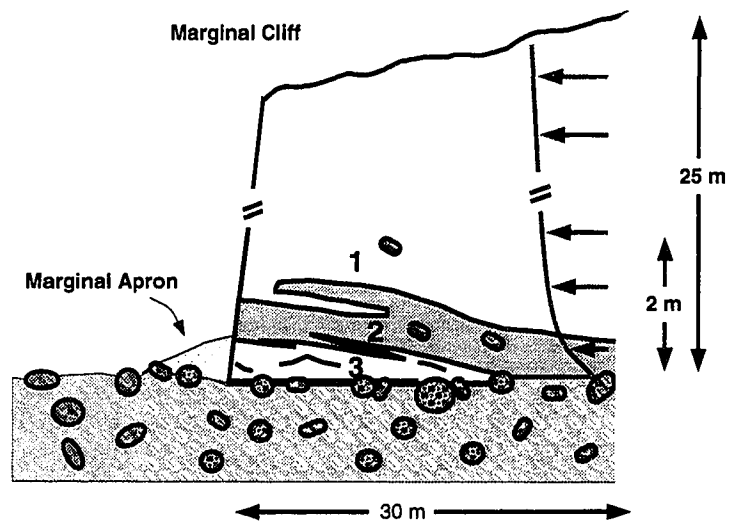


Figure 4.1: Vertical cross-section through the margin of the Meserve Glacier, showing the stratigraphy discussed by Holdsworth (1974) and re-exposed by us. Ice flow is shown schematically by velocity vectors on the right. The stratigraphy has three facies 1. relatively clean, bubbly, ordinary glacier ice, 2. bubbly amber ice with dispersed fine rock particles, and 3. strained mixture of glacier ice blocks, snow, and refrozen meltwater, with stringers of particles, inferred to be marginal apron material over-ridden by glacier advance. At my tunnel site, the glacier rests on bouldery till. Facies 3 tapers out at approximately 20m from the margin (Holdsworth and Bull, 1970). Physical mixing occurs by deformation at the facies boundaries.

composition of the liquid rather different from that of the atmosphere. After re-freezing, gas bubbles in the refrozen melt will have ratios different from atmospheric. In particular, the Ar/N_2 ratio will be higher than atmospheric due to the ≈ 2 times greater water solubility of Argon than Nitrogen. Further, the total gas content will be substantially reduced relative to that for normal bubbly glacier ice.

Beneath the Meserve, I expect the facies 3 gas composition to have a lower total gas content and increased Ar/N_2 than atmospheric, and it does (Figure 4.2). The amber layer composition, however, is essentially identical to that of the overlying bubbly glacier ice, except near the facies 2-3 boundary where physical mixing has combined the two. This is strong evidence that the amber layers were entrained without bulk melt and refreeze, the volume of interfacial films and grain boundary veins being too small to significantly alter the gas compositions (approximately 0.001 % in the most impure ices; Chapter 2).

4.1.3 Stable Isotope Composition

The stable isotopic composition of the basal ices supports this view. Simultaneous measurements of δD and $\delta^{18}O$ for ice samples from facies 1 and 2 mostly show (Figure 4.3) a strong linear relationship with a slope of eight, which is characteristic of precipitation (the meteoric water line of Craig, 1961). If there is bulk melt and partial re-freezing beneath a glacier, the isotopic composition of basal layers would deviate from the meteoric line (Jouzel and Souchez, 1982) because the preferential inclusion of heavy-isotope bearing water molecules in the solid phase is characterized by different fractionation coefficients than those for the vapor/solid-water phase transitions relevant to precipitation. Deviations of basal ice composition from that of meteoric water have been observed at several polar glaciers (Sugden et al., 1987; Souchez et al., 1988; Zdanowicz et al., 1996; Iverson and Souchez, 1996) and interpreted (reasonably) as evidence of temperate conditions beneath these glaciers. Here, the concordance of most of the dirty basal layer samples with the line defined by adjacent bubbly glacier ice suggests no bulk melt and refreeze has occurred. There are, however, two samples from the dirty ice, and one from the clean ice, that lie significantly off the

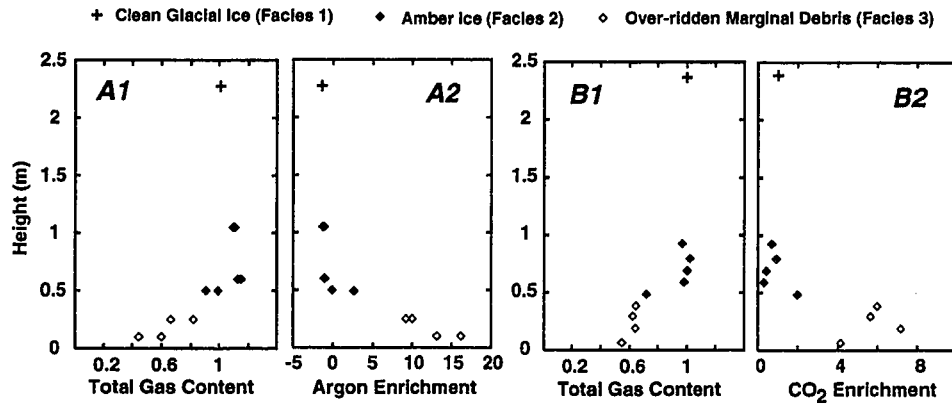


Figure 4.2: Gas composition measured on samples from two locations A and B in the subglacial tunnel. A. measurements of J. Severinghaus, B. measurements of R. Lorrain. Total gas content is normalized to that of the top clean ice samples in A1 and B1. Argon enrichment is defined as $\delta Ar/N_2$ for a sample (relative to atmospheric) normalized to $|\delta Ar/N_2|$ for the top two samples in A2 (which look like one point on the figure). The $\delta Ar/N_2$ value is negative in normal glacier ice because of gravitational separation in the firn column during initial densification. CO_2 enrichment is gas fraction of CO_2 normalized to that for the top sample in B2. This has a rather high CO_2 fraction (366ppmv) relative to the Holocene pre-industrial level, which suggests these data are rather noisy.

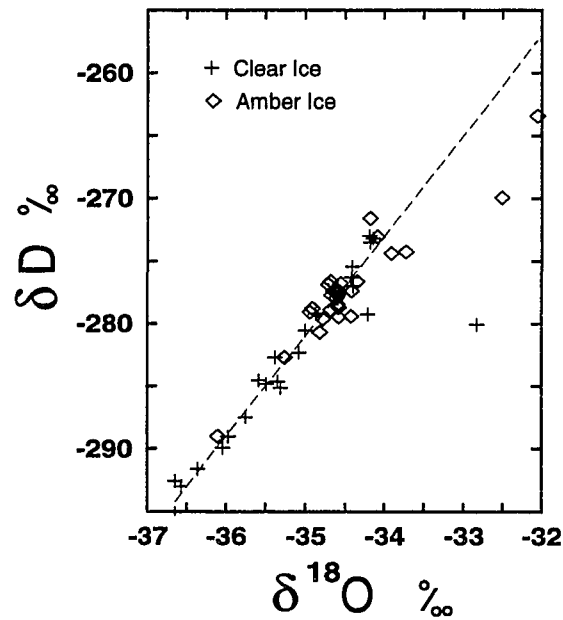


Figure 4.3: Co-isotopic analyses for amber ices and overlying glacial ice. The dashed line has a slope of eight.

line. Both of the anomalous dirty ices were adjacent to (within 2 centimeters of) clean ice interlayers. My ad hoc explanation for these is that the clear layers are refrozen meltwater from facies 3, and that my sampling method (extracting small cores 5 cm in length and 1 cm in diameter) lead to contamination. The relatively heavy values for these samples support this explanation. One of the samples is just above the facies 2-3 boundary, whereas the other is 30 cm above it. When sampling, I noticed nothing anomalous about the one sample from facies 1 with the odd composition, which was taken from 0.5m above the dirty ices.

The isotopic ratios are low ($\delta D \approx -270$ per mille) compared to that for modern precipitation in this region ($\delta D \approx -225$ per mille) indicating this ice accumulated during the last glacial period. The heart of the accumulation zone is 6 km from the sampling site. If this ice accumulated 15 kyr before present, near the end of the last glacial period, its average travel velocity was $\approx 0.4 \text{ m} \cdot \text{yr}^{-1}$, and this estimate would be lower if a greater age were assumed. This low velocity (compared to the surface ice velocity of $5 \text{ m} \cdot \text{yr}^{-1}$), plus the compressive flow regime of the ablation zone, suggests the ice has passed in close proximity to the bed for a significant fraction of its journey to the margin.

4.1.4 *Entrainment Summary*

As the stable isotopic composition and, especially, the gas content of the Meserve glacier basal amber ices strongly suggest that entrainment of bed material occurs here without significant alteration of the bubbly glacier ice, we can rule out several mechanisms for genesis of these layers, including over-riding of dirty marginal apron, basal freezing of groundwater (Wilson, 1979), and shear activation of permafrost. Though permafrost may have an isotopic composition identical to that of precipitation, it will likely have a low total gas content and high $\delta Ar/N_2$ compared to bubbly glacier ice.

More generally, it appears unlikely that entrainment occurred while the bed was at the bulk pressure-melting point. Partial loss of melt water would likely have occurred, driven by the steep surface slope of this glacier, altering the isotopic composition (Jouzel and Souchez, 1982) and gas composition (Tison et al., 1993), and water volumes may have been sufficient to affect isotopic composition during regelation (Iverson and Souchez, 1996). Thus entrainment probably occurred here at subfreezing temperatures. Moreover, entrainment quite likely is occurring under modern conditions; many other glaciers in the Dry Valleys region bear “amber” layers of this sort indicating the process is widespread and currently active (Holdsworth, 1974).

4.2 Geomorphic Work of the Subfreezing Meserve Glacier

Accepting that the modern debris flux to the margins of Meserve Glacier is the result of entrainment at subfreezing temperatures, has subfreezing erosion been a geomorphologically significant process here? The Dry Valleys environment has been cold and dry for at least the past 10 million years (Denton et al., 1993). Assuming that the modern debris flux is representative of long-term rates, I can estimate how much erosion has occurred in this time by this process. Two estimates follow. The first is based strictly on direct measurements near my tunnel site. The second is based more on inference but accounts for flux through the high-velocity central core of the ice tongue (Holdsworth, 1969, Figure 10) where I do not have direct measurements.

Fine rock particles account for 0.3% of the basal 2 meters of the glacier by volume (Chapter 2), and coarser particles (greater than 1 mm diameter) contribute approximately an equal amount (Holdsworth 1974, p. 43) so the thickness of rock λ_r in a vertical section of the glacier margin is approximately 1.2 cm. This is an underestimate because it neglects the occasional large boulders. Such layers are observed along the entire cliffed margin of the ablation zone (the lower ice tongue), which has perimeter length P_a . At my study site, the average velocity of these layers is $U_r \approx 0.3 \text{ m} \cdot \text{yr}^{-1}$ according to direct measurements (the average strain rate is 0.3 yr^{-1} and sliding is negligible). The total debris flux exuded by the Meserve Glacier tongue is thus approximately $\lambda_r U_r P_a \approx 10 \text{ m}^3 \cdot \text{yr}^{-1}$.

The more general estimate can be obtained from mass balance considerations. The gross flux of ice to the ablation zone is simply the product of accumulation area $A_b \approx 9.5 \times 10^6 \text{ m}^2$ and average accumulation rate ($\dot{b} \approx 0.05 \text{ m} \cdot \text{yr}^{-1}$ according to Carnein, 1967). This product equals the sum of mass loss by ablation processes occurring at rate \dot{a} over the ablation surface area $A_a \approx 2 \times 10^6 \text{ m}^2$ and mass loss at the marginal cliff, which is estimated in terms of average ice velocity \bar{U}_i (measured to be approximately $1.2 \text{ m} \cdot \text{yr}^{-1}$ at my study site), perimeter length, and cliff height ($H \approx 20 \text{ m}$) as $\bar{U}_i P_a H$. The ratios $f_u = U_r / \bar{U}_i$, $f_r = \lambda_r / H$, $f_b = \dot{a} / \dot{b}$ and $f_A = A_a / A_b$ are plausibly considered to be constant. The total debris flux exuded by the Meserve Glacier tongue is thus approximately $f_u f_r \dot{b} A_b (1 - f_b f_A)$. The average

surface ablation rate \dot{a} over the lower portion of the accumulation zone is approximately $0.13 \text{ m} \cdot \text{yr}^{-1}$, according to flux estimates based on Holdsworth's (1969, Figure 10) velocity and thickness maps, and an assumption of approximate steady state. Thus the ratios are $f_u = 0.25$, $f_r = .0006$, $f_b = 2.6$ and $f_A = 0.226$ and the debris flux is $\approx 30 \text{m}^3 \cdot \text{yr}^{-1}$.

The erosion rates corresponding to these two rock flux estimates are, as an average over the glacier bed, 9×10^{-7} to $3 \times 10^{-6} \text{m} \cdot \text{yr}^{-1}$, very low compared to those for temperate glaciers. Over 10 million years, the net erosion totals 10 to 30 meters if averaged over the glacier bed.

Radio-echo sounding measurements show that the upper tongue of the Meserve Glacier sits in a U-shaped trough, a classic landform of glacial erosion (Figure 4.4), with a depth of approximately 60m. The lower portion of the Meserve's ablation zone is known to rest on a planar bed, so the glacier has probably not eroded significantly here. Thus the bed-averaged erosion of 10 to 30 meters is an underestimate for the U-shaped trough, and the modern subfreezing entrainment rates are sufficient to account for much of this landform. It is not necessary to interpret this landform as a relict of past temperate conditions, though the possibility is certainly not excluded.

Dry Valleys glaciers provide a rather extreme example. The elapsed time of cold-based conditions has been very long compared to most locations. But also the temperatures here are very low. A $-17 \text{ }^\circ\text{C}$ basal temperature is much lower than the basal temperatures of most thicker polar ice masses. As erosion rates probably increase with basal temperature, it is difficult to generalize from this one example, other than to conclude that erosion at subfreezing temperatures may be a geomorphically significant process at other locations.

4.3 Mechanisms, Sliding, Interfacial Films

Entrainment of rock fragments at the bed of a cold glacier could occur simply by creep of ice engulfing rocks that are separated from bedrock by subglacial fracture (as suggested by Sugden and John, 1976) or which lay on the land surface prior to glacier coverage. However, the great viscosity of ice makes this mechanism a difficult one for fine-grained particles, such

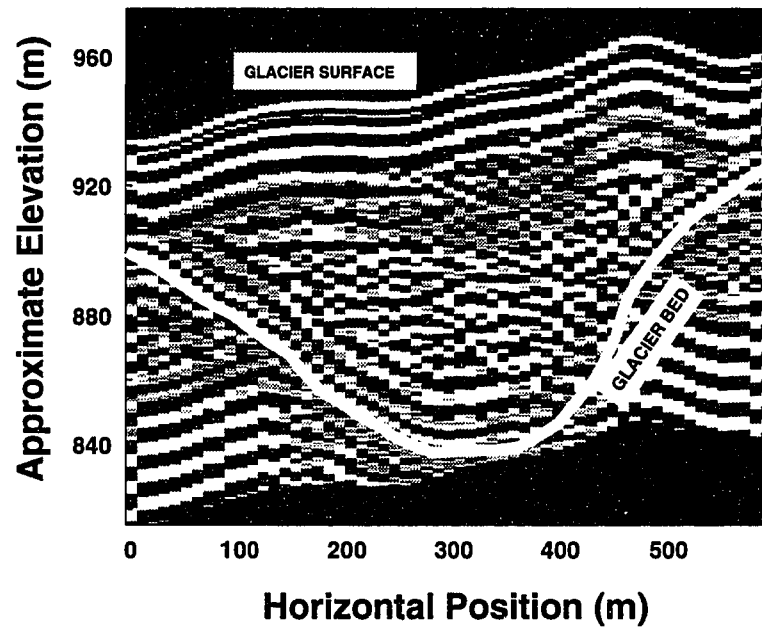


Figure 4.4: Radio-echo sounding image of the glacier bed along an East-West transect across the upper part of the ablation zone (the lower ice tongue) corrected for surface elevation. The migrated glacier bed is shown as a thick white line. Records collected at 10m spacing. Data were analyzed, and this figure made, by A. Gades, University of Washington.

as the silt and sand sizes of Holdsworth's amber ices. An additional mechanism that helps resolve this difficulty is local melt and refreeze accompanied by slip at ice-rock interfaces, which are made possible by the presence of interfacial water.

Traditionally, it has been almost universally accepted that sliding does not occur at ice-rock interfaces at temperatures lower than the bulk pressure-melting point (e.g. Sugden and John, 1976; Denton et al., 1993; Gow et al., 1997). The alternate view, that cold-based glaciers slide and ice negotiates small rock protrusions or particles by regelation was argued on theoretical grounds by Shreve (1984) as an application of Gilpin's (1979) empirical theory for interfacial films (thin layers of water at the interfaces between ice and immersed foreign solids such as rocks). There is now abundant laboratory evidence for the existence of interfacial films, including direct measurements of film thickness, to temperatures as low as $-30\text{ }^{\circ}\text{C}$ (Dash et al., 1995; Beaglehole and Wilson, 1994; Wettlaufer et al., 1996), and their existence in natural glacier ices should be assumed until contrary evidence is found. Their glaciological manifestation as slip at the ice-rock interface has been observed at temperatures of $-1\text{ }^{\circ}\text{C}$ (Hallet et al., 1986), $-4\text{ }^{\circ}\text{C}$ (Echelmeyer and Zhongxiang, 1987) and, during my investigations at Meserve Glacier, at the very low temperature $-17\text{ }^{\circ}\text{C}$ beneath the Meserve Glacier (Chapter 3; Cuffey et al., 1999).

Entrainment by regelation of ice past fine particles (due either to pressure gradients (Iverson and Semmens, 1995) or temperature gradients (Gilpin, 1979)) therefore should occur beneath cold glaciers. Interfacial slip will ease engulfment of larger particles. Such mechanisms may coexist with more traditional ones, and contribute to the overall entrainment flux.

Slip rates and the efficacy of associated entrainment mechanisms increase strongly as interfacial film thickness increases, which in turn is a strongly increasing function of both temperature and film solute concentration. In cold glaciers, interfacial layers probably have high solute concentrations even in relatively clean ice because of solute rejection during regelation and the strong segregation of impurities to grain boundaries (Chapter 3). However, the temperature should generally be the dominant control on film thickness. Geomorphic

activity at a very cold bed like that of the Meserve Glacier will generally only be important if the ice is very impure, as in the Dry Valleys glaciers. Polar glaciers whose beds are only a few degrees lower than the pressure melting point however might generally be important geomorphic agents, and basal contributions to total ice motion are likely important beneath such glaciers (Echelmeyer and Zhongxiang, 1987).

In all cases, erosion rates will, of course, depend strongly on the nature of bed material (unconsolidated till vs. hard bedrock). The U-trough under the Meserve Glacier is carved through crystalline bedrock. One possibility here is that this bedrock is subject to frost shattering when the glacier has retreated into its upper basin, and that the glacier subsequently entrains this loose material on re-advance and transports it down-slope.

4.4 *Striations and Abrasion*

The measurements of sliding beneath several cold glaciers, at temperatures as low as -17°C , indicate that abrasion, formation of striae and generation of fine material do occur beneath cold glaciers, though at rates probably much smaller than at warm beds (Shreve, 1984). This could explain the striations and grain crushing observed by Holdsworth (1974) and Mercer (1971). As melt rates are negligible in these cases, the vertical contact force of abrasive tools against their beds would (for typical abraders) result almost exclusively from viscous drag associated with longitudinal extension of the flow (see Hallet, 1979), and from the weight of very large boulders. Though abrasion beneath cold glaciers is presumably sluggish, the use of striations as indicators of warm-bed conditions and the assumption that cold glaciers do not slide or abrade (Summerfield, 1991; Gow et al., 1997, p. 26,573) should probably be abandoned.

4.5 *Conclusion*

Cold-based glaciers actively entrain basal material. This provides a general mechanism for formation of dirty basal layers, and may in some cases be an important geomorphic process.

Subfreezing entrainment is facilitated by interfacial water films, which also allow sliding and abrasion by cold glaciers. The common assumption that cold-based glaciers are “protective rather than erosional” (e.g. Denton et al., 1993, p. 168) is not true in the absolute sense, though this statement can be an accurate one if made relative to temperate glaciers.

Chapter 5

RECONSIDERING THE POLAR REGIONS METEORIC WATER LINE

Is the isotopic composition of precipitation largely determined by liquid water even at temperatures as low as -35 °C? Although contrary to current thinking, an affirmative answer to this question directly solves the decades-old puzzle of why there is a clear and persistent linear relation between deuterium and oxygen isotope ratios in polar regions precipitation. This view firmly supports the use of ice core deuterium excess measurements to learn past climates.

5.1 Background

One of the most remarkable characteristics of earth's environmental geochemistry is the very strong linear relationship between the isotopic ratios $\delta^{18}O$ and δD of precipitation (Craig, 1961; Dansgaard, 1964) ¹. This relationship is called the Meteoric Water Line (MWL), and is on average $\delta D = 8\delta^{18}O + 8.6$ ² (Jouzel et al, 1987). The singular clarity of this relationship makes measurements of deviations from it useful to paleoclimatologists (Jouzel et al, 1982; Johnsen et al, 1989), glaciologists, hydrologists, atmospheric scientists, and biologists (Dansgaard, 1964; Craig, 1966; Jouzel and Souchez, 1982; Federer et al, 1982; Frapre et al 1984; Yesikov et al, 1985; Sternberg et al, 1991; Gibson et al, 1996). The origins

¹ δ is defined for a sample as $\frac{R}{R_s} - 1$ where R is the number ratio of heavy to light isotope-bearing waters, and R_s is a standard value for the ratio. δD indicates the ratio is HDO to $H_2^{16}O$ and $\delta^{18}O$ indicates the ratio is $H_2^{18}O$ to $H_2^{16}O$. δ values are usually multiplied by 1000, in which case the units are "per mille". The ratios for two coexisting phases (e.g. ice and water vapor) differ by a proportionality constant (so that $R_1 = \alpha R_2$) which is called the fractionation factor, α . Fractionation factors are different for all the different isotope-bearing waters and ices, and are temperature-dependent.

²The MWL as originally defined by Craig has an intercept value of 10. Here I use MWL to refer to the best-fit line through isotopic data.

for the MWL, and its potential variability, are therefore of great interest.

Deviations from the MWL are described in terms of deuterium excess $d = \delta D - 8\delta^{18}O$, which has a global average value of 8.6. This non-zero value results from a natural isotopic separation process accompanying evaporation (Merlivat and Jouzel, 1979), and its magnitude depends on sea surface temperature and relative humidity in the vapor source regions. Measurements of d on ancient ice recovered by coring the polar ice sheets therefore may yield important information about past climates of the subtropics (Jouzel et al., 1982; Johnsen et al., 1989).

The slope value $d\delta D/d\delta^{18}O \approx 8$ (and the corresponding near constancy of d) is a consistent feature of precipitation over the polar ice sheets, through both spatial and temporal climate variations. A slope of 8 is seen clearly in modern precipitation in Greenland (Dansgaard, 1964; Johnsen et al., 1989), glacial-age precipitation in Greenland (Johnsen et al., 1989), and glacial-age precipitation in coastal Antarctica (Figure 5.1). Modern Antarctic precipitation deviates slightly from a slope of 8, with d rising by approximately 12 per mille in the cold interior of East Antarctica (Petit et al., 1991; Dahe et al., 1994), between $\delta^{18}O$ values of -43 and -55 per mille. Glacial-age precipitation in central Antarctica also very closely approximates a line of slope 8 (Jouzel et al., 1982). Thus, the MWL is an exceptionally robust feature of the polar environment.

The consistency of the polar MWL remains puzzling despite several decades of study. The standard model used to explain the MWL of the polar ice caps (Jouzel and Merlivat, 1984; Ciais and Jouzel, 1994) invokes kinetic (meaning rate-dependent) fractionations accompanying growth of ice crystals in clouds that are supersaturated with vapor. The most widely used form of this model (Jouzel et al., 1987; Johnsen et al., 1989; Jouzel and Merlivat, 1984; Ciais and Jouzel, 1994) successfully replicates deuterium excess data but is highly sensitive to its prescription for cloud supersaturation ratios as a function of temperature, and employs two adjustable coefficients which are tuned so the model calculations reproduce the MWL. As clearly recognized by the authors of the standard model (Jouzel and Merlivat, 1984), the high sensitivity to these parameters is problematic because supersaturations may

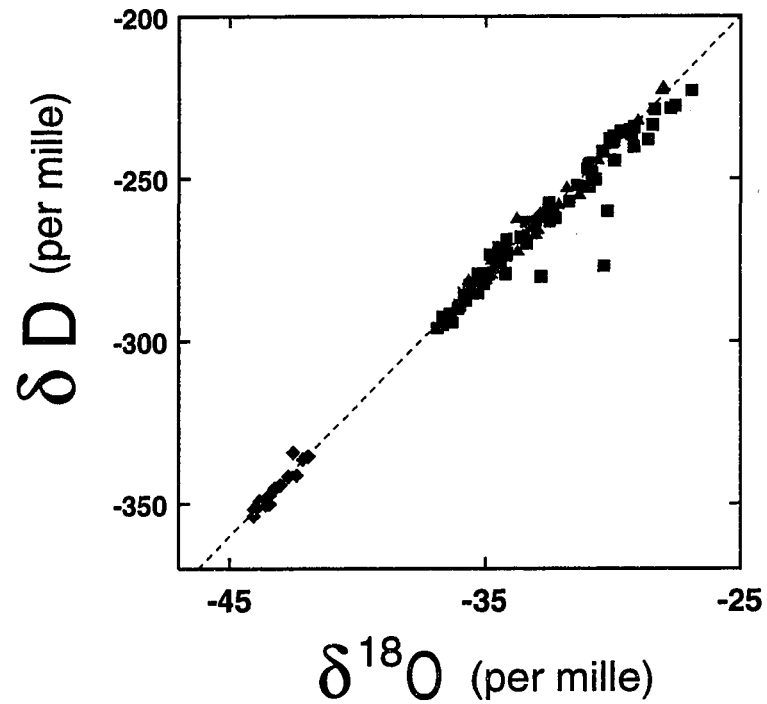


Figure 5.1: Isotopic data from three glaciers in the Dry Valleys region of southern Victoria Land, Antarctica, define a meteoric water line. The dashed line has a slope of eight. We collected these ice samples in Wright and Taylor Valleys, from the Meserve, Hart, and lower Taylor Glaciers. Analysis was subsequently done by mass spectrometry at the INSTAAR, University of Colorado, stable isotope lab by E.J. Steig, B. Vaughn, and J.W.C. White. The samples shown here mostly represent ice deposited during the last glacial period.

vary widely in clouds whereas deuterium excess varies little. Sensitivity tests exploring the full range of naturally permissible supersaturations (Jouzel et al., 1991) predict a possible range of over 100 per mille in central Antarctic d , a deuterium excess catastrophe in view of the observed 10 per mille variability (Dahe et al., 1994). Thus even a minor change in the average supersaturation of clouds during climate changes would cause a significant change to deuterium excess. The constancy of the MWL in space and through major environmental changes of the glacial-interglacial cycles indicates a more stable explanation for the MWL probably exists. A version of the standard model that calculates rather than prescribes supersaturation (Gedzelman and Arnold, 1994) is not as successful at reproducing either the polar regions MWL or the correlation of isotopic composition with temperature. This model incorporates a rather complete view of cloud microphysics, and therefore ought to reproduce the MWL nearly perfectly if its isotopic component is complete ³. Instead, it predicts a large rise of approximately 80 per mille in d between $\delta^{18}\text{O} \approx -25$ and $\delta^{18}\text{O} \approx -60$.

5.2 A New View

Here I show that a stable explanation for the polar regions MWL follows directly from two principles: 1. Fractionations are equilibrium fractionations and are therefore insensitive to cloud supersaturation. 2. The isotopic composition of precipitation is dominantly governed by liquid-vapor equilibrium down to approximately $-30\text{ }^{\circ}\text{C}$, and is partially governed by liquid-vapor equilibrium down to $-40\text{ }^{\circ}\text{C}$. A third important, though not essential, feature of our calculations is the use of refined temperature-dependent fractionation factors for liquid-vapor equilibrium (Horita and Wesolowski, 1994). These are nearly identical to previously used values for $D - H$ fractionation but are slightly larger for $^{18}\text{O} - ^{16}\text{O}$ fractionation. Fractionation factors for deeply supercooled water have never been measured, and I rely on extrapolations from higher temperature data. ⁴

³a precise replication of the isotope-temperature correlation should not be expected though.

⁴I use the temperature-dependent relations from Horita and Wesolowski (1994) for supercooled water. An extrapolation is reasonable because the temperature dependence of vibrational partition functions and

Following earlier researchers (Dansgaard, 1964; Johnsen et al., 1989; Jouzel and Merlivat, 1984; Ciais and Jouzel, 1994) I calculate isotopic composition of precipitation using a simple model that follows a single air mass from its oceanic source region pole-ward and upward over the interior of a polar ice sheet. A simple model of this sort is antiquated relative to General Circulation Models incorporating isotopic tracers (Jouzel et al., 1987; Jouzel et al., 1991) but serves to illustrate the predictions of an atmospheric model's isotopic component. My approach is to use a very flexible model that represents a broad array of cloud properties (*ice/liquid content and vapor/condensate ratio*) and that describes only the isotopic consequences of cloud microphysical processes, not the processes themselves ⁵.

The model air mass cools as it rises and radiates heat ⁶. The cooling causes condensation to liquid water or to ice, which are enriched in heavy isotope-bearing waters relative to the vapor. The vapor isotopic composition δ_v therefore decreases along the path as the number concentration of vapor-phase water molecules N_v decreases

$$\frac{d\delta_v}{1 + \delta_v} = \frac{\alpha^* - 1}{1 + f\alpha^*} \frac{dN_v}{N_v} + \frac{f}{1 + f\alpha^*} d\alpha^* \quad (5.1)$$

and ⁷ the condensate forming at any instant has composition

$$\delta_c = \alpha^* [1 + \delta_v] - 1 \quad (5.2)$$

Here α^* is the effective fractionation factor which is a linear combination of the fractionation

hydrogen bond fraction are necessarily smooth (Japas et al., 1995; Van Hook, 1968). Moreover, the relation for α_D in these formulae has a temperature dependence identical to that of the direct measurements for supercooled water (Merlivat and Nief, 1967) as far as the data go (-15 °C). The small absolute offset between these is well within the scatter of experimental fractionation data at 0 °C. Below (footnote [12]) I explore the sensitivity of our results to the extrapolations. For ice-vapor equilibrium fractionation factors I use Merlivat and Nief (1967) for deuterium and Majoube (1971) for oxygen 18.

⁵I in no way imply that such a model is a substitute for more complete physical models. Rather it is the appropriate tool for establishing criteria for a robust MWL.

⁶The meteorologic component of our model is identical to that of Johnsen et al. (1989)

⁷The derivation of equation (1) is due to Merlivat and Jouzel (1979). $d\alpha^* = (\beta - \alpha_w)d\lambda - [\lambda d\alpha_w + \zeta(1 - \lambda)d\beta]$ where β is the effective fractionation factor determining the composition of ice, α_w is the fractionation factor for liquid-vapor equilibrium, and λ is the fraction of condensate that forms and persists as liquid water rather than ice (λ does not include condensate that forms initially as liquid but is then rapidly converted to ice). See footnote [9] for the definition of ζ .

factors pertaining to water and to ice ⁸. The average composition of newly-formed ice is itself determined by an effective fractionation factor β which is a linear combination of the equilibrium fractionation factors for water-vapor equilibrium (α_w) and for ice-vapor equilibrium (α_i)

$$\beta = g\alpha_i + (1 - g)\alpha_w \quad (5.3)$$

Thus I envision that some ice forms directly in equilibrium with vapor, while other ices form directly from liquid precursors, or possibly have interfacial liquid layers which are in equilibrium with vapor (a remote possibility at such low temperatures, according to Dash et al., 1995). Because the composition of ice can be either governed by liquid-vapor or ice-vapor equilibrium, the distinction here between ice and liquid is that ice in a cloud does not necessarily maintain equilibrium with vapor, while water does. This is important only in defining f in equation 1. f is the molar ratio of equilibrated condensate to vapor in the cloud ⁹.

I assume that the effective ice/liquid partitioning g is 1 at all temperatures lower than -40 °C, approximately the apparent homogeneous nucleation temperature for water ¹⁰ (Stillinger, 1980). Otherwise I vary g with temperature T according to a simple exponential

⁸ $\alpha^* = \lambda\alpha_w + (1 - \lambda)\beta$.

⁹Equilibrated condensate being that portion of the ice plus liquid in a cloud which maintains equilibrium with the vapor. Define the ratio of total mass of condensate (ice plus liquid) to total mass of water vapor in a cloud as f_T . Then I define $f = f_T[\lambda + (1 - \lambda)\zeta]$ where ζ is a number between zero and one which prescribes the extent to which ice in the cloud maintains equilibrium with vapor. Typically accumulating ice will not maintain equilibrium with vapor at all and $\zeta = 0$. $\zeta > 0$ would result from a continual process of sublimation and redeposition of ice particles. The f_T is typically very low at high temperatures, and is unknown at very low temperatures. In between (at temperatures of -20 °C to 0 °C) condensate mass is typically 1% to 30% in precipitating clouds (Hobbs and Rangno, 1998) corresponding to $f_T = 0.01$ to 0.4. A cloud with 50% condensate would be unusually high, so $f_T = 1$ is a plausible extreme upper limit. In the calculations present here, I employ four scenarios for f_T : I. $f_T=0$ for all T . II. $f_T=0.1$ for all T . III. f_T attains a maximum value of 0.5 at -17 °C, and decreases in either direction, attaining a value of 0.05 at 0 °C and -35 °C. IV. Same as III except the maximum attained value is 1. The low temperature limit for f_T is nearly irrelevant because $\zeta \approx 0$.

¹⁰My results do not change if I decrease this nucleation temperature by up to 15 K.

decay with a characteristic scale Δ_g

$$g = \exp \left[\frac{233 - T}{\Delta_g} \right]; \quad T > 233K \quad (5.4)$$

The specific functional form is not important. The important proposition I make is that liquid-vapor equilibrium has a significant governing role even at a temperature of -30°C , which requires $\Delta_g < 20$.

I adopt this hypothesis by choosing $\Delta_g = 5, 10, \text{ or } 15 \text{ K}$, and solving equations 1 and 2 along a trajectory that starts over a warm subtropical ocean and ends on a high (3600-meter elevation) cold polar ice sheet ¹¹. The solutions for $\delta^{18}\text{O}$ and δD are found separately. The initial isotopic composition depends on sea surface temperature and relative humidity in accordance with Merlivat and Jouzel (1979), and I choose the relative humidity so that all initial d values equal nine. This is appropriate for precipitation on the Greenland ice sheet. To model precipitation on Antarctica, a lower initial d value would be used (Petit et al., 1991).

Calculations using all plausible values for the adjustable parameters in our model yield predicted meteoric water lines with slopes of approximately 8 and therefore nearly constant deuterium excess for the entire range $-43 < \delta^{18}\text{O} < 0$ (Figure 5.2). As this full range of parameters encompasses a vast array of natural conditions, this explanation for the MWL is stable, as observations require. Importantly, this result still holds if we prescribe substantial changes to the fractionation factors for supercooled water, as long as the changes are proportional for the $^{18}\text{O} - ^{16}\text{O}$ and $D - H$ systems ¹².

¹¹Johnsen et al. (1989) and Petit et al. (1991) have shown that vapour sources for polar precipitation must be warm and therefore must be located at low latitudes. As our model is essentially identical to Johnsen et al's for $T > 0^\circ\text{C}$, I use this condition. As with the Johnsen et al. calculations, our results are not at all sensitive to the details of the chosen trajectory otherwise. I use an initial ocean surface temperature of 300 K.

¹²The fractionation factors for deeply supercooled water may deviate significantly from those derived by extrapolating trends at warmer temperatures. Suppose that fractionation factors for supercooled water differ from the extrapolations α_w^* according to a parameter ϵ such that $\alpha_w = 1 + \epsilon(\alpha_w^* - 1)$. Let ϵ be a monotone function of supercooling, attaining a maximum or minimum of $1 + \epsilon^*$ at -40°C . I prescribe $\epsilon = 1 + \epsilon^* \left(\frac{273 - T}{40} \right)^m$ where m is a constant ≥ 1 . If I assume that ϵ is identical for ^{18}O and for D , so that the fractionation remains "water-like", then I find that deuterium excess deviates by no more than two per

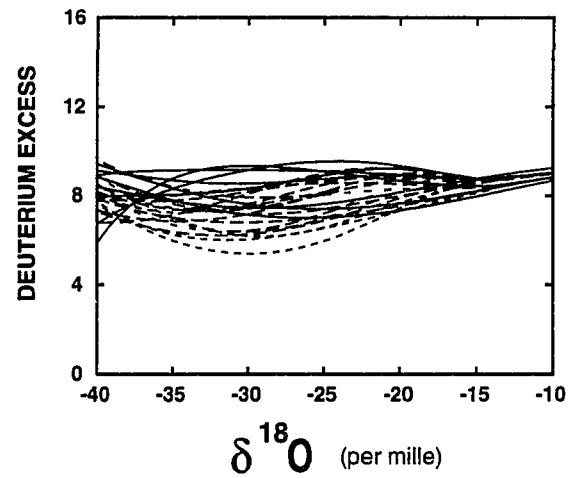


Figure 5.2: Modeled deuterium excess along air-mass trajectories for all combinations of the parameters $\Delta_g = 5, 10, 15$; $(T_\lambda, \Delta_\lambda) = (-15, 15), (-10, 8)$; $\zeta = 0, 1$; f_T given by scenarios I, II, III, IV (see Note 22). Solid lines are for $\Delta_g = 5$; long dashes for $\Delta_g = 10$; short dashes for $\Delta_g = 15$. The initial deuterium excess was chosen to be appropriate for modelling excess on the Greenland ice sheet, following (7).

Furthermore, this equilibrium model successfully replicates two independent features of polar precipitation. First, the 10 to 15 per mille rise in deuterium excess at very low temperatures on the East Antarctic Plateau is, on average, successfully predicted by the ensemble of model runs (panel A of Figure 5.3). Although individual trajectories are not all good, the ten per mille spread of d at given δ is not greater than the natural variability (Dahe et al., 1994). Second, our equilibrium model predicts a relationship between $\delta^{18}\text{O}$ and temperature that is a very satisfying match to the observed correlation between average $\delta^{18}\text{O}$ and average surface temperature (Dansgaard, 1964; Jouzel et al., 1987) (panel B of Figure 5.3), bearing in mind that model temperature refers to cloud temperatures during precipitation events (which become increasingly warmer than ground temperatures in the ice sheet interiors (Lorius and Merlivat, 1977)). My model's successful imitation of both this correlation and the d rise are not proof that the model is correct, but shows the model is consistent with the major features of isotopic data.

Thus I propose that an equilibrium isotopic model including a significant role for supercooled water explains the polar MWL and its consistency. This model should be viewed as the solution to an inverse problem, in which I have used the data (the persistent MWL) to construct the model. I do not argue for any particular interpretation of this forward model in terms of cloud microphysical processes. However, in our view there must be a quantitatively significant role for mechanisms of ice crystal formation that produce ice with composition close to that of liquid droplet precursors. These mechanisms must account for a mass fraction $1 - g$ of precipitating ice. I fully acknowledge that this view is unconventional and may prove to be wrong. It is justified by its ability to explain a major feature of geochemistry that remains puzzling to conventional models. Mechanisms that perform this task may involve

1. direct freezing of liquid droplets onto growing ice particles and

mille for ϵ^* in the range -0.3 to +0.3. This is a very large range, because $\epsilon^*=0.2$ increases the fractionation factor for supercooled water enough so that it equals the value for ice. If the fractionation factors do not maintain this "water-like" common relationship, but rather develop a more ice-like relationship, then this effect is included in the parameter g . Obviously, for our model to be correct, supercooled water cannot have a significantly ice-like ratio of fractionation factors for $T > -30^\circ\text{C}$.

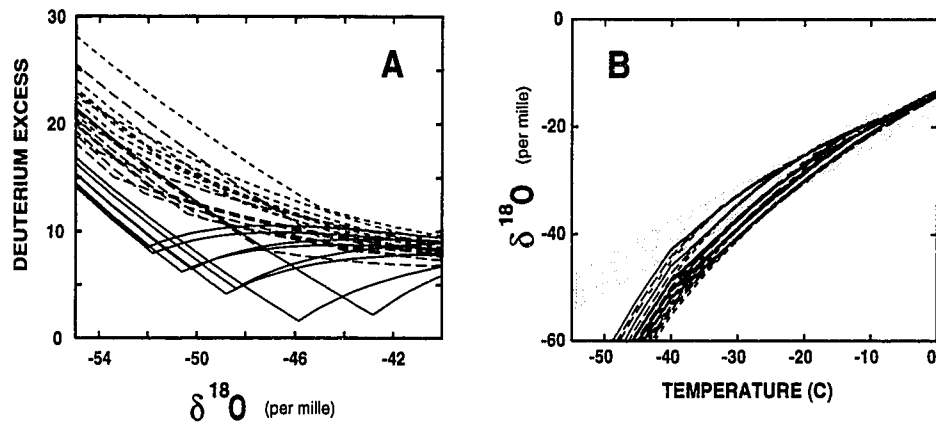


Figure 5.3: A. Model predictions for rise in deuterium excess at the very low temperatures of central Antarctica. Model parameters are same as above. The two trajectories with lowest d use the physically implausible limit $\zeta = 1$. B. Corresponding predictions for variation of isotopic composition as a function of cloud temperature. The light gray band represents the actual observations of isotopic composition versus ground temperature, whose mean is a line of slope 0.65 and intercept -14 (4).

2. growth of ice crystals from vapor in an environment that is locally dominated by liquid droplets.

Does our model admit a role for supersaturation-dependent kinetic fractionations (as identified by Merlivat and Jouzel, 1984)? Although I contend that such fractionations are not the reason for the MWL, I think they are plausible and wish to emphasize that our model does not argue against them. Rather, I suggest that these fractionations are not isotopically dominant because their cumulative effect, after integration of (1) over the range of natural temperatures, is small compared to that of liquid-vapor exchange. A sensitivity test illustrates this quantitatively. To maximize the kinetic effects I assume the largest permissible vapor pressures, those for liquid-vapor equilibrium, even at temperatures of -50 °C. Then replacing α_i in (3) by the kinetic fractionation factor ¹³ causes only a modest increase to predicted excess values (Table 1). In nature, supersaturations will vary and precipitation will reflect an average of these.

Despite the change I am proposing to the explanation for the polar MWL, our view strongly supports efforts to use ice-core deuterium excess measurements as an indicator of source-region paleoclimate conditions (Jouzel et al., 1982; Jouzel et al., 1989); in our view the constancy, and eventual rise, of deuterium excess along an air mass trajectory does not rely on a delicate balance between the temperature dependences of fractionation factors and cloud supersaturations. Thus, deuterium excess in an ice sheet interior is likely to reflect accurately the climate of the evaporative source regions which determine the deuterium excess of air masses crossing the margins of the ice sheets on their journey to ice core sites.

14

¹³ α_i is replaced by the kinetic fractionation factor $\alpha_k \alpha_i$, wherein according to Jouzel and Merlivat (1984) $\alpha_k = \frac{S_i}{(S_i - 1) \hat{D} \alpha_i + 1}$ and S_i is the supersaturation ratio (ratio of vapor pressure in the cloud to vapor pressure at an ice crystal surface) and \hat{D} is the ratio of diffusivities for different isotope-bearing waters.

¹⁴ The deuterium excess of air masses entering the ice sheet atmosphere should be properly interpreted according to Jouzel and Koster (1996).

Table 5.1: Average model deuterium excess values for various $\delta^{18}O$. The d column are averages of all models assuming no kinetic fractionation, whereas the d_{kin} assume the maximum possible kinetic fractionation (vapor pressure governed by liquid-vapor equilibrium). These models mimic Greenland precipitation. For Antarctic precipitation, a different initial condition must be used (Petit et al., 1991) which lowers d by approximately 5 per mille on average.

| $\delta^{18}O$ (per mille) | d (per mille) | d_{kin} (per mille) |
|----------------------------|-----------------|-----------------------|
| -20. | 8.2 | 8.8 |
| -30. | 7.3 | 10.1 |
| -40. | 8.4 | 13.4 |
| -50. | 14.7 | 20.1 |
| -60. | 26.1 | 25.7 |

BIBLIOGRAPHY

- Alley, R. B. (1988). Fabrics in polar ice sheets: development and prediction. *Science*, **240**, 493–495.
- Alley, R. B. (1992). Flow-law hypotheses for ice sheet modelling. *Journal of Glaciology*, **38**, 245–256.
- Alley, R. B. and Woods, G. A. (1996). Impurity influence on normal grain growth in the GISP2 ice core, Greenland. *Journal of Glaciology*, **42**(141), 255–260.
- Alley, R. B., Perepezko, J. H., and Bentley, C. R. (1986a). Grain growth in polar ice: I. theory. *Journal of Glaciology*, **32**, 415–424.
- Alley, R. B., Perepezko, J. H., and Bentley, C. R. (1986b). Grain growth in polar ice: II. application. *Journal of Glaciology*, **32**, 425–433.
- Alley, R. B., Cuffey, K. M., Evenson, E. B., Strasser, J. C., Lawson, D. E., and Larson, G. J. (1997). How glaciers entrain and transport basal sediment: physical constraints. *Quaternary Science Reviews*, **16**, 1017–1038.
- Anderton, P. W. (1974). Ice fabrics and petrography, Meserve Glacier, Antarctica. *Journal of Glaciology*, **13**, 285–306.
- Ashby, M. F. (1969). On the Orowan stress. In A. S. Argon, editor. *Physics of Strength and Plasticity*, pages 113–131, Cambridge MA. MIT Press.
- Ashby, M. F. (1980). The influence of particles on boundary mobility. In N. Hansen, A. R. Jones, and T. Leffers, editors, *Recrystallization and Grain Growth of Multiphase and Particle Containing Materials*, pages 325–336, Roskilde Denmark. Riso National Laboratory.

- Azuma, N. (1994). A flow law for anisotropic ice and its application to ice sheets. *Earth and Planetary Science Letters*, **128**, 601–614.
- Azuma, N. and Goto-Azuma, K. (1996). An anisotropic flow law for ice-sheet ice and its implications. *Annals of Glaciology*, **23**, 202–208.
- Azuma, N. and Higashi, A. (1985). Formation processes of ice fabric pattern in ice sheets. *Annals of Glaciology*, **6**, 130–134.
- Barnes, P., Tabor, D., and Walker, J. (1971). The friction and creep of polycrystalline ice. *Proceedings of the Royal Society of London, Series A.*, **324**, 127–155.
- Beaglehole, D. and Wilson, P. (1994). Extrinsic premelting at the ice-glass interface. *Journal of Physical Chemistry*, **98**, 8096–8100.
- Bower, K. N., Moss, S. J., Johnson, D. W., Choularton, T. W., Latham, J., Brown, P. R. A., Blyth, A. M., and Cardwell, J. (1996). A parameterization of the ice water content observed in frontal and convective clouds. *Quarterly Journal of the Royal Meteorologic Society*, **122**, 1815–1844.
- Buck, C. F., Mayewski, P. A., Spencer, M. J., Whitlow, S., Twickler, M. S., and Barrett, D. (1992). Determination of major ions in snow and ice cores by ion chromatography. *Journal of Chromatography*, **594**, 225–228.
- Budd, W. F. and Jacka, T. H. (1989). A review of ice rheology for ice sheet modelling. *Cold Regions Science and Technology*, **16**, 107–144.
- Carnein, R. C. (1967). *Mass balance of the Meserve Glacier, Wright Valley, Antarctica*. Master's thesis, Ohio State University, Columbus, OH.
- Ciais, P. and Jouzel, J. (1994). Deuterium and oxygen 18 in precipitation: Isotopic model, including mixed cloud processes. *Journal of Geophysical Research*, **99**(D8), 16793–16803.
- Clow, G. D. and Gundestrup, N. (1996). Borehole geophysics at GISP2 and GRIP. *Journal of Geophysical Research*, **in prep.**

- Craig, H. (1961). Isotopic variations in meteoric waters. *Science*, **133**, 1702–1703.
- Craig, H. (1966). Isotopic composition and origin of the Red Sea and Salton Sea geothermal brines. *Science*, **154**, 1544–1548.
- Cuffey, K. M., Conway, H., Hallet, B., Gades, A. M., and Raymond, C. F. (1999). Interfacial water in polar glaciers, and glacier sliding at -17°C . *Geophysical Research Letters*, in press.
- Dahe, Q., Petit, J. R., Jouzel, J., and Stievenard, M. (1994). Distribution of stable isotopes in surface snow along the route of the 1990 International Trans-Antarctica Expedition. *Journal of Glaciology*, **40**(134), 107–118.
- Dahl-Jensen, D. and Gundestrup, N. S. (1987). Constitutive properties of ice at Dye 3, Greenland. *International Association of the Hydrological Sciences*, **170**, 31–43.
- Dahl-Jensen, D., Thorsteinsson, T., Alley, R. B., and Shoji, H. (1997). Flow properties of the ice from the Greenland Ice Core Project ice core: The reason for folds? *Journal of Geophysical Research*, **102**(C12), 26831–26840.
- Dansgaard, W. (1964). Stable isotopes in precipitation. *Tellus*, **16**, 436–468.
- Dash, J. G., Fu, H., and Wettlaufer, J. (1995). The premelting of ice and its environmental consequences. *Reports on Progress in Physics*, **58**, 115–167.
- Denton, G. H., Sugden, D. E., Marchant, D. R., Hall, B. L., and Wilch, T. I. (1993). East Antarctic Ice Sheet sensitivity to Pliocene climate change from a Dry Valleys perspective. *Geografiska Annaler*, **75**(A4), 155–204.
- Durham, W. B., Kirby, S. H., and Stern, L. A. (1992). Effects of dispersed particulates on the rheology of water ice at planetary conditions. *Journal of Geophysical Research*, **97**(E12), 20883–20897.
- Duval, P., Ashby, M. F., and Anderman, I. (1983). Rate-controlling processes in the creep of polycrystalline ice. *Journal of Physical Chemistry*, **87**, 4066–4074.

- Echelmeyer, K. and Zhongxiang, W. (1987). Direct observations of basal sliding and deformation of basal drift at sub-freezing temperatures. *Journal of Glaciology*, **33**(113), 83-98.
- Echelmeyer, K. A., Harrison, W. D., Larsen, C., and Mitchell, J. E. (1994). The role of the margins in the dynamics of an active ice stream. *Journal of Glaciology*, **40**, 527-538.
- Etheridge, D. M. (1989). Dynamics of the Law Dome ice cap, Antarctica, as found from bore-hole measurements. *Annals of Glaciology*, **12**, 46-50.
- Federer, B., Brichet, N., and Jouzel, J. (1982). Stable isotopes in hailstones, I. The isotopic cloud model. *Journal of the Atmospheric Sciences*, **39**, 1323-1335.
- Fisher, D. A. (1987). Enhanced flow of Wisconsin ice related to solid conductivity through strain history and recrystallization. *International Association of the Hydrological Sciences*, **170**, 45-51.
- Fisher, D. A. and Koerner, R. M. (1986). On the special rheological properties of ancient microparticle-laden northern hemisphere ice as derived from bore-hole and core measurements. *Journal of Glaciology*, **32**(112), 501-510.
- Frape, S. K., Fritz, P., and McNutt, R. H. (1984). Water-rock interaction and chemistry of groundwaters from the Canadian Shield. *Geochimica et Cosmochimica Acta*, **48**, 1617-1627.
- Gedzelman, S. D. and Arnold, R. (1994). Modelling the isotopic composition of precipitation. *Journal of Geophysical Research*, **99**(D5), 10455-10471.
- Gibson, J. J., Edwards, T. W. D., and Prowse, T. D. (1996). Development and validation of an isotopic method for estimating lake evaporation. *Hydrological Processes*, **10**(10), 1369-1382.

- Gilpin, R. R. (1979). A model of the liquid-like layer between ice and a substrate with applications to wire regelation and particle migration. *Journal of Colloid and Interface Science*, **68**(2), 235–251.
- Goldsby, D. L. and Kohlstedt, D. L. (1997). Grain boundary sliding in fine-grained Ice I. *Scripta Materialia*, **37**(9), 1399–1406.
- Gow, A. J., Meese, D. A., Alley, R. B., Fitzpatrick, J. J., Anandkrishnan, S., Woods, G. A., and Elder, B. C. (1997). Physical and structural properties of the Greenland Ice Sheet Project 2 ice core: A review. *Journal of Geophysical Research*, **102**(C(12)), 26559–26576.
- Gross, G. W., McKee, C., and Wu, C. (1975). Concentration dependent solute redistribution at the ice/water phase boundary i. analysis. *Journal of Chemical Physics*, **62**, 3080–3084.
- Gudmundsson, G. H. (1997). Basal-flow characteristics of a non-linear flow sliding frictionless over strongly undulating bedrock. *Journal of Glaciology*, **43**, 80–89.
- Hallet, B. (1979). A theoretical model of glacial abrasion. *Journal of Glaciology*, **23**(89), 39–50.
- Hallet, B., Gregory, C., Stubbs, C., and Anderson, R. (1986). Measurements of ice motion over bedrock at subfreezing temperatures. *Mitteilungen der Versuchsanstalt für Wasserbau, Hydrologie und Glaziologie an der E.T.H., Zurich*, **90**, 53–54.
- Herron, M. M. and Langway-Jr, C. C. (1985). Chloride, nitrate and sulfate in the Dye 3 and Camp Century ice cores. In C. C. Langway-Jr, H. Oeschger, and W. Dansgaard, editors, *Greenland Ice Core: Geophysics, Geochemistry, and the Environment. Geophysical Monograph 33*, pages 77–84, Washington, DC. American Geophysical Union.
- Herron, M. M., Langway-Jr, C. C., and Brugger, K. A. (1985). Ultrasonic velocities and crystalline anisotropy in the ice core from Dye 3, Greenland. In C. C. Langway-Jr, H. Oeschger, and W. Dansgaard, editors, *Greenland Ice Core: Geophysics, Geochem-*

- istry, and the Environment. Geophysical Monograph 33*, pages 23–31, Washington, DC. American Geophysical Union.
- Hobbs, P. V. and Rangno, A. L. (1998). Microstructures of low and middle-level clouds over the Beaufort Sea. *Quarterly Journal of the Royal Meteorologic Society*, **124**, 2035–2071.
- Holdsworth, G. (1969). *Mode of Flow of Meserve Glacier, Wright Valley, Antarctica*. Ph.D. thesis, Ohio State University, Columbus, OH.
- Holdsworth, G. (1974). Meserve glacier, wright valley antarctica: Part 1. basal processes. Technical Report 37, Institute for Polar Studies, Columbus, OH.
- Holdsworth, G. and Bull, C. (1970). The flow law of cold ice; investigations on Meserve Glacier, Antarctica. *IAHS*, **86**, 204–216.
- Hooke, R. L., Dahlin, B. H., and Kauper, M. T. (1972). Creep of ice containing dispersed fine sand. *Journal of Glaciology*, **11**, 327–336.
- Horita, J. and Wesolowski, D. J. (1994). Liquid-vapor fractionation of oxygen and hydrogen isotopes of water from the freezing to the critical temperature. *Geochimica et Cosmochimica Acta*, **58**(16), 3425–3437.
- Huybrechts, P., Letreguilly, A., and Reeh, N. (1991). The Greenland Ice Sheet and greenhouse warming. *Paleogeography, Paleoclimatology and Paleoecology (Global and Planetary Change Section)*, **89**(4), 399–412.
- Iverson, N. R. and Semmens, D. (1995). Intrusion of ice into porous media by regelation: A mechanism of sediment entrainment by glaciers. *Journal of Geophysical Research*, **100**, 10219–10230.
- Iverson, N. R. and Souchez, R. (1996). Isotopic signature of debris-rich ice formed by regelation into a subglacial sediment bed. *Geophysical Research Letters*, **23**(10), 1151–1154.

- Jacka, T. H. (1984). Laboratory studies on relationships between ice crystal size and flow rate. *Cold Regions Science and Technology*, **10**, 31–42.
- Japas, M. L., Fernandez-Prini, R., Horita, J., and Wesolowski, D. J. (1995). Fractioning of isotopic species between coexisting liquid and vapor water: complete temperature range, including the asymptotic critical behavior. *Journal of Physical Chemistry*, **99**, 5171–5175.
- Johnsen, S. J., Dansgaard, W., and White, J. W. C. (1989). The origin of Arctic precipitation under present and glacial conditions. *Tellus*, **41**(B), 452–469.
- Jouzel, J. and Koster, T. D. (1996). A reconsideration of the initial conditions used for stable water isotope models. *Journal of Geophysical Research*, **101**(D17), 22933–22938.
- Jouzel, J. and Merlivat, L. (1984). Deuterium and oxygen 18 in precipitation: modelling of the isotopic effects during snow formation. *Journal of Geophysical Research*, **89**(D7), 11749–11757.
- Jouzel, J. and Souchez, R. (1982). Melting-refreezing at the glacier sole and the isotopic composition of the ice. *Journal of Glaciology*, **28**(98), 35–42.
- Jouzel, J., Merlivat, L., and Lorius, C. (1982). Deuterium excess in an East Antarctic ice core suggests higher relative humidity at the oceanic surface during the last glacial maximum. *Nature*, **299**, 688–691.
- Jouzel, J., Russell, G. L., Koster, R. D., Suozzo, R. J., White, J. W. C., and Broecker, W. S. (1987). Simulations of the HDO and H₂¹⁸O atmospheric cycles using the NASA GISS general circulation model: the seasonal cycle for present-day conditions. *Journal of Geophysical Research*, **92**(D12), 14739–14760.
- Jouzel, J., Koster, R. D., Suozzo, R. J., Russell, G. L., White, J. W. C., and Broecker, W. S. (1991). Simulations of the HDO and H₂¹⁸O atmospheric cycles using the NASA GISS general circulation model: sensitivity experiments for present-day conditions. *Journal of Geophysical Research*, **96**(D4), 7495–7507.

- Jun, L., Jacka, T. H., and Budd, W. F. (1996). Deformation rates in combined compression and shear for ice which is initially isotropic and after the development of strong anisotropy. *Annals of Glaciology*, **23**, 247–252.
- Kamb, W. B. (1962). Refraction corrections for universal stage measurements. I. Uniaxial crystals. *American Mineralogist*, **47**, 227–245.
- Koerner, R. M. (1989). Ice core evidence for extensive melting of the Greenland ice sheet in the last interglacial. *Science*, **244**, 964–968.
- Langway, C. C. (1958). Ice fabrics and the universal stage. Technical Report 62, SIPRE, Hanover, NH.
- Langway-Jr, C. C., Shoji, H., and Azuma, N. (1988). Crystal size and orientation patterns in the Wisconsin-age ice from Dye 3, Greenland. *Annals of Glaciology*, **10**, 109–115.
- Lipenkov, V. Y., Barkov, N. I., Duval, P., and Pimienta, P. (1989). Crystalline texture of the 2083 m ice core at Vostok Station, Antarctica. *Journal of Glaciology*, **35**(121), 392–398.
- Lliboutry, L. and Duval, P. (1985). Various isotropic and anisotropic ices found in glaciers and polar ice caps and their corresponding rheologies. *Annales Geophysique*, **3**, 207–224.
- Lorius, C. and Merlivat, L. (1977). Distribution of mean surface stable isotope values in East Antarctica: Observed changes with depth in a coastal area. *International Association of the Hydrological Sciences*, **118**, 125–137.
- Majoube, M. (1971). Fractionnement en oxygène 18 et en deuterium entre l'eau et sa vapeur. *Journal de Chimie et Physique*, **68**, 1423–1436.
- Mayewski, P. A. and six others (1997). Major features and forcing of high-latitude northern hemisphere atmospheric circulation using a 110,000-year-long glaciochemical series. *Journal of Geophysical Research*, **102**(C12), 26345–26367.

- Mercer, J. H. (1971). Cold glaciers in the central Transantarctic Mountains, Antarctica: dry ablation areas and subglacial erosion. *Journal of Glaciology*, **59**(10), 319–321.
- Merlivat, L. and Jouzel, J. (1979). Global climatic interpretation of the deuterium-oxygen 18 relationship for precipitation. *Journal of Geophysical Research*, **84**, 5029–5033.
- Merlivat, L. and Nief, G. (1967). Fractionnement isotopique lors des changements d'états solide-vapeur et liquide-vapeur de l'eau à des températures inférieures à 0 °C. *Tellus*, **19**(1), 122–127.
- Nakamura, T. and Jones, S. J. (1970). Softening effect of dissolved hydrogen chloride in ice crystals. *Scripta Metallurgica*, **4**, 123–126.
- Nye, J. F. (1957). The distribution of stress and velocity in glaciers and ice sheets. *Proceedings of the Royal Society of London, Series A.*, **239**, 113–333.
- Nye, J. F. (1969). A calculation on the sliding of ice over a wavy surface using a Newtonian viscous approximation. *Proceedings of the Royal Society of London, Series A.*, **311**(1506), 445–467.
- Paren, J. G. and Walker, J. C. F. (1971). Influence of limited solubility on the electrical and mechanical properties of ice. *Nature (Physical Sciences)*, **230**, 77–79.
- Paterson, W. S. B. (1991). Why ice-age ice is sometimes “soft”. *Cold Regions Science and Technology*, **20**, 75–98.
- Paterson, W. S. B. (1994). *The Physics of Glaciers*. Pergamon, Oxford.
- Peltier, W. R. (1998). Post-glacial variations in the level of the sea: implications for climate dynamics and solid-earth geophysics. *Reviews of Geophysics*, **36**(4), 603–689.
- Petit, J. R., White, J. W. C., Young, N. W., Jouzel, J., and Korotkevich, Y. S. (1991). Deuterium excess in recent Antarctic snow. *Journal of Geophysical Research*, **96**(D3), 5113–5122.

- Pimienta, P., Duval, P., and Lipenkov, V. Y. (1988). Mechanical behavior of ice along the 2040 m Vostok core, Antarctica. *Annals of Glaciology*, **10**, 137–140.
- Press, W. H., Teukolsky, S. A., Vetterling, W. T., and Flannery, B. P. (1992). *Numerical Recipes in FORTRAN. The Art of Scientific Computing, 2nd ed.* Cambridge University Press, Cambridge.
- Richardson, C. and Holmlund, P. (1996). Glacial cirque formation in northern Scandinavia. *Annals of Glaciology*, **22**, 102–106.
- Riley, N. W., Noll, G., and Glen, J. W. (1987). The creep of NaCl-doped ice monocrystals. *Journal of Glaciology*, **21**(85), 501–507.
- Shoji, H. and Langway-Jr, C. C. (1988). Flow-law parameters of the Dye 3, Greenland, deep ice core. *Annals of Glaciology*, **10**, 146–150.
- Shreve, R. L. (1984). Glacier sliding at subfreezing temperatures. *Journal of Glaciology*, **30**(106), 341–347.
- Souchez, R. (1997). The buildup of the ice sheet in central Greenland. *Journal of Geophysical Research*, **102**(C12), 26317–26323.
- Souchez, R., Lorrain, R., Tison, J. L., and Jouzel, J. (1988). Co-isotopic signature of two mechanisms of basal-ice formation in Arctic outlet glaciers. *Annals of Glaciology*, **10**, 163–166.
- Souchez, R. A., Janssens, L., Lemmens, M., and Stauffer, B. (1995). Very low oxygen concentration in basal ice from Summit, central Greenland. *Geophysical Research Letters*, **22**(15), 2001–2004.
- Sternberg, L. D., Ish-Shalom-Gordon, N., Ross, M., and O'Brien, J. (1991). Water relations of coastal plant communities near the ocean/freshwater boundary. *Oecologia*, **88**(3), 305–310.

- Stillinger, F. H. (1980). Water revisited. *Science*, **209**, 451-457.
- Sugden, D. E. and John, B. S. (1976). *Glaciers and Landscape*. Edward Arnold, London.
- Sugden, D. E., Clapperton, C. M., Gemmell, J. C., and Knight, P. G. (1987). Stable isotopes and debris in basal glacier ice, South Georgia, southern ocean. *Journal of Glaciology*, **33**(115), 324-329.
- Summerfield, M. A. (1991). *Global Geomorphology*. Longman Scientific and Technical, Essex.
- Thorsteinsson, T., Kipfstuhl, J., and Miller, H. (1997). Textures and fabrics in the GRIP ice core. *Journal of Geophysical Research*, **102**(C12), 26583-26600.
- Thorsteinsson, T., Waddington, E. D., Taylor, K. C., Alley, R. B., and Blankenship, D. D. (1999). Strain rate enhancement at Dye 3, Greenland. *Journal of Glaciology*, **in press**.
- Tice, A. R., Yuanlin, Z., and Oliphant, J. L. (1984). The effects of soluble salts on the unfrozen water contents of the Lanzhou, P.R.C., silt. Technical Report 84, Cold Regions Research and Engineering Laboratory, Hanover, NH.
- Tison, J. L., Petit, J. R., Barnola, J. M., and Mahaney, W. C. (1993). Debris entrainment at the ice-bedrock interface in sub-freezing temperature conditions (Terre Adelie, Antarctica). *Journal of Glaciology*, **39**(132), 303-315.
- Tison, J. L., Thorsteinsson, T., Lorrain, R. D., and Kipfstuhl, J. (1994). Origin and development of textures and fabrics in basal ice at Summit, central Greenland. *Earth and Planetary Science Letters*, **125**, 421-437.
- Underwood, E. E. (1970). *Quantitative Stereology*. Addison-Wesley Publishing Co., Reading, MA.
- vanderVeen, C. J. and Whillans, I. M. (1994). Development of fabric in ice. *Cold Regions Science and Technology*, **22**(2), 171-195.

- VanHook, W. A. (1968). Vapor pressures of the isotopic waters and ices. *Journal of Physical Chemistry*, **72**(4), 1234–1244.
- Waddington, E. D. and Rasmussen, L. A. (1993). Calculating strain rates and velocities from survey measurements of stake fields. *unpublished*.
- Wake, C. P., Mayewski, P. A., and Spencer, M. J. (1989). A review of central Asian glaciochemical data. *Annals of Glaciology*, **14**, 301–306.
- Weertman, J. (1972). General theory of water flow at the base of a glacier or ice sheet. *Reviews of Geophysics and Space Physics*, **10**(1), 287–333.
- Wettlaufer, J. S. (1998). Impurity effects in interfacial melting. *Physical Review Letters*, in press.
- Wettlaufer, J. S. and Worster, M. G. (1995). Dynamics of premelted films: Frost heave in a capillary. *Physical Review E*, **51**, 4679–4689.
- Wettlaufer, J. S., Worster, M. G., Wilen, L. A., and Dash, J. G. (1996). A theory of premelting dynamics for all power law forces. *Physical Review Letters*, **76**, 3602–3605.
- Wettlaufer, J. S., Worster, M. G., and Huppert, H. E. (1997). Natural convection during solidification of an alloy from above with application to the evolution of sea ice. *Journal of Fluid Mechanics*, **344**, 291–316.
- Wilson, A. T. (1979). Geochemical problems of the Antarctic dry areas. *Nature*, **280**, 205–208.
- Yesikov, A. D., Ivlev, A. A., Onipchenko, V. G., and Shnol, S. E. (1985). Isotope fractionation on movement of water in the xylem of higher plants. *Biophysics*, **29**(6), 1134–1139.
- Zdanowicz, C. M., Michel, F. A., and Shilts, W. W. (1996). Basal debris entrainment and transport in glaciers of southwestern Bylot Island, Canadian Arctic. *Annals of Glaciology*, **22**, 107–113.

VITA

Name: **Kurt M. Cuffey**

Date: January 20, 1999

Education:

B.S. Earth Science, Pennsylvania State University, 1992

M.S. Geological Sciences, University of Washington, 1995

Ph. D. Geological Sciences, University of Washington, 1999

Primary Research Interests:

Earth Surface Processes

Glacier Mechanics River Mechanics

Environmental Change

Ice Core Paleoclimatology Ice Sheet Growth and Decay

Environmental Geochemistry

Stable Isotopes of Water

Publications:

- Cuffey, K.M., H. Conway, B. Hallet, A.M. Gades and C.F. Raymond (1999). Interfacial water in polar glaciers and glacier sliding at -17°C . *Geophysical Research Letters* In press.
- Cuffey, K.M. and E.J. Steig (1998). Isotopic diffusion in polar firn: implications for interpretation of seasonal climate parameters in ice-core records, with emphasis on

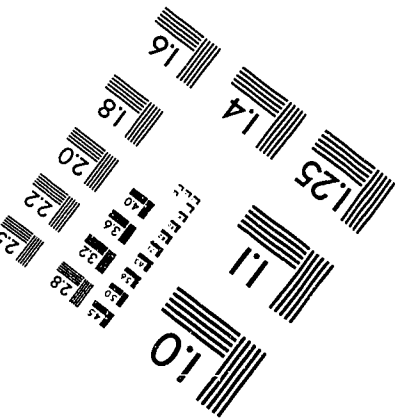
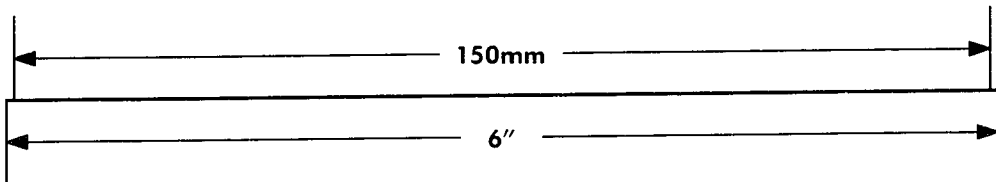
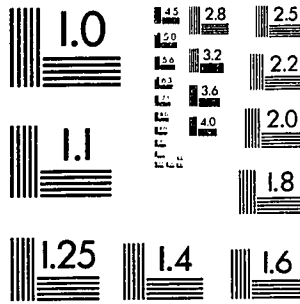
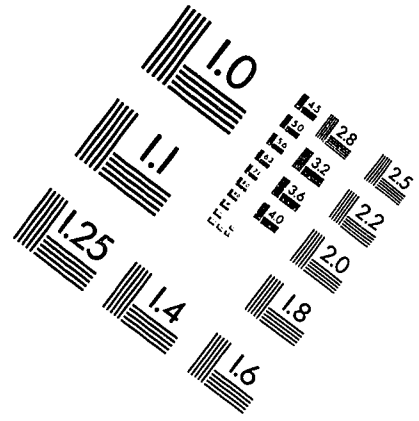
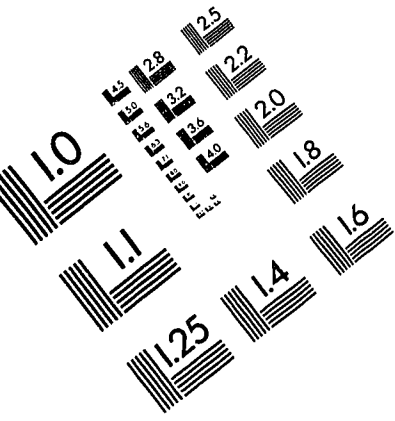
central Greenland. *Journal of Glaciology* **44**, 273-284.

- Cuffey, K.M. and G.D. Clow (1997). Temperature, accumulation and ice sheet elevation in central Greenland through the last deglacial transition. *Journal of Geophysical Research* **102**(C12), 26383-26396.
- Cuffey, K.M. and R.B. Alley (1996). Is erosion by deforming subglacial sediments significant? (Toward till continuity). *Annals of Glaciology* **22**, 17-24.
- Cuffey, K.M., G.D. Clow, R.B. Alley, M. Stuiver, E.D. Waddington and R.W. Saltus (1995). Large Arctic temperature change at the Wisconsin-Holocene glacial transition. *Science* **270**, 455-458.
- Cuffey, K.M., R.B. Alley, P.M. Grootes, J.M. Bolzan and S. Anandakrishnan (1994). Calibration of the $\delta^{18}\text{O}$ isotopic paleothermometer for central Greenland, using borehole temperatures. *Journal of Glaciology* **40**, 341-349.
- Cuffey, K.M., R.B. Alley, P.M. Grootes and S. Anandakrishnan (1992). Toward using borehole temperatures to calibrate an isotopic paleothermometer in central Greenland. *Global and Planetary Change* **6**, 265-268.
- Aalto, R., D.R. Montgomery, B. Hallet, T.B. Abbe, J.M. Buffington, K.M. Cuffey and K.M. Schmidt (1997). A hill of beans. *Science* **277**, 1911-1912.
- Alley, R.B., K.M. Cuffey, E.B. Evenson, J.C. Strasser, D.E. Lawson, and G.J. Larson (1997). How glaciers entrain and transport basal sediment: physical constraints. *Quaternary Science Reviews* **16**, 1017-1038.
- Alley, R.B., C.A. Shuman, D.A. Meese, A.J. Gow, K.C. Taylor, K.M. Cuffey, J.J. Fitzpatrick, P.M. Grootes, G.A. Zielinski, M. Ram, G. Spinelli and B. Elder (1997).

Visual-stratigraphic dating of the GISP2 ice core: basis, reproducibility, and application. *Journal of Geophysical Research* **102**(C12), 26367-26382.

- Alley, R.B., E.S. Saltzman, K.M. Cuffey and J.J. Fitzpatrick (1990). Summertime formation of depth hoar in central Greenland. *Geophysical Research Letters* **17**, 2393-2396.
- Jouzel, J., R.B. Alley, K.M. Cuffey, W. Dansgaard, P. Grootes, G. Hoffman, S.J. Johnsen, R.D. Koster, D. Peel, C.A. Shuman, M. Stievenard, M. Stuiver and J. White (1997). Validity of the temperature reconstruction from water isotopes in ice cores. *Journal of Geophysical Research* **102**(C12), 26471 - 26488.

IMAGE EVALUATION TEST TARGET (QA-3)



APPLIED IMAGE, Inc
 1653 East Main Street
 Rochester, NY 14609 USA
 Phone: 716/482-0300
 Fax: 716/288-5989

© 1993, Applied Image, Inc.. All Rights Reserved

